

# eScholarship@UMassChan

## Bacteria-Tumor-Drug Interactions: Investigating Bacterial Tumor Colonization and Bacterial Evolved Resistance to Anti-Cancer Therapy

Item Type	Doctoral Dissertation
Authors	Sayin, Serkan
DOI	<a href="https://doi.org/10.13028/cmw7-bc66">10.13028/cmw7-bc66</a>
Publisher	UMass Chan Medical School
Rights	© 2023 Serkan Sayin
Download date	2026-03-08 23:41:12
Item License	<a href="https://creativecommons.org/licenses/by-nc/4.0/">https://creativecommons.org/licenses/by-nc/4.0/</a>
Link to Item	<a href="https://hdl.handle.net/20.500.14038/52630">https://hdl.handle.net/20.500.14038/52630</a>

I

BACTERIA-TUMOR-DRUG INTERACTIONS: INVESTIGATING  
BACTERIAL TUMOR COLONIZATION AND BACTERIAL EVOLVED  
RESISTANCE TO ANTI-CANCER THERAPY

A Dissertation Presented

By

SERKAN SAYIN

Submitted to the Faculty of the  
Morningside Graduate School of Biomedical Sciences at UMass Chan Medical  
School in partial fulfillment of the requirements for the degree of  
DOCTOR OF PHILOSOPHY

September, 2023

Bioinformatics and Computational Biology

BACTERIA-TUMOR-DRUG INTERACTIONS: INVESTIGATING  
BACTERIAL TUMOR COLONIZATION AND BACTERIAL EVOLVED  
RESISTANCE TO ANTI-CANCER THERAPY

A Dissertation Presented

By

SERKAN SAYIN

This work was undertaken in the Morningside Graduate School of Biomedical Sciences

Bioinformatics and Computational Biology

Under the mentorship of

Amir Mitchell, Thesis Advisor

Marian Walhout, Member of Committee

Elinor Karlsson, Member of Committee

Josue FloresKim, Member of Committee

Sepepe Kuehn, External Member of Committee

Beth McCormick, Chair of Committee

Mary Ellen Lane, Ph.D.,  
Dean of the Graduate School of Biomedical Sciences  
September, 2023

**DEDICATION:**

To all *Felis catus* and other *Feline* species...

^\_^  
(o.o)  
> ^ <

**ACKNOWLEDGEMENTS:**

When I met **Amir Mitchell**, his lab was one of the newest in the Systems Biology Department and he had all the cool stuff like 3D printers, liquid handlers, an electronics bay, and Arduinos! And I have to say that Amir was also one of the smartest people I have ever met in my life. The scientific journey after joining his lab, since the beginning, has been a challenge but at the same time a great experience for me. We started with the evolution of antibiotic resistance, and jumped into chemotherapeutics; we used worms, then spheroids then the mice along the way! The number of research areas we explored was very diverse, and I developed large sets of skills, especially in data analysis. And of course, scientific discussions on Slack day and night really moved me to this dissertation. Amir you really helped me grow intellectually during my PhD journey, taught me critical thinking and coding skills, and gave me advice not just scientifically but also as a colleague. I can't believe how much I learned from you and I am so grateful to be the first PhD student joined to the lab. You have always supported me, and always gave me the courage to move on, even at the tough times of the PhD journey.

I also would like to thank my TRAC and DEC members for guiding me with scientific discussions. I especially thank **Marian Walhout**, **Beth McCormick**, and **Elinor Karlsson**. I really appreciate Marian's support both scientifically and on a personal level during the hard times of my Ph.D. I also thank the recent members **Josue FloresKim** and the external examiner **Seppe Kuehn**.

I would like to thank **Regino-Merdcao Lubo** for his experience and guidance with the mouse experiments, **Michael Brehm** and his lab members for preliminary mouse experiments, and **Greg Cottle** from Animal Medicine for training us and helping out. I also would like to thank our collaborators outside of the Umass, especially **Motasem Elgamel** and **Andrew Mügler** from University of Pittsburgh for their contributions to the quantitative modeling of the barcode data. I also thank **Leore Geller** from **Ravid Straussman** lab for performing an *in vivo* mouse experiment for us at the Weizmann Institute of Technology, Israel.

Anddd, all of the Mitchell lab members! It has been a blast to work with all of you. Early days of the lab with **Fang Xie**, **Payam Khoskenar**, and **Nicholas Vecchietti**. We had so much fun in and outside of the lab...Pizza nights, pixel art, late-night experiments... **Brittany Rosener**! I think we learned a lot from each other throughout the years. All the projects we did together, failed mouse experiments, and writing IACUC protocols. We will be always senior members of the Mitchell lab haha. Later members who joined Mitchell Lab; **Mariana Noto Guillén**, **Emily Lowry**, **Carmen Li**, and **Sydney Schock**. I always enjoyed our scientific discussions when someone had trouble with cloning when an experiment did not work and we had to troubleshoot. Also, our famous movie nights and lab hangouts... It was all so much fun and I think we have been an amazing group of friends besides being just coworkers. We generated a spectacular lab culture over the years supporting each other.

Walhout lab, Brewster lab, Lee lab, and all other systems biology colleagues... **Aurian Garcia-Gonzalez**, you were such a good friend, colleague, and mentor early times of my Ph.D. You were always very ambitious, motivated, and full of energy. Your vibe made all of the experiments we did together a very fun experience! I learned a lot from you. No doubt you will be a very successful woman in your medical career. **Brent Horowitz**, we always had a weird friendship that has been also acknowledged by many others. I think it all started meeting you on the first day of school. I think you will remember me always as “a Ph.D. student in Mitchell lab” haha. **Yong-uk Lee** you were always the weird and funny one. And **Olga Ponomarova**...you were the GC-MS master of Walhout lab. It has been a pleasure to work with you on the gemcitabine project. I also thank to **Gabrielle Giese** who is such a great colleague to work with and **Amy Levassaur** for her dedicated help the department with the reagents. **Vinuselvi Parisutham**! Every time we were stuck with a cloning problem when we needed a plasmid, had to set up a bacterial experiment or had questions with plate readers, you were always very helpful and solved all of our problems. I learned a LOT from you. **Sunil Guharajan** and **Zulfikar Ali**! You guys aka brew crew + Yong Uk - we had so much fun together. And **Peter Cruz-Gordillo**, you always felt like a brother to me! No doubt you will be an extraordinary Neurosurgeon! And, all other members of the systems biology department, you made all these years a great pleasure to work with. Everyone’s openness, scientific discussions, and friendship make this environment really nice.

I also want to express my thanks and gratitude to my classmates especially **Betul Akgol Oksuz, Sneha Suresh, Grant Weaver, Nanditha Un, Sarah Anderson, Melanie Walker,** and **Kris Holloway**. Getting used to a new country and a new school has been really fun and easy with you all. In the first year, we would always get lunches together which was the most fun of the day. I wish you all the best in your life and career.

And my housemate **Deniz Özata** and my dear friends/neighbors **Özgür Öksüz** and **Betül Öksüz**. Living in Worcester very close to made me feel at home. You were always there when I needed something and we had so much fun. Covid lockdown times, endless barbecues we did, buffalo wild wings. You have been my family here. My extended family here, **Tugba Ceren Gökoglan Barut**, Onur Barut! We had so much fun, travelled, celebrated and so on...Other close friends **Ahmet Bakirbas, Nehir Kurtas, Yetis Gultekin, Doga Tekbas, Ege Ozsar, Allan Pires, Kaan Eren**, and anyone I forgot to mention here. We built a great circle of friends here always up for something fun outside of work!

I also have friends who are living in Turkey or in other countries that I had so much interaction during my Ph.D. I especially thank to **Ilkcan Ercan, Burcu Ekinci**, and all other friends from IZTECH. I am thankful to my friends from my hometown, **Sükrü Gökhan Elçi, Ilkay Ayilmaz, Yasemin Martin,** and **Çaglar Çil**.

I want to express my gratitude and acknowledge my precious family who are always there for me to support me in my endeavors. My mom, **Ayşe Sayın**, who was on the phone with me literally every day, and my dad **Mehmet Sayın**,

who beat two cancers during my PhD! My dear sister **Funda Özgentas** who always supported me, believed in me, and talked to me whenever I needed it! I also want to thank my brother-in-law **Burak Özgentas** and my dear niece **Zeynep Özgentas**! I can imagine Zeynep being a very successful scientist in the future! And of course, I will acknowledge our cats who are part of the family: **Tekir, Kabarik, Angela, Firlama....**

I also would like to acknowledge all of my teachers, professors, and friends whom I could not mention here who had an impact on me to achieve my goal of being a scientist and the person today! I hope that this work will help and inspire future scientists for further investigations to improve the knowledge and well-being of humans.

## ABSTRACT

The human microbiome has been extensively studied, yet remains elusive due to its complexity. Recent findings showed that many solid tumors may harbor a microbiome. Bacterial presence in tumors may cause cancer progression, modify the chemical structures of anti-cancer treatments or alter the immune responses. Basic principles of how bacteria initiate a population and expand in tumors, and how they adapt to anti-cancer therapies is an underexplored area. For instance, gamma-proteobacteria found in pancreatic ductal adenocarcinomas cause chemoresistance by converting gemcitabine to its inactive form by the cytidine deaminase enzyme. Here, I first focused on this drug-bacteria interaction to understand bacterial evolution to gemcitabine and how it could affect existing bacteria-drug interactions. Using a genome-wide genetic screen, I showed that many loss-of-function mutations can cause gemcitabine resistance. I found that one-third of the resistance mutations increase or decrease bacterial drug breakdown, which can decrease or increase the gemcitabine load in the local environment. I also found that the adaptation of *E. coli* to gemcitabine resulted in the inactivation of the nucleoside permease *NupC*, which increased the drug burden on co-cultured cancer spheroids. Secondly, I focused on exploring the bacterial colonization of tumors *in vivo*. Using an isogenic barcoded *E. coli* library, I showed the presence of a narrow bottleneck during tumor colonization and skewed bacterial dissemination in the tumor environment. Overall, this study sheds

light on quantitative bacterial colonization principles in tumors and intra-species bacterial adaptation to anti-cancer drugs with implications to the cancer cells.

**TABLE OF CONTENTS:**

Dedication: .....	III
Acknowledgements:.....	IV
<b><i>Abstract</i></b> .....	<b><i>IX</i></b>
Table of Contents: .....	XI
List of tables: .....	XV
List of Figures:.....	XVI
List of copyrighted Materials Produced by the Author: .....	XVIII
List of Symbols, Abbreviations or Nomenclature .....	XIX
List of Multimedia Objects and Files.....	XX
<b><i>Chapter 1. introduction</i></b> .....	<b><i>1</i></b>
1.1. human microbiota in health and disease .....	1
1.2. Metabolic capabilities of the microbiome .....	4
1.3. interactions of microbiome with host targeted therapeutics.....	6
1.4. Tumor microbiome.....	9
1.5. Bacteria and chemoresistance in cancer .....	13
1.6. Bacteria as a therapeutic tool in cancer.....	16
<b><i>Chapter 2. evolved bacterial resistance to the chemotherapy gemcitabine modulates its efficacy in co-cultured cancer spheroids</i></b> .....	<b><i>19</i></b>

<b>2.1. Summary</b> .....	<b>19</b>
<b>2.2. Introduction</b> .....	<b>20</b>
<b>2.3. Materials and methods</b> .....	<b>24</b>
2.3.1. Bacterial strains and growth conditions.....	24
2.3.2. Barcoded strain library.....	27
2.3.3. Measurement of bacterial gemcitabine dose responses and IC50 .....	28
2.3.4. Pooled genetic screen .....	29
2.3.5. Rapid gemcitabine breakdown assay.....	31
2.3.6. GC-MS measurement of gemcitabine and dFdU .....	32
2.3.7. Spheroid experiments .....	34
2.3.8. Lab evolution experiment.....	36
2.3.9. Whole-genome sequencing and analysis of lab evolution experiment	37
2.3.10. Obtaining spontaneous <i>nupC</i> mutants.....	38
2.3.11. Luria-Delbruck fluctuation experiment.....	39
2.3.12. <i>In vivo</i> evolution experiment in murine model of cancer.....	40
<b>2.4. Results</b> .....	<b>41</b>
2.4.1. The <i>E. coli</i> resistome against gemcitabine.....	41
2.4.2. The impact of bacterial resistance on bacterial drug degradation.....	46
2.4.3. Evolved bacterial resistance against gemcitabine .....	57

2.4.4. inactivation of <i>nupC</i> underlies evolved drug resistance .....	59
2.4.5. mechanisms underlying convergence towards <i>nupC</i> inactivation.....	62
2.4.6. A bacterial evolution experiment against gemcitabine in a mouse model of cancer did not show indications of gemcitabine adaptation .....	67
<b>2.5. Discussion.....</b>	<b>69</b>
<b><i>Chapter 3. Bacterial population dynamics during colonization of solid tumors.....</i></b>	<b>74</b>
<b>3.1. Summary .....</b>	<b>74</b>
<b>3.2. Introduction.....</b>	<b>75</b>
<b>3.3. Materials and methods .....</b>	<b>78</b>
3.3.1. Bacteria and growth conditions .....	78
3.3.2. Construction of the <i>E. coli</i> Nissle 1917 Barcoded library.....	78
3.3.3. Preparation of <i>E. coli</i> Nissle 1917 Barcoded library for injection .....	79
3.3.4. Mouse experiments.....	80
3.3.5. Determination of bacterial CFU in the mouse tumors.....	80
3.3.6. Barcode Sequencing Library Preparation .....	81
3.3.7. Targeted Barcode Sequencing Analysis .....	82
<b>3.4. Results.....</b>	<b>84</b>
3.4.1. Generation of <i>E. coli</i> Nissle 1917 barcoded library.....	84

3.4.2. Exploring the host bottlenecks during tumor colonization .....	85
3.4.3. Exploring bacterial population expansion within the tumors.....	89
<b>3.5. discussion.....</b>	<b>92</b>
<b><i>Chapter 4. discussion.....</i></b>	<b>95</b>
<b>4.1. Intra-species bacterial evolution against anti-cancer drugs .....</b>	<b>95</b>
<b>4.2. Do tumor microbiomes in humans adapt to gemcitabine or other chemotherapies?.....</b>	<b>98</b>
<b>4.3. Understanding bacterial dynamics in the tumors .....</b>	<b>100</b>
<b>4.4. Conclusions .....</b>	<b>104</b>
<b>4.5. Implications of this work in the tumor microbiome field.....</b>	<b>106</b>
<b>5. <i>Appendix: Challenges in expanding gemcitabine lab evolution experiments to in vivo murine model .....</i></b>	<b>109</b>

**LIST OF TABLES:**

Table 2.1 : Bacteria used in this study.....	25
--	----

**LIST OF FIGURES:**

Figure 2.1 Statistics of the gemcitabine genetic screen performed with the <i>E. coli</i> barcoded knockout strain collection.....	45
Figure 2.2. Genetic screen identifies gemcitabine sensitive and resistant loss-of-function mutations in <i>E. coli</i> .....	48
Figure 2.3 Growth of top five resistant gemcitabine knockouts identified by the genetic screen in M9 minimal medium. ....	48
Figure 2.4 Individual growth curves of reporter strain ( <i>cdd</i> knockout) in the functional assay to estimate gemcitabine breakdown rate of the top 88 gemcitabine resistant genetic screen hits.....	52
Figure 2.5 Bacterial gemcitabine resistance can oppositely affect drug degradation and impact neighboring cancer cells .....	55
Figure 2.6: Validation of results of spheroid experiment.....	57
Figure 2.7 Changes in area under the EC50 front in spheroid fitness landscapes generated with co-incubation of gemcitabine and selected resistant knockout strains. ....	57
Figure 2.8 Gemcitabine selection leads to rapid evolved resistance in three <i>E. coli</i> strains .....	60
Figure 2.9 Evolved resistance converges to inactivation of the nucleoside permease <i>NupC</i> .....	61

Figure 2.10 Annotation of <i>nupC</i> mutations by evolutionary conservation .....	64
Figure 2.11 Plots showing the mutation rates in <i>nupC</i> (mutated in gemcitabine resistant mutants) and in <i>nfsA</i> (mutated in furazolidone resistant mutants) loci .	64
Figure 2.12: Adaptive bacterial evolution to gemcitabine was not observed <i>in vivo</i> .....	69
Figure 3.1: Cloning and growth dynamics of <i>E. coli</i> Nissle 1917 barcoded library .....	86
Figure 3.2: Colonization of the tumor by systemic infection reveals a major host bottleneck .....	88
Figure 3.3 : Unequal barcode expansion in the tumor suggests presence of micro-niches in the tumor which are advantageous for bacterial growth.....	90
Figure 3.4: Ranked frequency distribution of barcodes from the <i>i.t.</i> experiment with a slope of -1 indicative of power law .....	91
Figure 5.1: Overview of the preliminary <i>in vivo</i> experiments performed .....	111
Figure 5.2 Results of the <i>in vivo</i> competition experiments summarized in Figure 5.1.c and 5.1.d.....	112

**LIST OF COPYRIGHTED MATERIALS PRODUCED BY THE AUTHOR:**

Chapter 2 of this thesis has been previously published in a peer-reviewed journal and has been re-used here according to copyright regulations.

Serkan Sayin, Brittany Rosener, Carmen G Li, Bao Ho, Olga Ponomarova, Doyle V Ward, Albertha JM Walhout, Amir Mitchell (2023) Evolved bacterial resistance to the chemotherapy gemcitabine modulates its efficacy in co-cultured cancer cells eLife 12:e83140, <https://doi.org/10.7554/eLife.83140>

**LIST OF SYMBOLS, ABBREVIATIONS OR NOMENCLATURE**

AUC: Area under the curve

CDD: cytidine deaminase

CDDL: long isoform of cytidine deaminase

CRC: colorectal carcinoma

dFdC: 2',2'-Difluoro-2'-Deoxycytidine

dFdU: 2',2'-difluorodeoxyuridine

DHFR: Dihydrofolate reductase

*E. coli*: Escherichia coli

EcN: Escherichia coli Nissle 1917

FDR: False discovery rate

*F. nucleatum*: Fusobacterium nucleatum

GO: Gene ontology

HMP: Human Microbiome Project

*H. pylori*: Helicobacter pylori

KEGG: Kyoto Encyclopedia of Genes and Genomes

NIH: National Institutes of Health

PDAC: Pancreatic ductal adenocarcinoma

STAMP: Sequence tag-based analysis of microbial populations

## LIST OF MULTIMEDIA OBJECTS AND FILES

**Supplementary file 1:** Primary and validation screen results.

**Supplementary file 2:** Enriched and depleted pathways in the genetic screen using two databases: KEGG:yellow, GO:green, p-adj<0.1

**Supplementary file 3:** Mutations rates (per kb) for the *nupC* and *nfsA* genes determined by Luria-Delbrück fluctuation experiments.

**Supplementary file 4:** Summary of the mutation detected with the BreSeq tool in evolved strains.

**Supplementary file 5:** List of mutations and their annotations detected in gemcitabine resistant BW25113 colonies

**Supplementary file 6:** Mutations detected with BreSeq tool from the in vivo evolution experiment with *E. coli* Nissle 1917 (EcN). Each column is a single colony. Cohorts are GEM (gemcitabine treated), and VEH (vehicle treated).

**Supplementary file 7:** Mutations detected with Breseq tool. Each colony represent bacteria from the most frequent barcode found in that particular mouse. Wild-type EcN is shown in the last column as EcN\_wt.

**Supplementary file 8:** Mutations detected with BreSeq tool from the in vivo evolution experiment with *E. coli* F-18  $\Delta$ mutT. Each column is a single colony. Cohorts are GEM (gemcitabine treated), and VEH (vehicle treated).

**Supplementary file 9:** Metadata for the samples in Supp. Fig. 8

## **Chapter 1. INTRODUCTION**

### **1.1. HUMAN MICROBIOTA IN HEALTH AND DISEASE**

The human microbiota is the collection of all microbial species that live within our body, majorly consisting of bacteria but also containing members from Archaea, Eukaryota, and viruses as a minor fraction (Christian Milani, Sabrina Duranti, Francesca Bottacini et al., 2017). The microbiome is referred to as the collection of all genetic elements of the microbiota however, these terms could be used interchangeably in the field. Since the beginning of the field, the following have been the biggest questions to answer (Turnbaugh et al., 2007): How many species does the human microbiome consist of? What is the species diversity across the lifetime of an individual, between individuals, and between healthy and diseased subjects? Let's explore the scientific achievements aimed to answer these questions.

Human Genome Project, which revealed the sequence information of the human genome, would not be complete without characterization of the microbiota that lives within our bodies. A collaborative effort initiated by the National Institutes of Health (NIH), across many labs around the world, Human Microbiome Project (HMP) aimed to characterize a core healthy microbiome in 2008 (Huttenhower et al., 2012; Turnbaugh et al., 2007). In the first phase of the HMP, researchers tried to identify a healthy core microbiome at five body sites including the gut, urogenital area, skin, oral and nasal areas using 300 healthy subjects (Huttenhower et al.,

2012). 16S rDNA sequencing and shotgun metagenomic sequencing were commonly used to gather taxonomic information and gene compositions respectively. It produced a great amount of phylogenetic and genomic data, which is open to the public, to help the scientific community to further explore this dataset. No single species was present in all body sites, however, each body site had a distinct species composition that defined that niche across all individuals (Huttenhower et al., 2012). Firmicutes and Bacteroidetes are two dominant phyla constituting 90% of the gut microbiome, and the remaining 10% consist of the phyla Actinobacteria, Proteobacteria, Fusobacteria, and Verrucomicrobia (Arumugam et al., 2011; Huttenhower et al., 2012; Rinninella et al., 2019). These species coexist in a homeostatic state. Changes in species diversity and imbalance referred to as dysbiosis, can cause several pathologies (Oliva et al., 2021). These changes could be due to extrinsic or intrinsic factors such as delivery method at birth, nutrition/diet, antibiotic usage history, smoking and alcohol usage, or host genetics (Bonder et al., 2016; Capurso & Lahner, 2017; A. L. Goodman et al., 2011; McQuade, Daniel, Helmink, & Wargo, 2019; Penders et al., 2006; Pérez-Cobas et al., 2013) Since microbiome is very complex and intertwined with human health, characterizing the human core microbiome was a significant step in biomedicine to understand the microbiome's associations with human disease. Individuals have up to ~500-1000 species in their microbiomes, but the vast total number of bacterial species in the human microbiome across the population is estimated to be ~10,000 by the human microbiome project researchers (Gilbert et

al., 2018; Huttenhower et al., 2012; Turnbaugh et al., 2007). Besides the species diversity, the human microbiota consists of  $3.8 \times 10^8$  individual cells which is almost the same magnitude of cells as the human cells in our body (Sender, Fuchs, & Milo, 2016). The microbiome composition across individuals (beta diversity), was found to be very high across individuals and the major factors contributing to this were host genetics/race, diet, xenobiotics, and early microbial exposure (Huttenhower et al., 2012). The second phase of HMP aimed at characterizing the microbiome of the diseased individuals to understand the differences with respect to healthy subjects. Three cohorts in this phase represent preterm birth, inflammatory bowel disease, and diabetes. The researchers used not only the taxonomic information but multi-omics approaches including temporal sampling from the hosts to understand the function of the microbiome more drastically (Proctor et al., 2019). This multi-dimensional data serves as a valuable resource that is available to researchers to explore many aspects of human conditions, now and in the future (Proctor et al., 2019).

Another challenging question in the microbiome field has been if changes in microbiota composition between healthy and diseased individuals are either the cause or the consequence of the particular disease/human condition. (Carding, Verbeke, Vipond, Corfe, & Owen, 2015). This is an active area of research and there are studies that show examples of both possibilities. We need to keep in mind that microbiota and host interactions are very complex and bidirectional and the knowledge is constantly being updated by new research. There are many

studies that correlate certain bacteria species or compositional changes with human conditions, however, investigations that show the specific causality require more thorough studies including *in vivo* experiments. For example, changes in the species composition of the gut microbiota have been linked to obesity, diabetes, gastrointestinal disorders, depression, and anxiety disorders (Chassard et al., 2012; Cui et al., 2022; Duan et al., 2021; Simpson et al., 2021). Some toxins bacteria secrete have been linked to cancer initiation (Stone & Darlington, 2017). Furthermore, researchers found that members of the gut microbiota might access the bloodstream and translocate to the other parts of the body, due to the disruption of the barrier function and cell-cell junctions in the gut epithelium (Schoultz & Keita, 2020). Some studies have linked these changes in gut epithelial barrier to many human diseases such as irritable bowel syndrome, obesity, diabetes (Genser et al., 2018; Piche et al., 2009; Schoultz & Keita, 2020).

Overall, human health and well-being are closely associated with the microorganisms living within us. Any perturbations of this super organ can have dramatic consequences.

## **1.2. METABOLIC CAPABILITIES OF THE MICROBIOME**

The gut microbiome harbors ~3.3 million microbial genes which is about 150 times more than the total human genes according to metagenomic analyses (Qin et al., 2010). Since the metabolic potential of the gut microbiome is much more complex than a human cell metabolome, these commensal microorganisms

are considered to play a significant role in the digestion and biotransformation of foods, fiber, and xenobiotics (Koppel, Maini Rekdal, & Balskus, 2017; Valdes, Walter, Segal, & Spector, 2018). Even calorie extraction from the same food could vary from individual to individual based on the differences in their microbiome profiles (Boekhorst et al., 2022).

Gut bacteria provide many essential nutrients for the host. For instance, microbiota produce short-chain fatty acids (SCFA) such as butyrate, propionate, and acetate by fermentation (Ramakrishna, 2013). SCFAs have plenty of health benefits including the protection of the intestinal barrier function (Chambers, Preston, Frost, & Morrison, 2018), regulating gluconeogenesis in the gut, and involvement in gut-brain communication (De Vadder et al., 2014). Various members of gut bacteria also synthesize K and B groups of vitamins including thiamine, folate, biotin, riboflavin, and pantothenic acid (Said & Mohammed, 2006).

Germ-free animals served as an integral tool for researchers to understand many aspects of the microbiome on host metabolism. Germ-free mice completely lack the total microbiome and are only viable if proper nutrition is provided. They are raised in special containers and provided with sterile food and water. Indeed, the lack of the microbiome results in many physiological differences compared to the conventionally raised mice (reviewed in detail here, Smith, McCoy, & Macpherson, 2007). Some of those characteristics are as follows: Germ-free mice are smaller in body size, have lower body fat, require vitamin K and B supplementation, have an immature immune system, and have a much larger

cecum and a smaller liver (Smith et al., 2007) These observations show how the host is reliant on the microbiota for metabolism and energy production as well as healthy physiology and developed immune system.

### **1.3. INTERACTIONS OF MICROBIOME WITH HOST TARGETED**

#### **THERAPEUTICS**

Pharmacomicrobiomics is an interdisciplinary field that spans microbiology, pharmacology, and genomics and investigates the interaction of the microbiome with xenobiotics (any external compound present within the organism including drugs). Bacterial enzymes are able to modify host-targeted drugs or their metabolites, affecting treatment efficacy (Spanogiannopoulos, Bess, Carmody, & Turnbaugh, 2016). These mechanisms are classified as direct interactions and they include modifications to the chemical structures such as reduction or hydrolysis reactions (Haiser & Turnbaugh, 2013; Spanogiannopoulos et al., 2016). For instance, irinotecan (CPT11) is a topoisomerase I inhibitor used to treat many types of cancer (Pommier, 2006). After intravenous administration, irinotecan is metabolized by liver enzymes and converted to both the inactive form SN38G and active form SN38 (Haaz, Rivory, Jantet, Ratanasavanh, & Robert, 1997; Iyer et al., 1998; Satoh et al., 1994; Yue, Gao, Wang, & Dou, 2021). Beta-glucuronidase enzymes of gut microbiota can convert SN38G into SN38 increasing the therapeutic and toxic effects of irinotecan as shown by *in vivo* experiments (Haiser & Turnbaugh, 2013; Takasuna et al., 1996). Antibiotic administration with

irinotecan reduces the toxic effects of this chemotherapy by reducing the abundance of such microbial enzymes (Takasuna et al., 1996). Methotrexate is another drug that can be modified by gut bacteria resulting in reduced efficacy (Haiser & Turnbaugh, 2013; Widemann et al., 2000). Methotrexate inhibits dihydrofolate reductase enzyme (DHFR) disrupting nucleotide synthesis and cell division, while reducing nitric oxide production and leading to immunosuppression (Bedoui et al., 2019). However, oral administration of methotrexate was found only effective in half of rheumatoid arthritis patients (Detert et al., 2013; Emery et al., 2008). A clinical study showed that the microbiome composition of a patient could predict if the patient would respond to methotrexate therapy (Artacho et al., 2021). They first found that the microbiome of non-responders was more diverse. During *ex vivo* co-incubation of patient stool samples, measurement of methotrexate levels by LC-MS showed that the microbiota of the responder group metabolizes methotrexate while the microbiota of non-responders did not (Artacho et al., 2021). Conversely, the gut microbiota can also play roles in the activation of prodrugs. For instance, Prontosil and sulfasalazine are two drugs that are processed by bacterial azoreductases to produce active compounds (Gingell, Bridges, & Williams, 1971; Haiser & Turnbaugh, 2013; Peppercorn & Goldman, 1972). All of these examples show significant effects of the host microbiome on the treatment efficacy of host-targeting therapeutics.

In recent years, systematic large-scale genetic screens using a library of drugs and representative species from the human gut microbiome have identified

many bacteria drug pairs that have a metabolic interaction. Intriguingly, these interactions are bidirectional meaning that although many species of bacteria modify drug structure, some bacterial species' growth can also be inhibited by non-antibiotic drugs. Zimmerman et. al used 76 representative bacterial species from the human gut microbiome and performed a chemical screen with them in a combinatorial way using 271 orally administered drugs (Zimmermann, Zimmermann-Kogadeeva, Wegmann, & Goodman, 2019). They incubated the drugs with bacteria and measured the drug levels in the supernatant using LC-MS. They observed that more than 20% of drugs were metabolized by at least one bacterial species. They observed that chemical structures that contained esters or amide groups were hydrolyzed while chemical structures that had azo and nitro groups were reduced. One species, *Bacteroides thetaomicron* metabolized a very high number of drugs (total of 46). A gain of function screen using a library of *E. coli* containing genomic DNA fragments of *B. thetaomicron* revealed the specific gene-drug pairs that play a role in the biotransformation of the specific drug.

Maier et al.'s systematic approach has also shown that these bacteria-drug interactions could be bidirectional, where some of the host-targeted drugs can have antimicrobial activity on certain bacteria species (Maier et al., 2018). In this study, they screened 1197 FDA-approved drugs from the Prestwick Chemical library against 40 representative species of gut microbiota in anaerobic conditions. They used physiologically relevant drug dosing of 20  $\mu$ M in the screen which is thought to be an underestimated drug level that gut bacteria are normally exposed

to. They analyzed growth inhibition by the drugs using bacterial growth curves and found that 24% of drugs inhibited the growth of at least one species. The drug categories of antimetabolites, antipsychotics, and calcium channel blockers were enriched among the hits. This study shows that many of these drugs targeting the host, could have detrimental effects on the gut microbiota because of these anti-microbial features. Thus, a person who chronically uses such drugs may develop resistance against many antibiotics without any antibiotic usage.

Furthermore, research has shown that not only do bacteria-drug interactions occur, but also bioaccumulation of host-targeted drugs by gut bacteria. Klünemann et al. used 25 representative species from the gut microbiota and 15 human drugs and measured the intracellular drug levels in bacterial cells after co-incubation (Klünemann et al., 2021). They found 70 bacteria-drug interactions of which 29 of them were novel. Half of these novel interactions were bioaccumulation events and the rest were biotransformation of the active drug molecule. Duloxetine (selective serotonin reuptake inhibitor used to treat depression) and rosiglitazone (used in the treatment of diabetes) were especially observed to accumulate in a high number of bacterial species.

#### **1.4. TUMOR MICROBIOME**

According to 2018 statistics, 13% of cancers are caused by microorganisms and viruses (de Martel, Georges, Bray, Ferlay, & Clifford, 2020). Human papillomaviruses, *Helicobacter pylori* (*H. pylori*), hepatitis B and C viruses, and

*Fusobacterium nucleatum* are some examples of pathogens that are known to cause carcinogenesis in humans (van Elstrand & Neefjes, 2018). The mechanisms responsible for carcinogenesis include exposure to microbial toxins such as CagA of *H. pylori* and colibactin of bacteria with the polyketide synthesis (pks) island, as well as prolonged chronic inflammation induced by bacteria (Armstrong, Bording-Jorgensen, Dijk, & Wine, 2018; Pleguezuelos-Manzano et al., 2020; Suzuki et al., 2015). The CagA toxin of *H. pylori* activates oncogenic signaling pathways and inhibits the expression of tumor suppressor genes in the host cells (reviewed here: Hatakeyama, 2017). On the other hand, colibactin is a genotoxic compound synthesized by pks+ bacteria. Colibactin has been shown to induce mutations in DNA by directly binding to the DNA and causing double-stranded breaks during DNA damage repair (Nougayrède et al., 2006; Wilson et al., 2019). It causes a specific mutational signature which has been observed in patient tumor samples and has been recapitulated in human intestinal organoids colonized with pks+ bacteria (Dziubańska-Kusibab et al., 2020; Pleguezuelos-Manzano et al., 2020).

Conversely, some bacterial species are associated with anti-tumorigenic effects, including, inhibition of pathogenic species by other members, synthesis of anti-inflammatory short-chain fatty acids, metabolism of nutrients that produce anti-inflammatory molecules and modulation of the immune system to enhance immune surveillance, and improving the efficacy of anticancer treatments (Andreeva, Gabbasova, & Grivennikov, 2020). In addition to the pro and anti-oncogenic properties of some microorganisms, many research groups have

reported bacterial presence within multiple tumor tissues over the years however, a systematic and comprehensive study was missing until recently. In 2020, Nejman *et al.* characterized the tumor microbiome in seven cancer types in a rigorous investigation (Nejman et al., 2020). This study serves as a proof of concept of the tumor microbiome with negative controls and spans the tumors of the bone, brain, breast, lung, pancreas, ovary, and skin (melanoma). They used qPCR to detect bacterial 16S rDNA in tumor samples along with lipopolysaccharide/lipoteichoic acid staining and 16S rRNA fluorescence in situ hybridization. According to Nejman et al.'s findings, breast tumors had the highest proportion of bacterial presence, bacterial load, and diversity while melanomas ranked lowest in these categories.

Although the tumor microbiome field is currently very critical about the results of some major studies, the consensus is that there is a microbial presence in at least some of the tumors in some patients. So, where does the tumor bacteria originate from? Most of the infections actually originate from the patient's own microbiome (Cummins & Tangney, 2013; Rolston, 2017). In addition, cancer patients are one of the most vulnerable groups to infections due to the following risk factors: presence of neutropenia (low neutrophil count), disruption of the epithelial barrier function, and obstruction by the tumor and medical procedures (Rolston, 2017). Translocation of microorganisms from commensal sites into the tumor environment has been shown in many cancer types. For instance, both clinical and pre-clinical models indicate that retrograde bacterial colonization is

responsible for the bacterial presence in pancreatic cancer, and the PDAC microbiome mostly consists of gamma-proteobacteria in most patients (Geller et al., 2017; Pushalkar et al., 2018). In colorectal cancer, *Fusobacterium nucleatum* (*F. nucleatum*) has been shown to increase in tumors compared to adjacent tissues (Castellarin et al., 2012), however, some studies have only found *F. nucleatum* only in some tumors and the increase was not statistically significant when compared to adjacent healthy tissue (Errington et al., 2021).

There are certain aspects of tumors that make them a suitable environment for the bacteria. Disrupted vasculature causes microorganisms to spread into tumors easily, while expression of immunosuppressive receptors (such as CTLA-4) reduces immune activity. Additionally, hypoxic areas are advantageous for anaerobic bacteria, and areas where cancer cells die (necrosis) contain many nutrients bacteria can use to grow (Cummins & Tangney, 2013; Ma, Zhu, & Liu, 2021; Walker, Tangney, & Claesson, 2020)

Overall, bacteria can be causative and opportunistic colonizers in cancer. Many features of the tumors make this environment suitable for bacterial colonization. Although much evidence exists about the bacterial presence within solid tumors, we still need to be very critical about interpreting the results of these studies since much contradicting evidence weakens the findings of the major papers in this field.

## 1.5. BACTERIA AND CHEMORESISTANCE IN CANCER

The American Cancer Society defines chemotherapy as the use of cytotoxic medicines to kill cancer cells. Historically, the first chemotherapy was discovered by Louis Goodman and Alfred Gilman, by using nitrogen mustard, a chemical weapon used in world war I, to treat xenografted lymphoid tumors in mice (Chabner & Roberts Jr, 2005; Papac, 2001). These compounds are alkylating agents which can make covalent bonds with nucleic acids, halting DNA replication. Gustav Lindskog used this chemical on a human non-Hodgkin's lymphoma patient for the first time (Chabner & Roberts Jr, 2005; Gilman, 1963). This treatment regressed the tumor masses at first, but then the tumors continued growing again (Chabner & Roberts Jr, 2005). This phenomenon is known as chemoresistance, the ability of the cancer cells to find a way to circumvent the cytotoxic effects of the chemotherapy and continue the cell division.

Other types of chemotherapy agents include antimetabolites, anti-microtubule agents, topoisomerase inhibitors, and cytotoxic antibiotics. Chemotherapy is considered a non-targeted therapy since it acts on all dividing cells (including healthy cells). Targeted therapies work to kill cancer cells through the molecules with cancer specific targets. I won't go into details of targeted therapies but I will refer to combination chemotherapies and targeted therapies as anti-cancer drugs. Cancer cells can develop resistance to these agents through multiple mechanisms. There are six main types of resistance mechanisms achieved by cancer cells: modification of the drug target, increased expression of

drug efflux pumps, upregulation of detoxification mechanisms, decreased cell death rate, enhanced DNA repair rate, and change in the cell proliferation rate (Cree & Charlton, 2017).

Bacteria were thought to contribute to chemoresistance through their interactions with anti-cancer drugs as well since they are present in many cancerous tumors (Nejman et al., 2020a). Lehouritis et al., have used *E. coli* and *Salmonella* to test if co-incubation of multiple chemotherapy drugs with bacteria changes their efficacy and potentially contributes to chemoresistance (Lehouritis et al., 2015). Intriguingly, they observed stability, enhancement, or reduction in drug efficacy for the cancer cells after co-incubation of the drug with bacteria. Furthermore, they used mass spectrometry to identify if bacteria were transforming the drugs into different forms. They found out that the drugs Claribine and Fludarabine were hydrolyzed and that CB1954 was reduced by the bacteria. They also discovered the potential acetylation of gemcitabine by the bacteria. Their *in vivo* mouse experiment utilizing subcutaneous tumors, bacteria, and gemcitabine showed that tumors colonized with bacteria had reduced gemcitabine efficacy compared to tumors without bacteria. More research on this topic has led to the discovery of a native chemoresistance mechanism against gemcitabine mediated by *Mycoplasma hyorhina* and other tumor bacteria (Geller & Straussman, 2018; Liekens, Bronckaers, & Balzarini, 2009; Voorde et al., 2014). Mycoplasma-infected cancer cell lines had reduced efficacy of gemcitabine compared to mycoplasma-free cell lines. In addition, treatment of mycoplasma-infected cancer cells either

with the antibiotic tetracycline or the cytidine deaminase inhibitor, tetrahydro-uridine, restored gemcitabine efficacy (Voorde et al., 2014). Voorde et al. have observed reduced levels of active phosphorylated gemcitabine metabolites in the cells infected with *M. hyorhinis* and suggested that gemcitabine could be converted into the less active form of 2',2'-difluorodeoxyuridine (dFdU) (Vande Voorde, Vervaeke, Liekens, & Balzarini, 2015). Others confirmed that gemcitabine can be converted into dFdU, and found that only a long form of cytidine deaminase can perform this reaction (Geller et al., 2017). Phylogenetic analysis showed that a significant amount of bacteria in the Gammaproteobacteria class are found to possess this long form of cytidine deaminase (Geller & Straussman, 2018). 16S rDNA sequencing of PDAC patients, in which gemcitabine is used as a frequent treatment option, showed that the majority of the patient tumors were actually infected with Gammaproteobacteria which are thought to migrate from the duodenum (Geller & Straussman, 2018).

Additionally, there are more mechanisms of chemoresistance through bacterial interactions with the host cells. Although widespread enrichment of *Fusobacterium nucleatum* in CRC tumors is under debate, there is an increased presence of *Fusobacterium* in cancer tissue compared to healthy tissue in some patients (Castellarin et al., 2012; Repass et al., 2018) In CRC, *Fusobacterium nucleatum* was shown to cause chemoresistance (Yu et al., 2017). According to Yu et al.'s findings, *Fusobacterium nucleatum* activates toll like receptor 4 to induce activation of the autophagy pathway in the cancer cells through regulation

of two miRNAs. Furthermore, *in vivo* data supported this for the chemotherapeutics 5-FU and oxaliplatin as well. Activation of autophagy results in reduced apoptosis in the presence of the chemotherapy. Analysis of the patient tumors which were derived from the subjects with relapsed disease has also supported these findings (Yu et al., 2017).

## **1.6. BACTERIA AS A THERAPEUTIC TOOL IN CANCER**

The ability of certain bacteria to specifically colonize tumors makes it possible to exploit them as a shuttle to deliver anti-cancer molecules, peptides, or toxins specifically into the tumor microenvironment (Forbes, 2010). Many preclinical and a handful of clinical studies have been pursuing this treatment option (Gupta, Nowicki, Giurini, Marzo, & Zloza, 2021). A single FDA approved bacteria based anti-cancer therapy utilizing *Mycobacterium bovis* is already in use in the treatment of bladder cancer in the US, while it is used as a preventative vaccination against Tuberculosis in other countries (Morales, Eidinger, & Bruce, 1976; Sieow, Wun, Yong, Hwang, & Chang, 2021),.

Synthetic genetic modifications are usually made to enhance anti-tumor activities of bacteria and make them safer for *in vivo* use (Forbes, 2010). The various strategies of improvements/modifications are; engineering the immunomodulatory activity, expression and delivery of cytotoxic proteins/peptides, expression of enzymes for the conversion of prodrugs into active compounds, expressing factors that modify angiogenesis in tumor tissue, siRNA delivery to

control cancer cell gene expression, and increasing tumor specificity of bacteria (Sieow et al., 2021).

Gram-negative probiotic bacterial strains such as *Escherichia coli* Nissle 1917 and attenuated strains of pathogenic bacteria such as *Salmonella*, *Clostridium* and *Leisteria* species are commonly used in the development of anti-cancer therapies. For instance, the type-III secretion system of *Salmonellae* is used to transfer certain virulence factors into the host cell cytosol (Haraga, Ohlson, & Miller, 2008), a feature that makes these bacteria a great tool for delivering cytotoxic agents into the tumors. The SipA protein of *S. typhimurium* was linked to reduced P-glycoprotein (P-gp) in cancer cells which are involved in the multidrug resistance (Siccardi, Mummy, Wall, Bien, & McCormick, 2008). In a preclinical study, Mercado-Lubo et al. used gold nanoparticles attached to SipA to downregulate P-gp on cancer cells thereby overcoming the multidrug resistance phenotype (Mercado-Lubo et al., 2016). This paves the way for using these nanoparticles in combination with other anti-cancer drugs to increase the efficacy of the treatment for the patients.

Furthermore, researchers used bacteria and cancer spheroids to perform a high throughput screening of bacteria-based anti-cancer therapies using synthetic gene circuits (Harimoto et al., 2019). This model allows rapid discovery of promising therapies before testing them in animal models which are lower throughput, expensive, and time-consuming. In their spheroid model, they encapsulated attenuated *S. typhimurium* inside the spheroids, controlling

excessive growth of the bacteria outside of the spheroid with gentamicin, a non-penetrative antibiotic. They screened ten bacterial toxins and anti-cancer peptides using their synthetic gene circuit and bacteria-spheroid model to find that azurin, thetatoxin, and hemolysin E were the most effective ones for the cancer spheroid growth inhibition (Harimoto et al., 2019). Furthermore, they validated some of their results in a mouse model and observed a high correlation with the *in vitro* findings.

Besides the preclinical research, some bacteria-based treatments have been tested in human clinical trials either on their own or in combination with other therapies (Gupta et al., 2021; Sieow et al., 2021). *Listeria monocytogenes*-based therapy combined with chemoradiation has made it to phase III clinical trial to treat high-risk and advanced cervical cancer (clinicaltrials.gov ID: NCT02853604). Many other clinical trials in phase I and II include the use of *Salmonella* and *Bifidobacterium* species, some of which are in the form of a vaccination (Sieow et al., 2021, clinicaltrials.gov IDs: NCT03762291, NCT01562626). With our current knowledge, there are no clinical trials yet exploiting probiotic strains, such as *E. coli* Nissle 1917, in cancer treatment. In the near future, we anticipate that more bacteria-based cancer therapies will be available for cancer patients if safety concerns are overcome.

## Chapter 2. EVOLVED BACTERIAL RESISTANCE TO THE CHEMOTHERAPY GEMCITABINE MODULATES ITS EFFICACY IN CO-CULTURED CANCER SPHEROIDS

### 2.1. SUMMARY

Drug metabolism by the microbiome can influence anti-cancer treatment success. We previously suggested that chemotherapies with antimicrobial activity can select for adaptations in bacterial drug metabolism that can inadvertently influence the host's chemoresistance. We demonstrated that evolved resistance against fluoropyrimidine chemotherapy lowered its efficacy in worms feeding on drug-evolved bacteria (Rosener et al., 2020). In this chapter, we examine a model system that captures local interactions that can occur in the tumor microenvironment. Gammaproteobacteria colonizing pancreatic tumors can degrade the nucleoside-analog chemotherapy gemcitabine and, in doing so, can increase the tumor's chemoresistance. Using a genetic screen in *Escherichia coli*, we mapped all loss-of-function mutations conferring gemcitabine resistance. Surprisingly, we infer that one-third of top resistance mutations increase or decrease bacterial drug breakdown and therefore can either lower or raise the gemcitabine load in the local environment. Experiments in three *E. coli* strains revealed that evolved adaptation converged to inactivation of the nucleoside permease *NupC*, an adaptation that increased the drug burden on co-cultured cancer cells. The two studies provide complementary insights on the potential

impact of microbiome adaptation to chemotherapy by showing that bacteria-drug interactions can have local and systemic influence on drug activity.

## **2.2. INTRODUCTION**

Clinical research on the influence of intratumor bacterial infection can be dated back to more than 150 years ago (Sepich-Poore et al., 2021). However, in the past decade, research of the tumor-microbiome gained significant momentum with the maturation of DNA sequencing technologies and advancement of microbiome research. Multiple recent studies of bacterial colonization in human tumors outlined the magnitude of this phenomenon (reviewed here, Cullin, Azevedo Antunes, Straussman, Stein-Thoeringer, & Elinav, 2021; B. Goodman & Gardner, 2018; Sepich-Poore et al., 2021). Collectively, these works establish that the proportion of infected tumors greatly varies across tumor types and that many tumors harbor microbiomes with a distinctive and characteristic composition of bacterial species. In some cases, as in breast and pancreatic cancer, more than 60% of tumors harbored a tumor-microbiome (Nejman et al., 2020a). The microbiome, in turn, is known to influence cancer disease through multiple independent mechanisms, including promotion of neoplastic processes in healthy host cells, modulation of the host anti-tumor immune response, and by bacterial biotransformation of anticancer drugs (Alexander et al., 2017; Cullin et al., 2021; Riquelme et al., 2019; Roy & Trinchieri, 2017).

Bacterial metabolism of xenobiotics, including breakdown of host-targeted drugs, is prevalent (Spanogiannopoulos et al., 2016). Estimates from recent drug screens show that two thirds of human-targeted drugs can be metabolized by at least one bacterial species that is present in the human gut microbiome (Zimmermann et al., 2019). Yet, these interactions are reciprocal, bacteria both metabolize the host-targeting drugs and are also frequently impacted by them (Zimmermann, Patil, Typas, & Maier, 2021). Roughly 25% of host-targeted drugs are potent inhibitors of bacterial growth at physiological concentrations (Maier et al., 2018). This proportion is doubled for antineoplastic drugs and almost all anticancer drugs that belong to the antimetabolite drug class have potent antimicrobial activity (Maier et al., 2018). A key underexplored question that arises from these reciprocal drug-microbiome interactions is how they impact one another given the ability of microorganisms to evolve and change over short time scales within the host (Garud, Good, Hallatschek, & Pollard, 2019; Gatt & Margalit, 2021; Lieberman, 2022; Snitkin et al., 2013; S. Zhao et al., 2019). Specifically, given that bacteria rapidly evolve resistance to antimicrobial drugs, it is plausible that adaptation to host-targeting drugs that are also antimicrobial will alter bacterial drug metabolism or its transport (Kyono et al., 2022; Rosener et al., 2020). Such adaptations have been repeatedly observed with standard antibiotics (Alekshun & Levy, 2007). In such cases, evolved resistance in tumor-colonizing bacteria may increase or decrease drug availability to the tumor cells which, in turn, may interfere with the efficacy of the chemotherapy.

The tumor-microbiome in pancreatic cancer has attracted much attention recently due to the prevalence of infections in PDAC (Aykut et al., 2019; Geller & Straussman, 2018; McAllister, Khan, Helmink, & Wargo, 2019; Nejman et al., 2020b; Pushalkar et al., 2018; Riquelme et al., 2019). Studies have uncovered multiple independent mechanisms through which microbes influence oncogenesis (Aykut et al., 2019; Pushalkar et al., 2018), disease progression (Riquelme et al., 2019), and treatment success (Geller & Straussman, 2018) in the pancreas. Bacterial infection is attributed to retrograde bacterial migration from the gastrointestinal tract into the pancreas (McAllister et al., 2019; Pushalkar et al., 2018). Characterization of the PDAC tumor-microbiome by 16S rRNA gene sequencing showed that proteobacteria are highly enriched relative to the gut microbiome and that they are highly prevalent in pancreatic tumors (Geller et al., 2017; Nejman et al., 2020b; Pushalkar et al., 2018). Recent work suggested that pancreatic colonization can impede therapy with gemcitabine (dFdC), a front-line chemotherapy drug that is used for PDAC treatment (Geller et al., 2017). Further clinical data provided circumstantial evidence indicating that this interaction may indeed take place in treated patients (Meriggi & Zaniboni, 2021; Mohindroo et al., 2021). Gemcitabine drug metabolism is well-understood in the model gamma-proteobacteria *E. coli* (Geller & Straussman, 2018) (Figure 2.2A).

The antimetabolite gemcitabine, a nucleoside analog, is imported into the bacterial cell through the nucleoside transporter *NupC* and is then phosphorylated. Gemcitabine triphosphate may be incorporated into a newly synthesized DNA

strand and then may interfere with chain elongation by masked chain termination (similar to mammalian cells (De Sousa Cavalcante & Monteiro, 2014)). Therefore, despite its clinical use as an anticancer drug, gemcitabine's mechanism of action potentially makes it a broadly toxic, antimicrobial compound. Previous works showed that some bacterial species can rapidly convert gemcitabine into the less toxic metabolite dFdU (Geller et al., 2017; Voorde et al., 2014). In gamma-proteobacteria, gemcitabine degradation proceeds through a specific isoform of the cytidine deaminase enzyme (CddL)(Geller et al., 2017). The well-characterized interactions between tumor cells, gemcitabine and gamma-proteobacteria put forth a good model system for testing how bacterial adaptation can impact drug metabolism and potentially influence the tumor's chemoresistance.

Through a pooled genetic screen, we systematically mapped all loss-of-function mutations that increase *E. coli*'s resistance to gemcitabine and found that inactivation of over than forty genes increased bacterial resistance by more than 16-fold. This observation led us to conclude that resistance can rapidly emerge under natural selection through gene inactivation within a single evolutionary step. Using a functional assay, we found that one third of top resistance mutations impacted extracellular drug concentrations (gemcitabine activity). Co-culturing bacteria harboring these loss-of-function mutations with cancer cells confirmed that these adaptive mutations have the potential to alter chemoresistance of neighboring tumor cells. Finally, through in-vitro evolution we studied which adaptations emerge under drug selection in three *E. coli* strains. We found that

inactivation of the drug transporter *NupC* arises in all evolved strains. This inactivation leads to decreased bacterial drug import and therefore reduces the rate of gemcitabine breakdown. Reduced bacterial breakdown, in turn, increases gemcitabine availability for neighboring tumor cells. Our work reveals that bacterial adaptation to the frontline chemotherapy drug gemcitabine can take place rapidly in-vitro. If similar adaptation takes place in gemcitabine treated patients, it may ultimately increase the chemosensitivity of the hosting tumor. Our in-vitro work suggests that monitoring bacterial adaptation to chemotherapy may be required to decide if chemotherapy should be augmented with antibiotic treatments. Such decisions are nontrivial given that administration of antibiotics can be detrimental to cancer patients (Corty et al., 2020; Elkrief et al., 2019; Gao et al., 2020; Meriggi & Zaniboni, 2021).

## **2.3. MATERIALS AND METHODS**

### **2.3.1. Bacterial strains and growth conditions**

Bacterial strains used in this study are shown in Table 2.1. We used the *E. coli* barcoded knockout strain collection for the pooled genetic screen (similarly to (Noto Guillen, Rosener, Sayin, & Mitchell, 2021; Rosener et al., 2020)). All experiments measuring gemcitabine breakdown were performed with strains from the KEIO strain collection (Baba et al., 2006). For spheroid experiments, double knockout strains were generated with P1 transduction method (Thomason, 2007) using *pyrD* knockout strain from the barcoded library and the desired gene

knockout from the KEIO collection. The *pyrD* knockout background was used since it is a pyrimidine auxotroph that cannot grow in the media used to culture the spheroids.

For all experiments, bacteria were inoculated into Lysogeny Broth (LB) and grown overnight at 37°C, 200 rpm orbital shaking. Knockout strains were grown in LB media supplemented with 50 µg/mL kanamycin (KEIO strain collection) or 25 µg/mL chloramphenicol (barcoded strain collection). All growth and serial evolution experiments were performed in M9 minimal media supplemented with 0.2% ampicase and 0.4% glucose. Experiments designed to monitor gemcitabine breakdown were performed in PBS (functional assay) or in 0.9% saline (GC-MS).

**Table 2.1 : Bacteria used in this study**

<b>Strain/Resource</b>	<b>Source</b>	<b>Remarks</b>
<i>E. coli</i> BW25113	Walhout Lab, University of Massachusetts Chan Medical School, MA, USA	
<i>E. coli</i> Nissle 1917	ArdeyPharm GmbH, (Pharma Zentrale GmbH), Germany	

<i>E. coli</i> F-18	McCormick Lab, University of Massachusetts Chan Medical School, MA, USA	
<i>E. coli</i> MG1655	Brewster Lab, University of Massachusetts Chan Medical School, MA, USA	
KEIO knockout collection	Dharmacon (GE life sciences)	Parent Strain: BW25113
Barcoded knockout collection	Hirota Mori, Nara Institute of Science and Technology, Japan	Parent Strain: BW38028
BW25113 $\Delta$ <i>pyrD</i> :: <i>tGFP- chl'</i> -barcode $\Delta$ <i>cytR</i> :: <i>kan'</i>	Barcoded library, KEIO Collection	Double knockout was generated by P1 transduction

BW25113 $\Delta$ <i>pyrD</i> ::tGFP- <i>chl</i> <sup>f</sup> -barcode $\Delta$ <i>cdd</i> ::kan <sup>r</sup>	Barcoded library, KEIO Collection	Double knockout was generated by P1 transduction
BW25113 $\Delta$ <i>pyrD</i> ::tGFP- <i>chl</i> <sup>f</sup> -barcode $\Delta$ <i>nupC</i> ::kan <sup>r</sup>	Barcoded library, KEIO Collection	Double knockout was generated by P1 transduction

### 2.3.2. Barcoded strain library

The *E. coli* barcoded deletion library was used in our previous studies (Noto Guillen et al., 2021; Rosener et al., 2020). The parent strain of this library is BW38028 with the genotype  $\Delta$ (*araD-araB*)567 *lacZ*<sub>p-4105(UV5)</sub>-*lacY* *hsdR*514, *rph*<sup>+</sup> (Conway et al., 2014). The library includes two sets of 3,680 knockout strains (each set with different barcodes: odd and even libraries). After overnight growth in nutrient-poor synthetic media (M9) we identified 3,512 barcodes in one set and 3,226 barcodes in the other set (3,145 knockout strains were detected in both collections). In each strain, the open reading frame of a single gene was replaced in-frame with a fragment containing turbo GFP, chloramphenicol resistance cassette, and a unique 20 bp sequence that serves as an identification barcode. Since the barcode is the only variable region across strains, it can be amplified from a mixed culture of strains with a single pair of primers. We used primers that amplify a 325 bp region.

### **2.3.3. Measurement of bacterial gemcitabine dose responses and IC50**

On the day of the experiment, a 384-well plate containing serially diluted gemcitabine in M9 was prepared at 2x concentration in a volume of 35  $\mu$ L. For the day-to-day IC50 measurements (Figure 2.8B) a sample from daily evolving populations was directly diluted 1:200 into the microtiter plate with gemcitabine. For measurement of gemcitabine resistance of evolved populations (Figure 2.8C), a sample from frozen last-day glycerol stocks of evolution experiment was inoculated into 3 mL LB for overnight culture. Overnight cultures were diluted to OD (600 nm) of 1 in M9 and were added to the 384-well plate (1:200 final dilution). For single-colony gemcitabine IC50 experiments (Figure 2.2B and Figure 2.8D), single colonies were grown overnight in 3 mL LB, and the same dilution protocol was followed as evolved populations. The prepared microplates (with bacteria and gemcitabine dilutions) were incubated at 37°C and 360 rpm double orbital shaking in an automated plate reader (BioTek Eon) and absorbance (600 nm) was monitored every 10 minutes for 18 hours. All measurements were performed in technical triplicates. Each evolved population is considered as a separate biological replicate (three biological replicates per evolution condition. One biological replicate is shown on the figure for control evolved population.) A MATLAB script was used to fit the dose-response curves and infer the IC50 values. Individual growth curves were assessed for quality control and to determine the exclusion criteria for analysis.

#### 2.3.4. Pooled genetic screen

We thawed a frozen glycerol stock of the pooled barcoded strain collection and inoculated 15  $\mu$ L of the stock into 25 mL of M9 supplemented with chloramphenicol for overnight growth at 37°C and 200 rpm shaking. In the morning, the culture was diluted to OD<sub>600</sub> of 1, and then diluted 1:400 into 7 ml of M9 with or without 140  $\mu$ M gemcitabine. We prepared triplicates for each of the two conditions (quadruplicates in validation screens). The tubes were incubated at 37°C shaker and OD was monitored periodically. Once the culture crossed OD (600 nm) 0.6, we collected the cells and extracted genomic DNA with a commercial kit (Zymo Quick DNA miniprep Plus Kit, Cat#D4068). Library preparation was identical to the protocol we previously developed (Rosener et al., 2020). Briefly, genomic DNA isolated from endpoint of the genetic screen was quantified using Qubit dsDNA high sensitivity kit (Thermo-fisher, Cat#Q32854). We used 6.25 ng DNA to prepare the DNA library. First, barcoded region was amplified using the following primers and 2x KAPA HiFi Hotstart ReadyMix (Kapa Biosystems, Cat#KK2602) which yielded ~350 bp product. PCR products were purified using AMPure XP beads (Beckman Coulter, Cat#A63881). Nextera XT Index Kit protocol (Illumina, Cat#FC-131– 1024) was used to add indices and Illumina sequencing adapters to each PCR sample. Next, products were purified using AMPure XP bead (Beckman Coulter, Cat#A63881) purification protocol. The libraries were then run on a 3% agarose gel and the product was extracted using NEB Monarch DNA Gel Extraction Kit (NEB, Cat# T1020L). Next, we used Agilent High Sensitivity

DNA Kit (Agilent Technologies, Cat# 5067–4626) to evaluate the quality and average size of the libraries. Using Qubit dsDNA high sensitivity kit, we measured the concentration and calculated the molarity of each library. Libraries were normalized to 4 nM, denatured, and diluted according to Illumina MiniSeq / NextSeq System Denature and Dilute Libraries Guide. After pooling, sequencing was performed using MiniSeq High Output Reagent Kit, 75-cycles (Illumina, Cat# FC-420–1001) or NextSeq 500/550 High output Reagent Kit v 2.5, 75-cycles (Illumina, Cat# 20024906). Raw reads were converted to barcode counts using a Matlab script which compared a database of all barcodes to the reads (Rosener et al., 2020).

We identified the enriched or depleted hits by comparing the relative frequency of individual barcodes when the pooled library grew in the presence or absence of gemcitabine. For this analysis, we used the barcode counts and we identified barcodes with significant changes in their relative frequency with DEBRA (Akimov, Bulanova, Timonen, Wennerberg, & Aittokallio, 2020). We discarded barcodes with less than 10 counts. We used “Wald statistical test” and a cutoff value of 16-fold for enrichment and false discovery rate adjusted  $p$ -value of 0.05. Next, we performed gene set enrichment analysis with GAGE (Luo, Friedman, Shedden, Hankenson, & Woolf, 2009) using KEGG (Kanehisa, Sato, Kawashima, Furumichi, & Tanabe, 2016) and GO (The Gene Ontology Consortium, 2000) databases at a false-discovery-rate adjusted  $p$ -value of 0.1. We used published data on the KEIO strain collection (Supplementary File 3 on Baba et al., 2006) to

classify slow-growing knockouts. Specifically, we used the optical density measurements made after 24 hours of growth of the strain collection on minimal defined media (MOPS) and defined a cutoff value of 0.11 to discriminate normal and slow growth. We chose this cutoff value by the bimodal distribution of the density measurements in the dataset (this value separated the data into two unimodal histograms with 124 slow-growing strains and 4,178 strains with normal growth).

### **2.3.5. Rapid gemcitabine breakdown assay**

We picked from the KEIO strain collection the top 88 gemcitabine resistant knockouts that were identified in the genetic screen. Knockout strains that were not found in the KEIO collection were picked from the barcoded knockout collection. The strains were grown in LB media with appropriate antibiotic at 37°C and 200 rpm shaking. We included six overnight cultures of the wild-type strain (BW25113) as controls. The next day, all strains were diluted to OD (600 nm) of 0.5 into 1 mL PBS with gemcitabine (200  $\mu$ M) in a 96-deep well plate. The plate was incubated in a shaker at 37°C, 900 rpm orbital shaking. 250  $\mu$ L of the supernatant was sampled after 15 and 45 minutes and filtered by spinning down at 5000G using a 96-well plate 0.22  $\mu$ m filters (PALL Corporation, Cat#8119). We repeated this procedure for obtaining conditioned buffer three times on different days as independent biological replicates.

After we obtained the conditioned buffers, we evaluated the amount of residual gemcitabine left by monitoring the growth of a gemcitabine sensitive

reporter strain (*cdd* knockout). The *cdd* knockout was grown overnight in 3 mL M9 media at 37°C, 200 rpm shaking. The next day, the culture was first diluted to OD (600 nm) 1 and then further diluted 1:500 into M9 media. We aliquoted 150 µL of this culture into a 96-well plate and added 50 µL of conditioned buffer to each well. The plate was incubated at 37°C and 360 rpm double orbital shaking in an automated plate reader (BioTek Eon/TECAN). Absorbance (600 nm) was monitored every 10 minutes for 7 hours. We used the growth measurements from media supplemented with buffer after 15 minutes of incubation to identify fast degraders and growth measurements from media supplemented with buffer after 45 minutes of incubation to identify slow degraders. We used a statistical test to identify fast and slow degraders. For this test, we calculated the area under the growth curve (AUC) after blank subtraction for each replicate and used a one-tailed t-test to test if the conditioned buffer from a knockout strain (three biological replicates) reduced or increased the AUC of the reporter strain compared to the buffer prepared with the wild-type strain (eighteen replicates). We used an FDR adjusted *p-value* of 0.1 as a cutoff for statistical significance.

#### **2.3.6. GC-MS measurement of gemcitabine and dFdU**

We picked the knockout strains directly from the frozen glycerol stock of the barcoded knockout collection and grew them overnight in 3 mL M9 media at 37°C, 200 rpm shaking. The next day, cultures were washed in saline (distilled water with 0.9% NaCl) and cultures were diluted to an OD (600 nm) of 0.125 in 1,350 µL of saline in a 96-deep well plate. Gemcitabine was added to each well to reach a final

concentration of 80  $\mu\text{M}$  and cultures were incubated in a microplate shaker at 900 rpm and 37°C. We sampled 450  $\mu\text{L}$  from the cultures at predetermined time points and filtered the samples using 0.22  $\mu\text{m}$  filters by centrifugation at 5000G for 5 minutes. We froze the conditioned supernatants at -20°C until the GC-MS measurements were performed. This experiment was performed as three biological replicates (independent three overnight cultures and independent co-incubations).

For GC-MS measurements, first 200  $\mu\text{L}$  of bacterial culture supernatants (or standard solution) were dried under vacuum. Dried samples were derivatized by adding 20  $\mu\text{L}$  of pyridine and 50  $\mu\text{L}$  of *N*-methyl-*N*-(trimethylsilyl) trifluoroacetamide (Sigma-Aldrich, Cat#M-132) followed by incubation for 3 hours at 37 °C. The derivatization reaction was allowed to complete for 5 hours at room temperature. Measurements were performed on an Agilent 7890B single quadrupole mass spectrometer coupled to an Agilent 5977B gas chromatograph with an HP-5MS Ultra Inert capillary column (30 m  $\times$  0.25 mm  $\times$  0.25  $\mu\text{m}$ ). Helium was used as carrier gas at flow rate of 1 ml/min (constant flow). The temperatures were set as follows: inlet at 230 °C, the transfer line at 280 °C, the MS source at 230 °C and quadrupole at 150 °C. 1  $\mu\text{L}$  of sample was injected in a splitless mode. Initial oven temperature was set to 80 °C, held for one minute and then increased to 270 °C at a rate of 20 °C/min, then further increased to 285 at a rate of 5 °C/min. MS parameters were: 3 scans/sec with 30-500 *m/z* range, electron impact ionization energy 70 eV. Analytes were identified based on retention time, one quantifier and

two qualifier ions that were manually selected using a reference compound. Gemcitabine was quantified as m/z 241 ion eluted at 13.14 min, 2',2'-difluorodeoxyuridine was quantified as m/z 242 ion eluted at 11.42 min and Peak integration and quantification of peak areas were done using MassHunter software (RRID: SCR\_015040).

### **2.3.7. Spheroid experiments**

We plated CT-26 mouse colon carcinoma cell-line (RRID:CVCL\_7256) on 96-well low attachment plates (Costar, Cat#7007) as 4000 cells/well to form spheroids. Cells were incubated in RPMI 1640 media (Gibco, Cat#11875-093) with 2mM L-Glutamine, 5% Fetal Bovine Serum (Gibco, Cat#26140-079) and 25 mM HEPES Buffer (Corning, Cat#25-060-CI). The plates were centrifuged at 3000G for 5 minutes and kept at in a tissue culture incubator with 37°C with 5% CO<sub>2</sub>. After four days of spheroid growth, we serially diluted bacterial cultures into the spheroid microplate and incubated the co-culture for four hours with gemcitabine (1.6-fold serially diluted across the columns). Note that all the tested bacterial mutants in this experiment were on *pyrD* knockout background (a pyrimidine auxotroph) to avoid bacterial proliferation in cell culture media that does not contain any nucleotides. Next, the plate was washed with cell culture media with 50 µg/ml gentamicin three times. To achieve this, we used 96 channel handheld electronic pipette (Integra, Viaflo 96), and made use of gravity force. 100 µL media was aspirated capturing the spheroid from the bottom of the wells. After the spheroids sank to the bottom of the tips, the tips were touched to the surface of a fresh plate

containing culture media with 50 µg/mL gentamicin, leaving the spheroids in the new plate. We chose a four-hour time interval to address two opposing requirements of the co-culture system – mitigate overgrowth of the bacterial cultures (which hinders spheroid growth irrespective of the drug) while still allowing enough incubation time to allow for drug degradation. While removal of bacteria after 4 hours may limit the bacterial impact, such a limitation will only result in underestimation the bacterial impact (but will have no impact on how we evaluate how strains compare to one-another).

After three washes, the 96-well plate was transferred to an S3 imaging platform (Incucyte, Sartorius) which is housed inside a tissue culture incubator. The plate was imaged every six hours to track spheroid growth and validate that there was no residual contamination of resistant bacteria (evident by bacterial overgrowth). After seven days of growth, spheroids were washed once using cell culture media with 50 µg/mL gentamicin to get rid of any dead cell and cellular debris and a final microscopy image was captured. We calculated the area of individual spheroids using the Incucyte software (Segmentation sensitivity:40, Minimum Area Filter: 2000 µm<sup>2</sup>). A matlab script was used to make the fitness landscapes by fitting polynomial equations. The following are the steps followed:

1. Normalization by timepoint zero: we divided the last day spheroid area to day zero spheroid area (4 days post cell seeding).
2. Normalization by plate: we subtracted the minimum spheroid area from all spheroid areas and divided that value by second largest spheroid area in the plate minus minimum spheroid area

3. Fitting 3D surface and calculating EC50 lines: we fitted a mesh surface using normalized spheroid areas (2D) using a four-degree polynomial function ('poly44'). Lastly, we marked the EC50 line by calculating the coordinates of the 3D mesh surface where the values corresponded to a mid-response (value of 0.5). This experiment was performed with high-resolution of conditions (12 x 8 conditions) which did not require technical replication.

### **2.3.8. Lab evolution experiment**

We evolved bacteria in sub-inhibitory doses of gemcitabine using a standard serial transfer protocol (200  $\mu$ M for BW25113, 750  $\mu$ M for Nissle 1917, 100  $\mu$ M for F-18) in a deep 96-well plate. For each strain, a single colony was picked for each individual evolution line and grown overnight in M9 media (three biological replicates per condition). The cultures were normalized to OD (600nm) 1 and diluted 1:200 to a total volume of 1,200  $\mu$ l M9 (with or without gemcitabine). The 96-well plate was incubated at 37 °C, 200 rpm shaking and was diluted 1:200 daily into fresh media for a period of 7 days (~53 generations). Resistance of evolving populations was measured daily by diluting the cultures 1:200 into a 384-well plate (35 $\mu$ l per well) containing serially diluted gemcitabine (prepared in M9 at 2x concentration at a volume of 35  $\mu$ L). The microplate was incubated at 37°C and 360 rpm double orbital shaking in automated plate reader (BioTek Eon) and absorbance (600 nm) was monitored every 10 minutes for 18 hours. All absorbance measurements were performed in technical triplicates. All

downstream experiments were performed using the frozen last day populations.

### **2.3.9. Whole-genome sequencing and analysis of lab evolution experiment**

We isolated single individual colonies from last day of the independently evolved populations by streaking them on LB agar plates. Eight colonies were selected and gemcitabine IC50 levels were determined using microtiter plate-based assay. The gDNA was extracted from selected clones using Zymo Quick-DNA Fungal/Bacterial Miniprep Kit (Cat # 11-321). Ancestor gDNAs from the replicates of each strain were pooled at equal ratio and processed as a single sample. DNA sequencing was performed by Seqcenter (Pittsburg, PA). Seqcenter prepared libraries using Illumina DNA Prep Kit and IDT 10 basepair UDI indices. Sequencing was performed on Illumina NextSeq 2000 device (2x151 bp reads). For all samples, demultiplexing, quality control and adapter trimming was performed with bcl2fastq (Illumina) and trimgalore (Trim Galore, RRID:SCR\_011847). DNA sequencing yielded a median coverage of ~120x per reference genome. We used Breseq tool to identify and annotate mutations<sup>42</sup>. Mixed ancestor populations were run in breseq population mode to evaluate all existing mutation variants and all other samples were run as pure clones. Following are the NCBI accession numbers for the reference genomes we used in the analysis: CP009273 for *E. coli* BW25113; CP058217.1 for *E. coli* Nissle 1917 and MLZI01000000.1 for F-18. The Breseq gdttools SUBTRACT/COMPARE was used to subtract mutations that

existed in the ancestor population (mutations existing 30% or more were considered) from the independently evolved clones. Then, we inspected Breseq reports to resolve unassigned junction evidence (we did not evaluate the unassigned missing coverage). Supplementary File 3 includes the mutations identified in all clones after manual inspection of the Breseq reports. Only the mutations which exist in the evolved clones but not in the ancestor were visualized on concentric circles shown in Figure 2.9A using circa software (OMGenomics). Since, F-18 genome consists of 113 contigs, the genomic locations shown on F-18 circa plot are undetermined. Mutations identified on contigs with low/unusual coverage were ignored (these are usually observed on small contigs which are shorter than 1 kb and frequently arise due to challenges in read mapping).

### **2.3.10. Obtaining spontaneous *nupC* mutants**

We cultured 96 cultures of the BW25113 strain from individual colonies overnight in LB media (96 biological replicates). In the morning 100  $\mu$ L of each culture were plated with glass beads on M9 agar plates containing 0.5 mM gemcitabine. A day after, a single colony, corresponding to single spontaneous resistant mutant, was isolated from each agar plate. A 1.3 kb region spanning the entire *nupC* coding region was amplified by colony PCR and Sanger sequenced with forward (5' TCACAGGACGTCATTATAGTG 3') and reverse (5' TGAGAGTAATTCATCGGCAC 3') primers. We annotated mutations by pairwise alignment of the sanger sequencing results with the *nupC* coding sequence of the reference genome (Supplementary File 5). Short insertions and deletions identified

in the alignment were annotated as indels. Point mutations identified in the alignment were annotated as missense or nonsense mutations according to their impact on the coding sequence. Insertion of transposon were inferred by a truncated (local) alignment to a region in the *nupC* coding sequence followed by alignment of the remaining sequence to a known transposon. We note that mutations in the promoter region were not sequenced or annotated by this method due to the position of the primers. However, some mutations in this region may account for some of the spontaneous resistant mutants that were not annotated as having *nupC* mutation (Figure 2.9B).

### **2.3.11. Luria-Delbruck fluctuation experiment**

For each strain, we inoculated 4 single colonies into 1 mL M9 medium and grew them at 37°C, 200 rpm shaking for 12 hours. Cultures were diluted to OD (600 nm) of 1 in M9. A  $10^{-6}$  dilution of OD1 was used to determine accurate CFU/OD (600nm) by plating on LB agar plates. A  $10^{-4}$  dilution of OD 1, was further diluted 27-fold and transferred into 10 wells of a 96-well plate as 200  $\mu$ L/well (initial population size ( $N_0$ ): approximately 730 cells/well). The 96-well plate was incubated at 37°C, 1000 rpm shaking overnight. Next day, OD (600 nm) of 2 wells from the 96-well plate was measured to estimate the final population size ( $N_t$ ). Next, all cultures were diluted 1:40 into 1 mL of 0.9% saline. We plated 200  $\mu$ L of each cell suspension on M9 agar plates (Plating efficiency ( $\epsilon$ ), 1:40) containing selective amounts of gemcitabine (0.5 mM for BW25113, Nissle 1917, MG1655; 62.5  $\mu$ M for F-18) or furazolidone (1mg/mL for BW25113, Nissle 1917, MG1655; 2

mg/mL for F-18). Plates were incubated at 37°C for 18 hours and the number of colonies was determined. Then, mutation rates were calculated using the RSalvador package in R(Zheng, 2017). First, mutation frequency ( $m$ ) was calculated using the function `newton.LD.plating` (and 95% confidence intervals were calculated using `conf.LD.plating`). Then mutation frequency ( $m$ ) was divided to  $N_t$  to find mutation rate per generation ( $p$ ). These numbers later normalized to a gene that is 1000 bp long.

### **2.3.12. *In vivo* evolution experiment in murine model of cancer**

Female BALB/c mice (N=20), were subcutaneously injected with one million CT-26 cells on the right flank. After sixteen days of tumor formation and growth, mice were then injected with  $5 \times 10^6$  CFUs of mid-log phase bioluminescent *E. coli* Nissle 1917 bacteria through the retroorbital vein. This bacteria strain contains chromosomally integrated *luxCDABE* operon from *Photobacterium luminescens* and erythromycin resistance cassette. Bacterial homing to tumors was monitored by IVIS imaging after two days and animals were started being given gemcitabine (at a dose of 150mg/kg) or vehicle every four days. Treatment has been continued up to seven injections or the experimental endpoint was reached due to enlarged tumor size, whichever was reached first. After mice were euthanized, tumors were extracted and flash-frozen. Bacteria were isolated from the tumors by chopping the tumor in a sterile petri dish as 1-2 mm sizes and inoculating liquid LB with erythromycin (25 mg/mL) with pieces. Tubes were then incubated at 37°C shaker and if

bacteria growth was observed single colonies were further isolated by streaking the culture on LB agar plates with erythromycin (25 mg/mL).

## **2.4. RESULTS**

### **2.4.1. The *E. coli* resistome against gemcitabine**

We first set out to determine the inhibitory concentration of gemcitabine in three *E. coli* strains: BW25113 (a K-12 lab strain), F-18 (a human fecal isolate), and Nissle 1917 (a human fecal isolate that is used as probiotic). We characterized the inhibitory concentrations by monitoring bacterial growth inhibition after 12 hours.

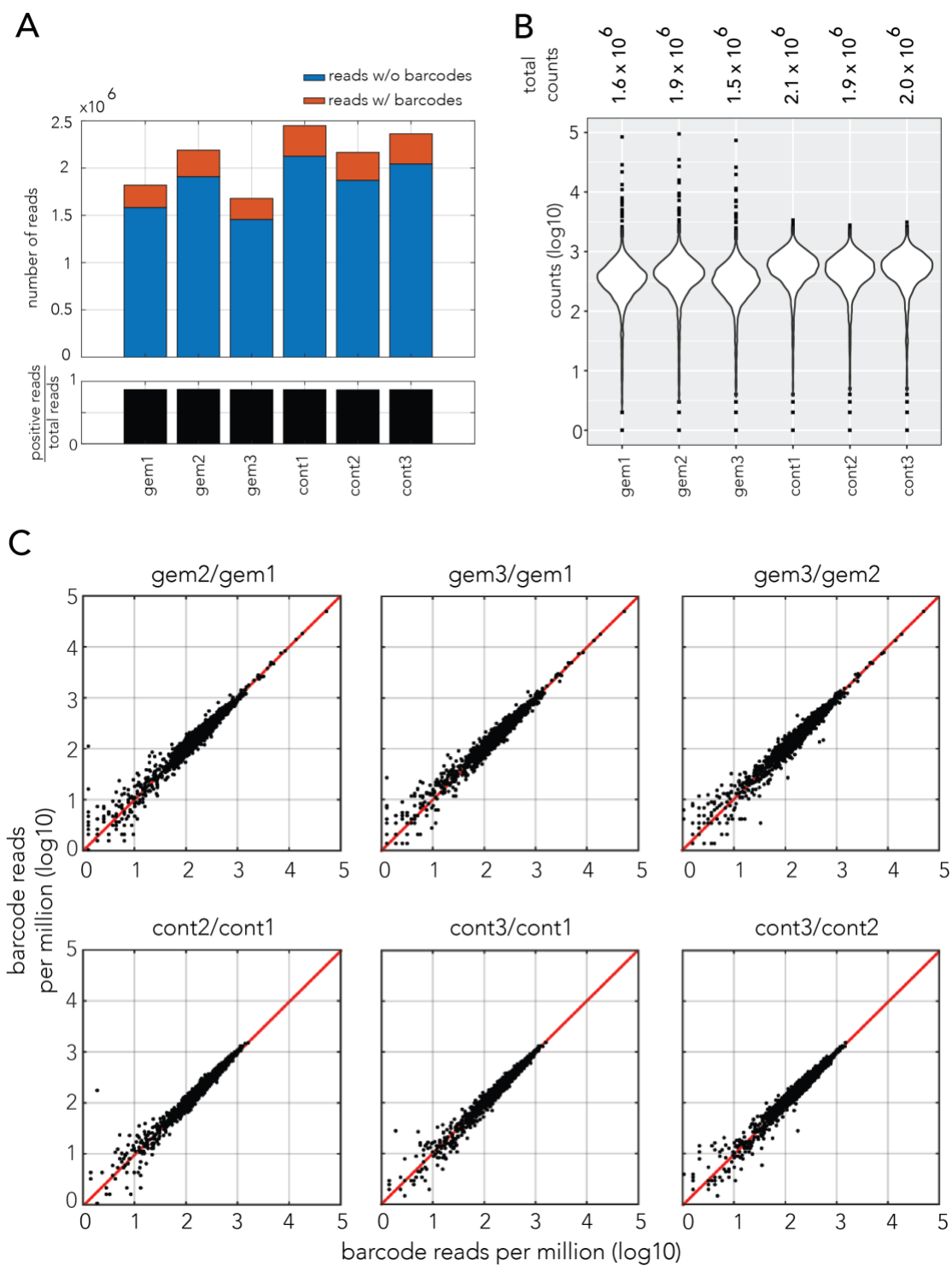
Figure 2.2B shows the sensitivity curves and the inhibitory concentration that reduced culture density by 50% (IC<sub>50</sub>). We observed that gemcitabine can completely inhibit the growth of all three strains, with F-18 being most sensitive (IC<sub>50</sub>=0.7 μM) and BW25113 being most resistant (IC<sub>50</sub>=103 μM). These concentrations are comparable to the IC<sub>50</sub> reported for 29 pancreatic adenocarcinomas in the GDSC2 dataset that tested hundreds of toxic compounds on a thousand cell-lines (Yang et al., 2013) (boxplot above Figure 2.2B).

We next conducted a genetic screen with a collection of 3,680 single-gene knockout strains to systematically map all non-essential genes that influence gemcitabine resistance when depleted (typically referred to as the drug resistome). We used a pooled screening approach that we recently developed which relies on

sequencing DNA barcodes that are unique for each gene-knockout in the strain collection (Noto Guillen et al., 2021; Rosener et al., 2020).

Figure 2.2C outlines the main steps of the screening method: the pooled knockout strains were inoculated and grown in media containing a high gemcitabine concentration (140  $\mu$ M) while a control culture was inoculated in media without drug. Once the cultures reached a late logarithmic growth phase, cells were lysed, and DNA was extracted for amplification and sequencing of the barcode region. Lastly, we compared the frequency of each barcode, corresponding to an individual gene-knockout, in the drug and control conditions. This comparison revealed strains whose frequency was significantly increased or decreased in gemcitabine. Such enrichment or depletion correspond to increased or decreased drug resistance, respectively. We used three biological replicates, biological experiments conducted side-by-side, in three separate tubes, to infer statistical significance. We identified over a million and a half barcode containing reads in each replicate that corresponded to roughly 3,500 unique barcodes (knockout strains). Figure 2.1 shows detailed information on the screen coverage and replication quality. To validate the screen results we repeated the entire screen two additional times, once with the same collection of knockout strains and once with a collection knockout strains that were cloned independently (again, each with three internal replicates). The results (resistance/sensitivity) from the two additional screens were highly correlated with the original screen (Figure 2.1D). Results of all screens and replicates appear in Supplementary File 1.

Figure 2.2D shows a volcano plot representation of the screen results. Using very strict cutoff values for fold-change ( $>16$ ) and FDR-adjusted p-value ( $<0.05$ ), we identified 42 gemcitabine-resistant knockout strains and 6 gemcitabine-sensitive strains (Figure 2.2D). The screen results, including all statistically significant hits without a strict cutoff on enrichment, appear in Supplementary File 1. Reassuringly, we found that knockout of the known drug transporter (*nupC*) is among the top resistors. When we inspected the gene annotation of the top resistors, we identified multiple hits from the known target pathway of the drug (Figure 2.2E). These included the permease (*nupC*), the transcriptional regulator *cytR* (a repressor of both *nupC* and *cdd*), and the cytidylate kinase (*cmk*) that likely phosphorylate intracellular gemcitabine. We also found multiple hits that encode membrane proteins or transporters, including *ompR* and *envZ* that together regulate permeability channels for nutrients, toxins, and antibiotics (MIZUNO & MIZUSHIMA, 1987). Lastly, we observed a high prevalence of genes coding for metabolic enzymes that can considerably slow down growth when mutate (Noto Guillen et al., 2021) Indeed, a statistical test revealed that gene knockouts that were previously identified as reducing growth (Baba et al., 2006) were highly enriched in the set of gemcitabine resistant strains ( $p\text{-value}= 8.6186\text{e-}18$ , Fisher exact test). The overlap between resistant strains and slow growing strains is sensible given that slow growth reduces the rate of DNA synthesis. Since gemcitabine is quickly degraded by the bacterial Cdd enzyme, it was only transiently present in the extracellular media during the screen experiment. Under



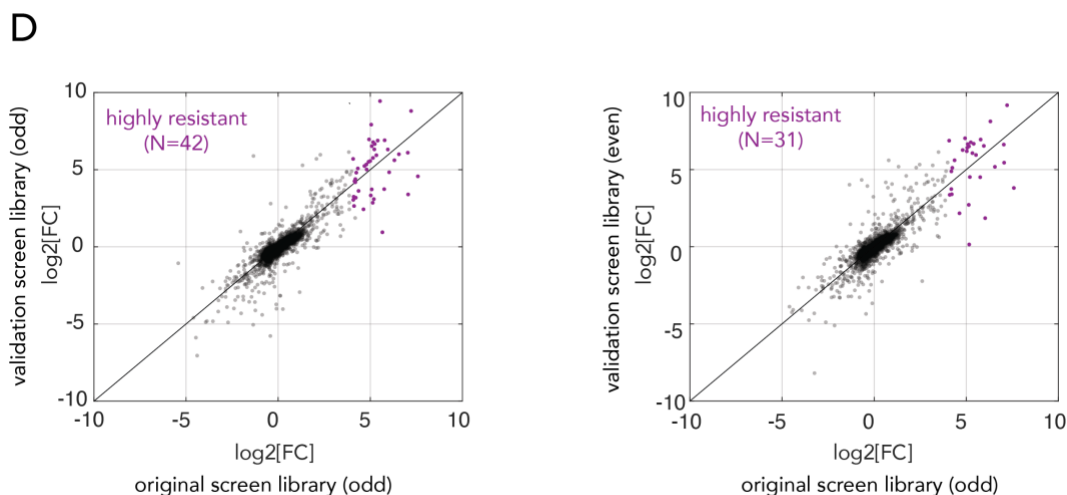


**Figure 2.1 Statistics of the gemcitabine genetic screen performed with the *E. coli* barcoded knockout strain collection.**

A. Bar plots showing the number of reads with or without barcodes across samples (three biological replicates with gemcitabine and without drug). B. Violin plots showing the frequency of individual barcode counts. C. Scatter plots of barcode counts across biological replicates D. Comparison of between independent biological replicates of the genetic screen for gemcitabine resistance. Left panel - Comparison between the log-fold change in strain enrichment between the original screen and a screen performed with the same strain collection (odd collection) on the different day. Right panel - Comparison between the log-fold change in strain enrichment between the original screen and a screen performed with the knockout strain collection that was independently cloned (even collection). Strain marked in purple are resistant knockout strains that were identified in the original screen (figure 1E). Eleven knockout strains that were gemcitabine resistant in the original screen were not detected at all newly used strain collection (even collection).

such a transitory stress, slower consumption of the antimetabolite is likely beneficial (normal growers incorporated much more gemcitabine into their DNA and remain arrested while slow growers incorporated less and therefore avoid arrest). Next, we used the gene set enrichment analysis tool GAGE (Luo et al., 2009) to test for functional enrichment using the Kyoto Encyclopedia of Genes and Genomes (KEGG) (Kanehisa et al., 2016) and Gene Ontology (GO) databases (The Gene Ontology Consortium, 2000). This analysis is complementary to the

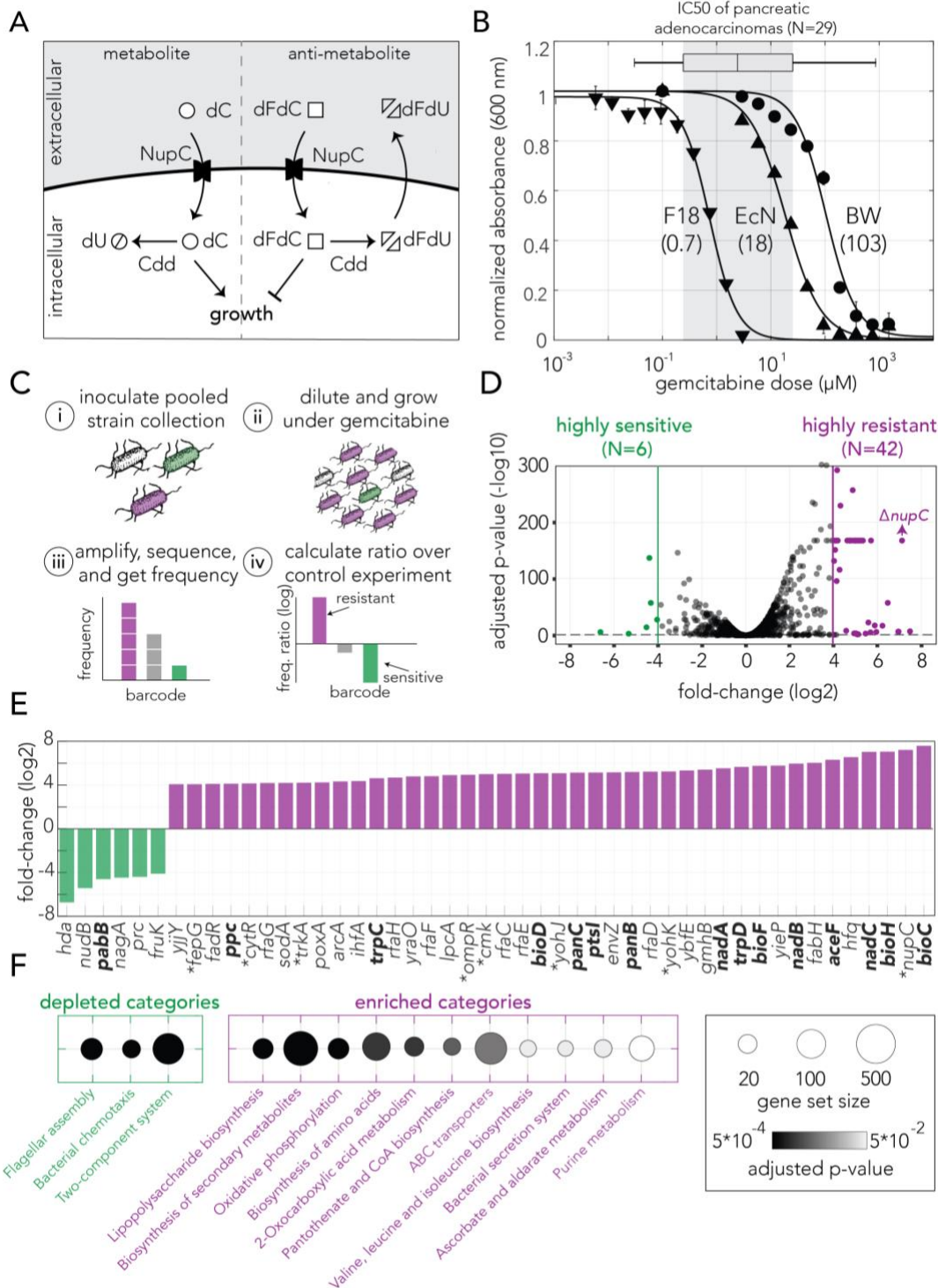
previous analysis, since it considers the enrichment values from all strains, rather than only the limited set of hit strains obtained by imposing strict cutoffs.

Figure 2.2F shows the functional enrichment by KEGG pathways (enrichment indicates that pathway inactivation increased resistance). Reassuringly, we observed a high agreement between the functional enrichment by GAGE and the annotation of the top hits. Specifically, we observed enrichment in purine synthesis and membrane transporters as well as multiple metabolic pathways impacting bacterial growth rate (Noto Guillen et al., 2021). Supplementary File 2 provides the full list of enriched and depleted categories.

Taken together the results from our genetic screen outline three adaptation strategies that increase bacteria's gemcitabine resistance: reduced drug import by inactivating membrane proteins and transporter systems, changes in the drug metabolism through mutations in the target pathway, and inactivation of metabolic genes that slowdown bacterial growth. Importantly, since these resistance adaptations arise from knockout of single genes, they are all accessible within a single evolutionary step (e.g., a single gene inactivating mutation).

#### **2.4.2. The impact of bacterial resistance on bacterial drug degradation**

Our genetic screen revealed alternative adaptation strategies that increase bacterial resistance against gemcitabine. However, for most loss-of-function mutations, it remains to be determined how they will influence the rate of bacterial



**Figure 2.2. Genetic screen identifies gemcitabine sensitive and resistant loss-of-function mutations in *E. coli***

A. Gemcitabine transport and metabolism in *E. coli*. Similar to deoxycytidine (dC), gemcitabine (dFdC) is imported into the cell through the nucleoside permease *NupC*. Intracellular gemcitabine is either converted into the less toxic metabolite dFdU the cytidine deaminase *Cdd* or is phosphorylated and incorporated into the DNA. B. Gemcitabine dose response curves for three *E. coli* strains (three technical replicates, performed once). The inferred IC<sub>50</sub> are shown in parenthesis. Gemcitabine IC<sub>50</sub> range of 29 pancreatic adenocarcinomas are shown as a box plot above the graph. C. Overview of the pooled screening approach. Pooled cultures of the knockout strain collection were inoculated (i) and grown for multiple hours with or without gemcitabine (ii), DNA extracted from cells was used to amplify, sequence and calculate the frequency of barcodes that correspond to individual strains (iii), The ratio of barcode frequencies of each strain in gemcitabine and control conditions were used to identify sensitive and resistant knockouts (iv). Experiment includes three biological replicates (independent inoculums). D. Volcano plot of the genetic screen results. Green and purple dots represent sensitive and resistant knockout strains, respectively. E. Highly sensitive and resistant strains. Asterisk sign marks the gene knockouts likely involved in gemcitabine transport and phosphorylation. Knockouts marked in bold were characterized as slow growing strains. F. Statistically significant enriched and depleted KEGG categories identified by the genetic screen. The marker size shows the number of genes in the category and the gray scale marks the statistical significance.

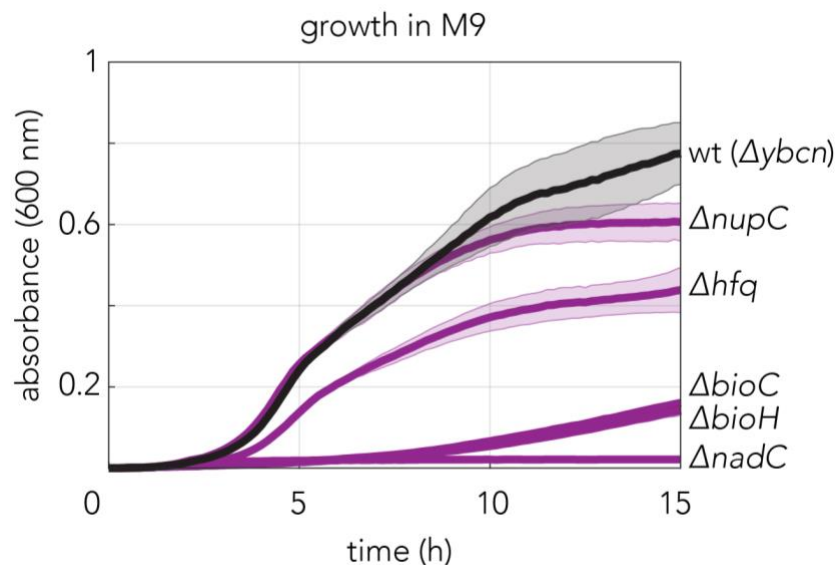


**Figure 2.3 Growth of top five resistant gemcitabine knockouts identified by the genetic screen in M9 minimal medium.**

The *ybcn* deletion strain was used as a wild-type control since this gene deletion does not impact *E. coli* growth and the genetic background of this strain is comparable to the other mutants used in the experiment

drug degradation (and ultimately drug availability for neighboring cancer cells). We therefore designed a functional assay to detect changes in drug activity, after bacterial incubation with the drug, relative to its activity after incubation with the wild-type strain (outlined in Figure 2.5A). We incubated a knockout strain of interest in saline with a high gemcitabine concentration and collected the conditioned supernatant after a short incubation period (15 or 45 minutes). We diluted the conditioned supernatant into regular media and monitored the growth of a drug-sensitive reporter strain (a *cdd* knockout that cannot degrade gemcitabine) in this media. Finally, we used growth curves of the reporter strain as a proxy for the gemcitabine concentration in the conditioned supernatant. We reasoned that a conditioned supernatant containing high drug concentration is indicative of slow degradation by the strain of interest. This difference in drug concentration will in turn manifest as slow growth of the reporter strain (blue curve in Figure 2.5A). We note that this detection method is insufficient to resolve the mechanism underlying the slowed degradation since it only measures drug availability in the extracellular environment after incubation (e.g., both slow import and slow deamination will be interpreted as slow degradation).

We evaluated drug activity after incubation of the 88 most resistant strains, the top 42 resistors found by the strict enrichment cutoff (Figure 2.2E) and the next 46 resistant strains (supernatant collection was repeated three times on different days). Figure 2.5B shows a summary of the results of this assay (Figure 2.4 shows observed growth curves). We found one-third of the tested knockout strains

modulated extracellular drug availability (33 of 88). Specifically, 11% of all strains were fast degraders and 26% of strains were slow degraders (one-tailed t-test, FDR-adjusted  $p$ -value < 0.1). We next decided to validate the conclusions of our functional assay using an independent chemical approach for the wild-type and three knockout strains. We focused on the fastest and the slowest degraders and *cdd* knockout as a control. We incubated each strain with gemcitabine and sampled aliquots of the supernatant at predetermined time points (20, 45 and 75 minutes). We then used gas chromatography–mass spectrometry (GC-MS) to measure the concentration of gemcitabine and its degradation product in the conditioned supernatant (Figure 2.5C). In agreement with our functional assay, the GC-MS measurements confirmed that the gene knockouts indeed altered the availability of gemcitabine and in the extracellular environment. The increased availability of the drug breakdown product (dFdU) supports the conclusion that rate of drug metabolism is underlying this change (as opposed to intracellular drug accumulation (Klünemann et al., 2021)).

Lastly, we tested if bacterial resistance mutations influence the drug sensitivity of co-cultured cancer cells. While previous works relied on sequential exposure to the drug (Geller et al., 2017; Lehouritis et al., 2015), using conditioned bacterial supernatant on cancer cells, we reasoned that a co-culture system will reveal if bacterial degradation is sufficient to impact drug efficacy in neighboring cancer cells that are simultaneously exposed to the drug. We co-cultured with spheroids of the CT-26 murine cancer cell-line and simultaneously treated them

with gemcitabine for 4 hours (gemcitabine cytotoxicity can be recapitulated in this cell-line (Geller et al., 2017)). Spheroids were then washed and left to grow for a week in media supplemented with antibiotics. Lastly spheroids were washed again to remove dead cells and the area of the spheroids was measured to evaluate gemcitabine's efficacy on the cancer cells. Figure 2.5D shows microscopy images of a representative microwell plate. As the figure shows we observed sensible trends in these experiments: First, we observed that spheroid size was inversely correlated with gemcitabine concentration (lower spheroid row in Figure 2.5D) and that bacterial concentration, without any drug, did not significantly impact spheroid growth (left spheroid column in Figure 2.5D). Reassuringly, we observed that co-cultured bacteria can mitigate gemcitabine damage and that the magnitude of rescue depended on the bacterial concentration (spheroid area is overall increased in upper spheroid rows in Figure 2.5D).

We used our systematic measurements of spheroid area to fit a fitness landscape. This procedure allowed us to infer the effective drug concentration that leads to a 50% change in area (EC50) for any bacterial concentration. Figure 2.5E shows the landscapes for the wild-type strain, a control non-degrader (*cdd* knockout) and the fastest and slowest degraders (*cytR* and *nupC* knockouts, respectively). As evidenced by the changes in the EC50 fronts, we observed that the spheroid fitness landscapes were considerably different depending on the co-

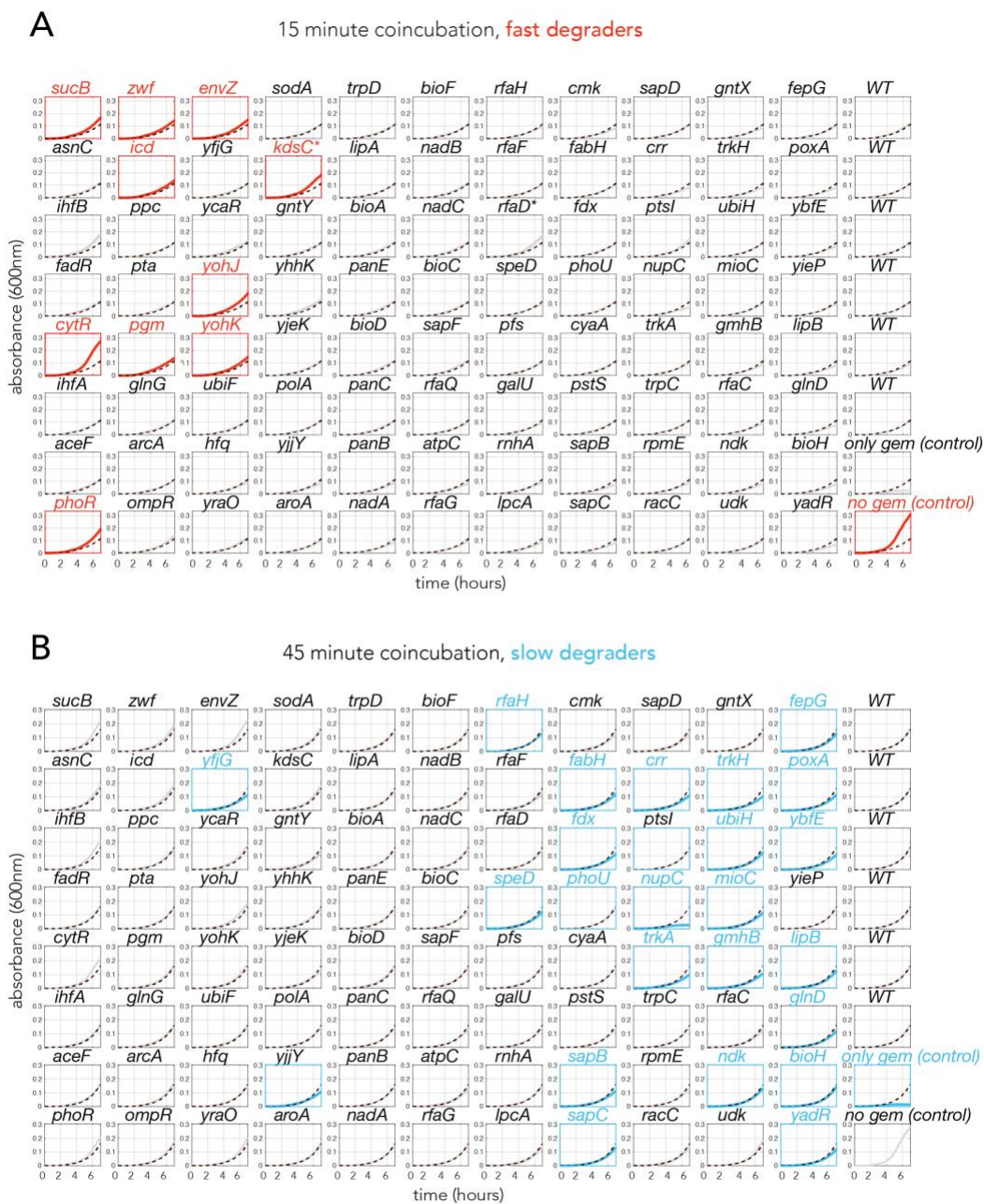


**Figure 2.4 Individual growth curves of reporter strain (*cdd* knockout) in the functional assay to estimate gemcitabine breakdown rate of the top 88 gemcitabine resistant genetic screen hits**

The title of each graph shows the knockout strain that was incubated with gemcitabine before the reporter strain was inoculated into the filtered conditioned supernatant. A. Mean growth curves of the reporter strain in the conditioned supernatant filtered after 15 min of co-incubation with the 88 tested knockout strains. Statistically significant fast degraders are shown with red color. (One tailed student's t-test with FDR corrected  $p\text{-adj}<0.1$ ). B. Mean growth curves of the reporter strain in the conditioned supernatant filtered after 45 min of co-incubation with 88 tested knockout strains. Statistically significant slow degraders are shown with blue color. (One tailed student's t-test with FDR corrected  $p\text{-adj}<0.1$ ).

cultured bacteria during drug exposure. In agreement with our functional and chemical assays, increased chemoresistance relative to the wild-type strain was observed when spheroids were co-incubated with the fast degrader (*cytR* knockout). In contrast, decreased chemoresistance relative to the wild-type strain was for co-incubation was with the slow degrader (*nupC* knockout). A replicated spheroid experiment with *cytR* and *nupC* knockouts and the wild-type strain revealed similar shifts in the EC50 fronts (Figure 2.6). Additional experiments with nine more bacterial resistors showed they also impacted spheroid chemoresistance (Figure 2.7).

Taken together, the results of the spheroid experiments demonstrate that mutations impacting gemcitabine degradation rates in bacteria can indeed impact neighboring cancer cells simultaneously with the drug. Importantly, we observed that bacterial resistors can have opposite influences on gemcitabine sensitivity of co-cultured cancer cells. For examples, the *nupC* knockout decreased chemoresistance while the *cytR* knockout increased it. A key question remaining is which adaptations will naturally transpire during bacterial evolution under drug selection.

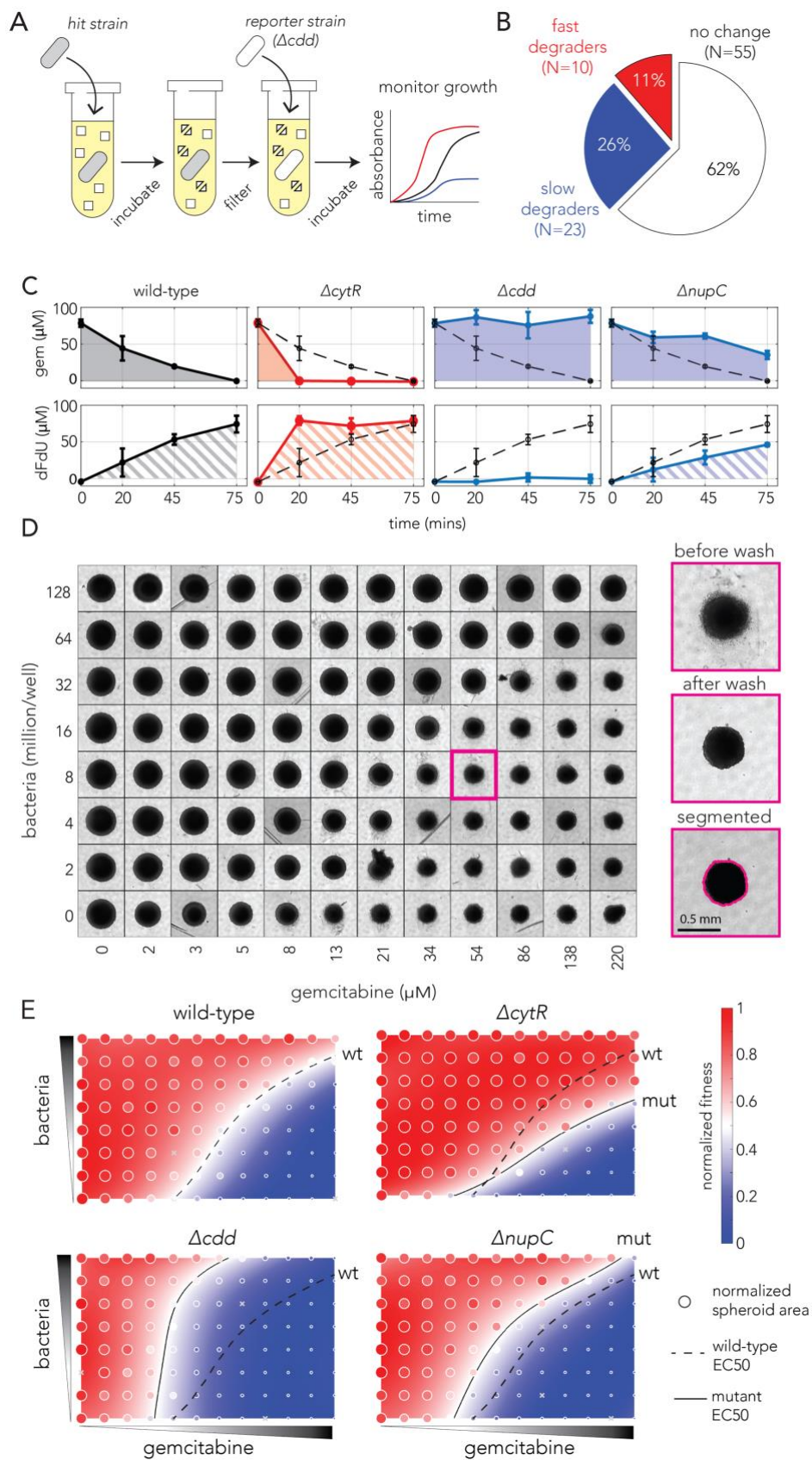


**Figure 2.5 Bacterial gemcitabine resistance can oppositely affect drug degradation and impact neighboring cancer cells**

A. The functional drug breakdown assay. Each knockout strain was inoculated in saline containing gemcitabine and incubated for 15 or 45 minutes. Conditioned supernatant was then filtered and mixed with fresh media before inoculating a reporter strain. Reporter strain growth was used as a proxy for changes in gemcitabine availability in the conditioned supernatant. B. Results of the drug breakdown assay for the top 88 resistant knockouts. A third of all tested knockouts (33/88) influenced the drug degradation rate. C. Chemical validation of the functional assay for the slowest and fastest degraders. GC-MS was used to measure gemcitabine concentration (shaded area, top panels) and its degradation product dFdU (hatched area, lower panels) in conditioned supernatant (colors as in A). The dashed black curve marks the measurements after incubation with the wild-type strain. The error bars show the standard deviation of three biological replicates. D. Co-culture experiments shows bacterial mutations can influence gemcitabine efficacy in neighboring spheroids of cancer cells. Representative microscopy images of spheroids that were co-cultured with wild-type bacteria across multiple concentrations of drug and bacteria (large images show the same spheroid before the wash, after the wash that removed dead cell debris, and after image segmentation). E. Bacterial mutations that modulate drug degradation can impact drug efficacy neighboring cancer cells. Results of spheroid experiments with the slowest and fastest degraders and the inferred fitness landscapes. Each panel shows the fitness landscape calculated from spheroid size across a range of gemcitabine and bacteria concentrations (as in D). The color code shows the normalized spheroid size (ranging from the smallest spheroid to the largest one). The dashed black line marks the parameter combination (bacteria and gemcitabine concentrations) that reduce spheroid growth by 50% (EC50 front) and solid lines show the EC50 front for the knockout strains. Shifts in the EC50 front, relative to the wild-type front, indicate that co-incubation with the knockout strain during drug exposure altered the spheroid's chemo-resistance.

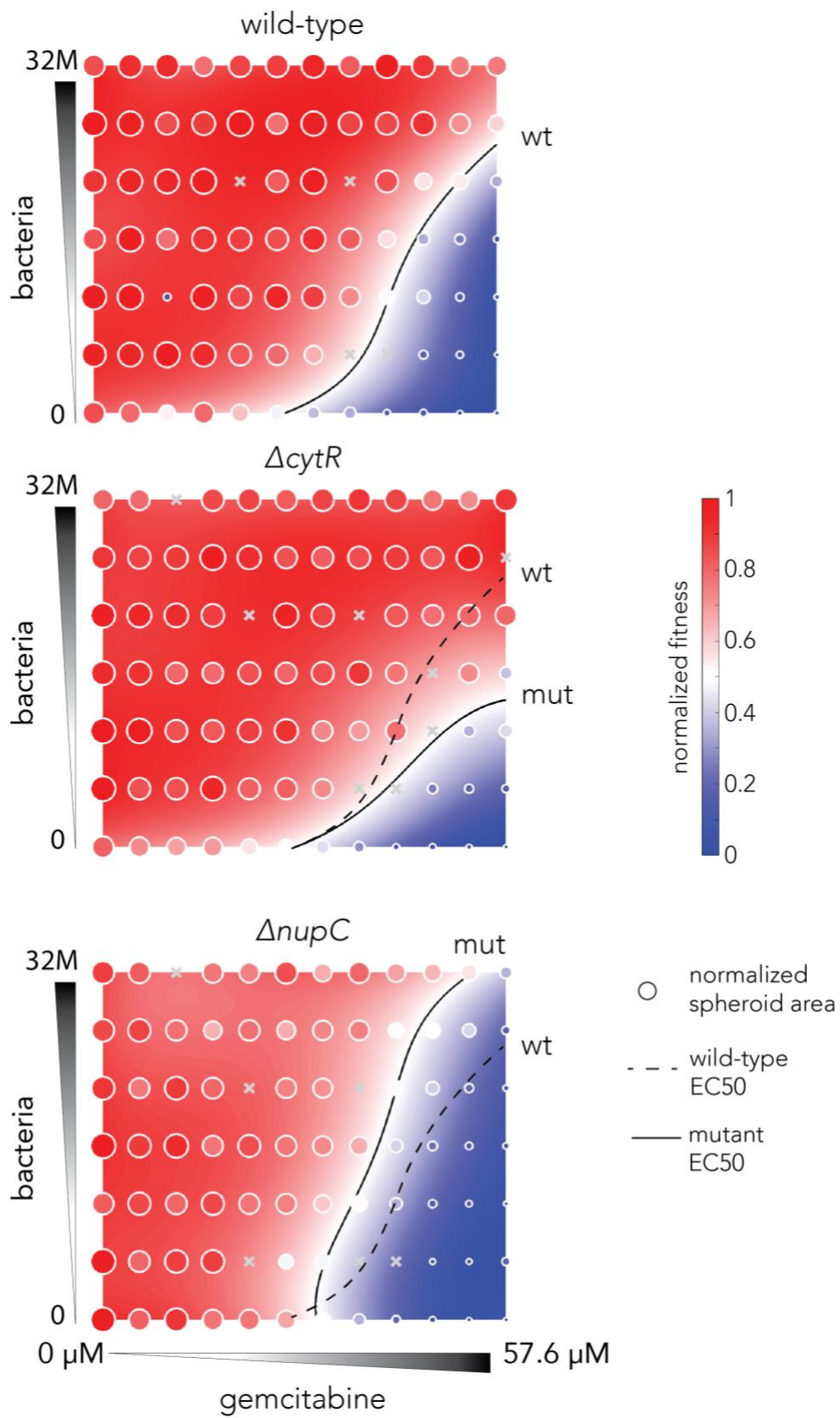


### Figure 2.6: Validation of results of spheroid experiment

The fitness landscape inferred for the slowest and fastest bacterial degraders relative to the wild-type strains. Each panel shows the fitness landscape calculated from spheroid size across a range of gemcitabine (0  $\mu\text{M}$  to 57.6  $\mu\text{M}$  as 1.5 fold dilutions) and bacterial concentrations (0 to 32 million as 2 fold dilutions). The color code shows the normalized spheroid size (ranging from the smallest spheroid to the largest one). The dashed black line marks the parameter combination (bacteria and gemcitabine concentrations) that reduce spheroid growth by 50% (EC50 front) and solid lines show the EC50 front for the knockout strains. Shifts in the EC50 front, relative to the wild-type front, indicate that co-incubation with the knockout strain during drug exposure altered the spheroid's chemo-resistance.

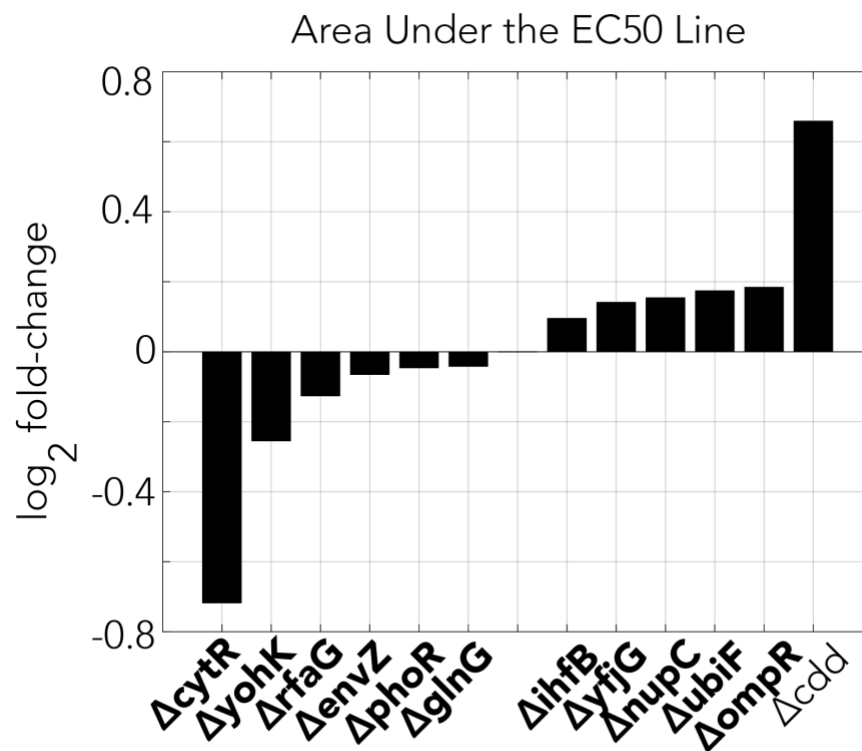


Figure 2.7 Changes in area under the EC50 front in spheroid fitness landscapes generated with co-incubation of gemcitabine and selected resistant knockout strains.

#### 2.4.3. Evolved bacterial resistance against gemcitabine

The genetic screen uncovered multiple loss-of-function mutations that confer bacterial gemcitabine resistance. Yet, such screens are insufficient for

determining which gene inactivation, if any, will emerge under natural selection. Moreover, since evolution can leverage additional processes beyond gene-inactivation, such as gain-of-function, adaptation may follow an entirely different evolutionary trajectory. We applied the widely used serial transfer approach to select for evolved drug resistance in bacteria (Dragosits & Mattanovich, 2013). Such in-vitro experiments can shed light on the mechanisms underlying resistance and the time scale needed to acquire resistance. To test if reoccurring adaptations emerge, we used the three *E. coli* strains that were characterized by different drug sensitivity levels (Figure 2.2B). Once the serial transfer experiment ended, we evaluated if drug resistance increased in the population and isolated single resistant clones for whole genome-sequencing (Figure 2.8A).

We evolved three independent populations of each *E. coli* strain in sub-inhibitory concentrations of gemcitabine (methods) and three control populations without any drug. We monitored drug resistance in all populations daily throughout the experiment (Figure 2.8B). We observed that resistance emerged within a day or two for the Nissle 1917 and F-18 strains, while it emerged more slowly for the BW25113 strain. Last day populations from all strains that evolved in gemcitabine were resistant to the drug across all tested drug concentrations (Figure 2.8C). In order to isolate individual resistant clones, we streaked each of the evolved population on agar plates and measured IC50 does for 8 independent colonies. (Figure 2.8D). Almost all clones from Nissle 1917 and F-18 drug evolved strains were resistant. However, clones from the BW25113 populations showed

heterologous levels of resistance. All clones isolated from the populations that evolved without the drug were drug sensitive. We chose a single clone from each population for further analysis (marked as extruding slices in the pie charts on (Figure 2.8D). These individual clones represent lineages that evolved completely independently from one another.

#### **2.4.4. inactivation of *nupC* underlies evolved drug resistance**

Phenotypic measurements revealed that all drug-evolved populations became highly resistant. We next sequenced the genomes of evolved clones to identify the underlying adaptive mutations and identified mutations with the BreSeq software (Barrick et al., 2014). Figure 2.9A shows the mutations we identified in the single clones as circa plots (concentric circles representing the bacterial chromosomes). Annotation of mutations in F-18 required careful manual inspection since its reference genome consists of 113 contigs. As the figure shows, we observed that the genomes of all the drug-evolved clones harbored *nupC* mutations while none of the control-evolved clones had such mutations. Supplementary File 3 provides the BreSeq information the mutations we identified. Importantly, while we found additional mutations beyond those in the *nupC* gene, we did not observe another gene that was repeatedly mutated across all independent replicates in all of the *E. coli* strains. The only other repeated mutation we identified involved the *yahF* gene in two lines of F-18 that also shared an identical *nupC* mutation (transposon). Inspecting the BreSeq report and the contig

files led us to believe both lines shared single new junction that impacted both the *nupC* and *yahF* loci.

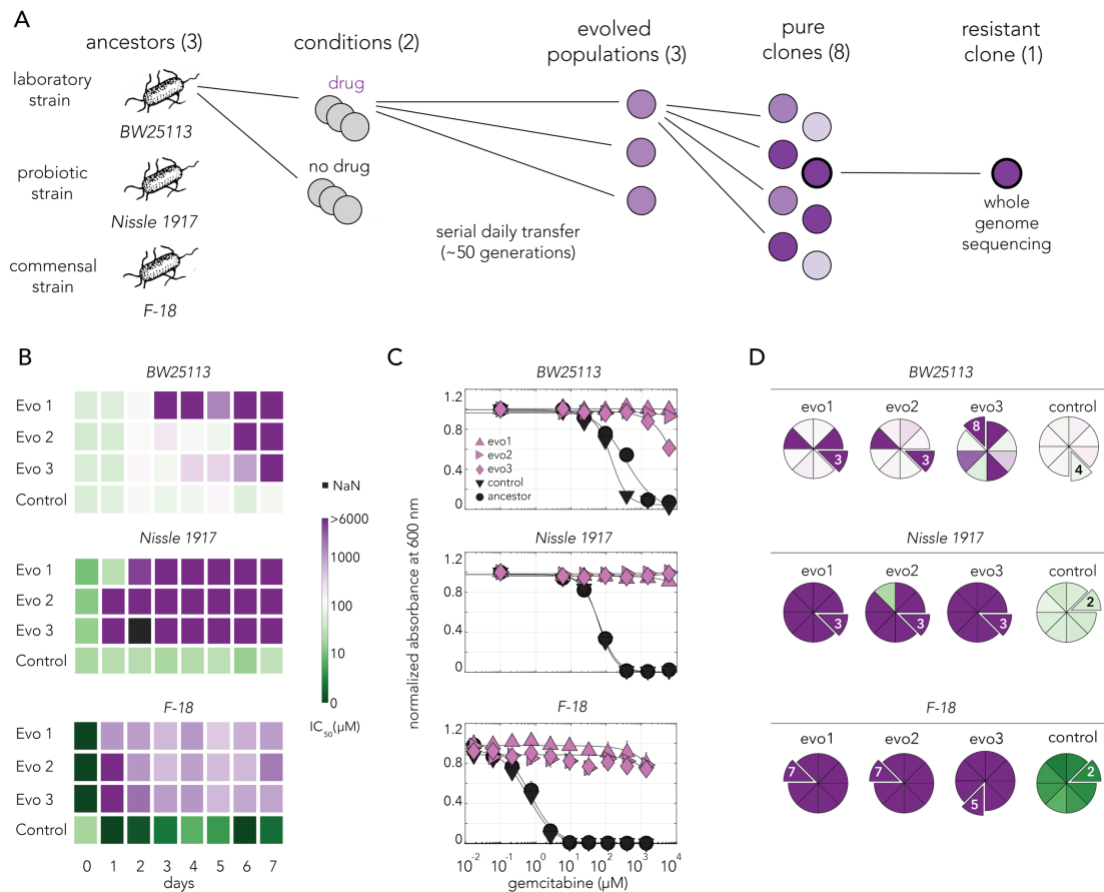


**Figure 2.8 Gemcitabine selection leads to rapid evolved resistance in three *E. coli* strains**

A. Overall approach for the lab evolution experiment. Three *E. coli* strains were evolved over 50 generations in serial transfer evolution experiment. We measured gemcitabine resistance of last day populations and eight single clones were isolated from each population. A single resistant clone was used for the whole genome sequencing and for identifying of the underlying mechanism for drug resistance. B. Heatmaps showing the temporal changes in gemcitabine  $IC_{50}$  of evolving populations in each day of the serial transfer experiment. C. Gemcitabine dose response curves of last day populations from lab evolution experiment. All of the gemcitabine evolved lines, but not the control evolved lines, developed a high resistance against gemcitabine. D. Pie charts showing the gemcitabine  $IC_{50}$  levels of screened clones. Slices represent the clone selected for whole genome sequencing. Color scale is the same as panel B.

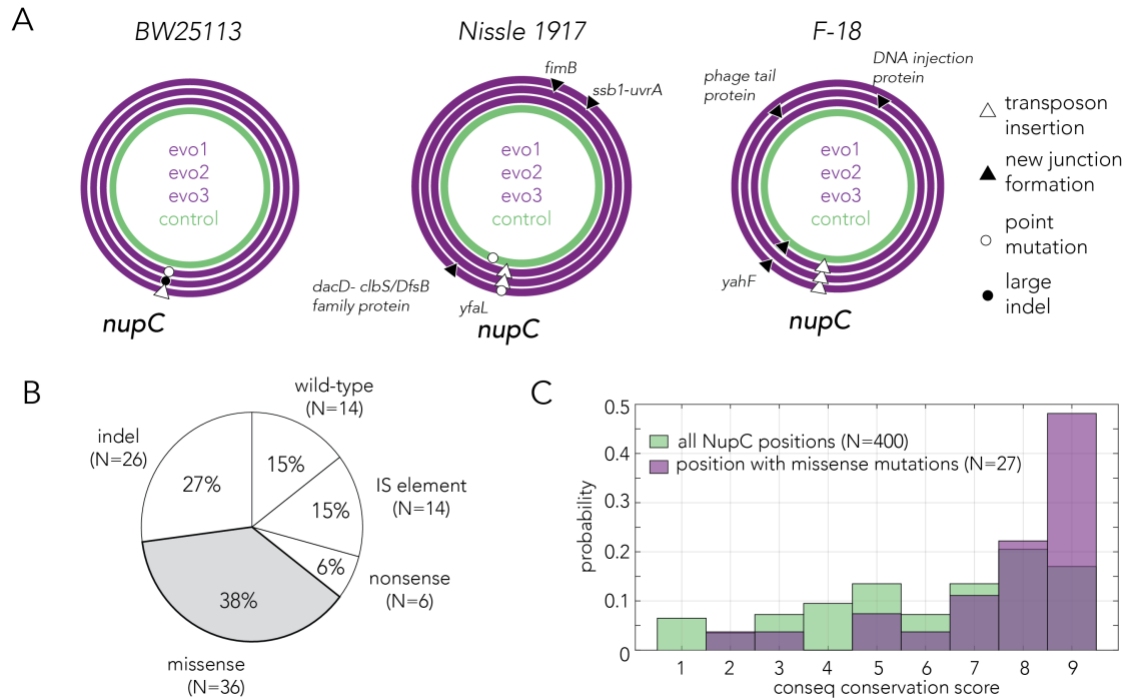


**Figure 2.9 Evolved resistance converges to inactivation of the nucleoside permease *NupC***

A. Circa plots showing the mutations identified by whole-genome sequencing in pure clones isolated from independently evolved populations. Mutations in the coding region of the *nupC* gene were observed across all gemcitabine-evolved clones but not in the no-drug control evolved clones. Since the F-18 genome is not fully assembled, relative positions on the F-18 circa plot are not real genomic positions. B. Pie chart showing the frequency of various mutation types identified by sequencing the *nupC* across 96 spontaneous gemcitabine resistant mutants in the BW25113 strain. C. A comparison of the evolutionary conservation of missense mutation positions relative to the conservation of all position in *NupC*. The positions of the missense mutations are statistically biased towards the conserved positions ( $p$ -value =  $1.95 \cdot 10^{-4}$  in Wilcoxon rank sum test).

The mechanism of mutation in the *nupC* gene varied across the gemcitabine-evolved strains, and included point mutations, large deletions, and new junction formation within *nupC* coding region that can stem from transposon insertions and genomic rearrangements. The two of the point mutations we identified, were missense mutations (S175P and V249A). To evaluate if these point mutations likely interfere with the permease function, we used the ConSurf Server

that identifies evolutionarily conserved positions (Ashkenazy et al., 2016). The analysis revealed that both positions are highly conserved and are therefore likely important for the permease function (positions marked in red in Figure 2.10). Lastly, we examined the function of all other genes that were mutated in evolved strains to pinpoint additional putative adaptive mutations. We identified a new genomic junction, likely originating a transposon insertion, upstream to the *uvrA* gene. The *uvrA* gene codes for A subunit in the UvrABC nuclease that is involved in nucleotide excision repair pathway (Keseler et al., 2017). The mutation impacted the annotated promoter of the gene according to regulonDB (Gama-Castro et al., 2016) Taken together, we concluded that resistance emerged across all twelve sequenced and independently gemcitabine-evolved strains primarily through inactivation of the nucleoside permease *NupC*.

#### **2.4.5. mechanisms underlying convergence towards *nupC* inactivation**

Gemcitabine adaptation in our evolution experiments likely emerged through inactivation of *nupC* across all evolved strains. This convergence can be driven by multiple mechanisms that are not necessarily exclusive to one another. Evolutionary trajectories are influenced by multiple parameters, including the adaptation benefit (e.g., the level of resistance the mutation confers), the adaptation cost (e.g., if it reduces growth) and the likelihood that the mutation will appear spontaneously. We reasoned that quantifying these parameters for the *nupC* gene would provide insight on the forces underlying the evolutionary convergence we observed.



The conservation scale:

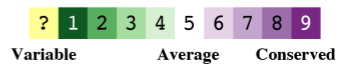


**Figure 2.10 Annotation of *nupC* mutations by evolutionary conservation**

The color code shows the conservation level inferred for the *NupC* protein with the ConSurf server. Mutations shown in black are found in spontaneous mutants isolated from agar plates containing high concentrations of gemcitabine. Mutations shown in red are missense mutations found in the gemcitabine evolved strains. Abbreviations; del:deletion, ins: insertion, fs:frameshift causing mutation, IS: insertion element(transposon insertion)

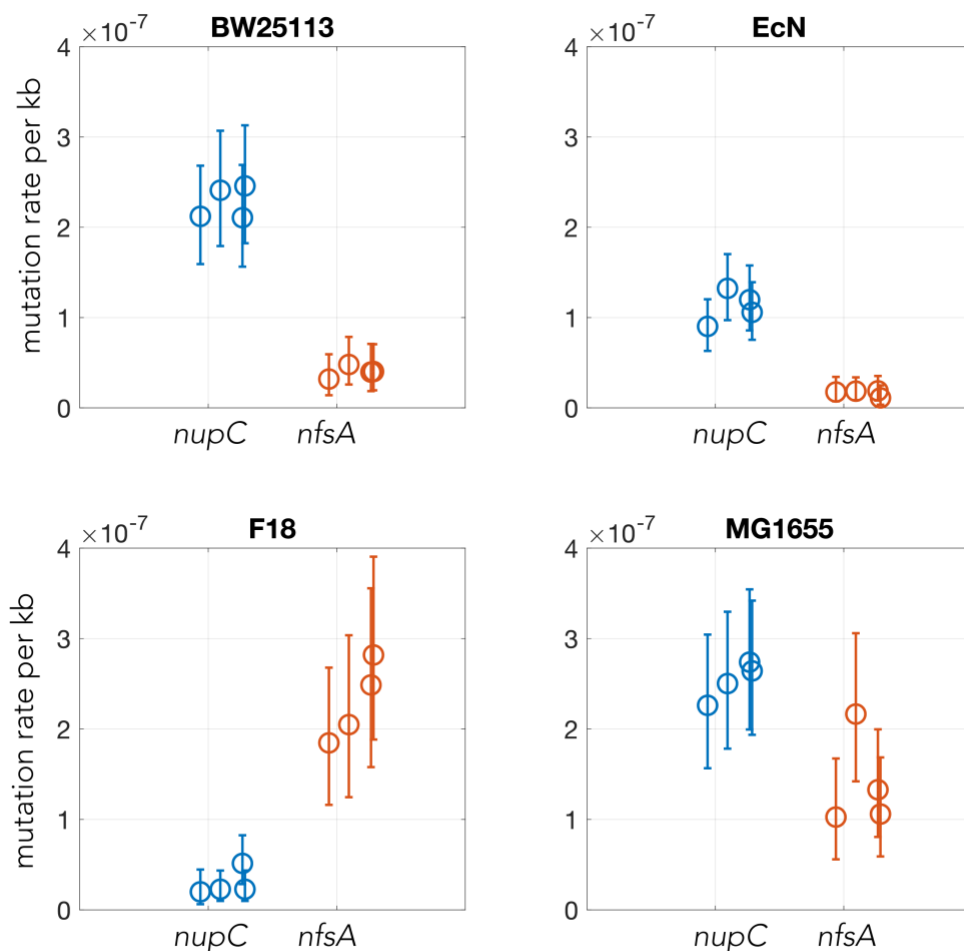


**Figure 2.11 Plots showing the mutation rates in *nupC* (mutated in gemcitabine resistant mutants) and in *nfsA* (mutated in furazolidone resistant mutants) loci**

The rates were calculated with a Luria-Delbrück fluctuation experiment in four *E. coli* strains. We repeated each fluctuation experiment four times.

Our genetic screen already revealed that *nupC* is among top loss-of-function mutations conferring resistance (Figure 1E), yet it remains unclear whether *nupC* inactivation is associated with any cost to the cells. We therefore monitored the growth rate of the top five resistant knockouts identified in the genetic screens (Figure 2.3). The experiment revealed that a *nupC* knockout grows as fast as the wild-type strain (*ybcN* knockout) for most of the growth phases and slows down only during the stationary phase. In contrast, all other top resistant knockouts were significantly slower than the wild-type strain (and *nupC*) during all growth phases. We concluded that *nupC* inactivation is unique among the resistant mutations since its associated with only a small fitness cost for bacteria when the drug is not present.

We next tested whether the *nupC* locus contains a mutation hotspot. We reasoned that a mutation hotspot will be evident if we observed that multiple independent resistant clones will share a specific site or region within the *nupC* locus or will leverage on a specific mutation mechanism. We obtained independent clones by picking 100 individual colonies of the wild-type strain. We grew them overnight and plated them on agar plates with an inhibitory gemcitabine concentration (0.5 mM). We reasoned that at this high concentration, only the most resistant and fast-growing mutants, namely *nupC* mutants, will be able to form large colonies within an overnight growth. We then picked a single resistant colony from each of the 100 agar plates and Sanger sequenced the *nupC* coding sequence locus. We found that 85% of colonies were mutated in this region, with

mutations spanning multiple types. Missense mutations and short indels were the most frequent mutations observed (Figure 4B). In order to annotate the missense mutations, we tested if they likely disrupt positions important for permease function. We used the ConSurf sequence analysis tool and identified evolutionarily conserved positions (Figure 2.10). The analysis revealed that missense mutations we identified were significantly biased towards the highly conserved regions of the permease (Figure 4C,  $p$ -value =  $1.95 \times 10^{-4}$  in Wilcoxon rank sum test).

Lastly, we decided to test if the *nupC* is naturally poised for frequent mutations in the absence of gemcitabine. We reasoned that since our agar plating experiment showed that most resistant colonies have been *nupC* mutants, we could estimate the mutation rate ( $\mu$ ) of in this gene with a Luria Delbrück fluctuation test (Luria & Delbrück, 1943). We compared this mutation rate to a reference gene (*nfsA*) that confers resistance to furazolidone (Lourenço et al., 2016). We performed this experiment as four replicates using four different genetic backgrounds (the strains used for the evolution experiments and the MG1655 lab strain). Figure 2.11 and Supplementary File 4 shows the calculated mutation rates for *nupC* and *nfsA* loci in all strains (normalized to a gene with 1000 basepairs). In all cases we found rates comparable to the average gene mutation rate previously inferred for *E. coli* ( $2.1 \times 10^{-7}$  per gene per generation) (Chen & Zhang, 2013). For BW25113, the mutation rate of *nupC* was 5.7-fold higher than that of *nfsA*. For Nissle, this difference was 6.8-fold and for MG1655 it was 1.8-fold. For F-18 strain, in contrast, the mutation rate of *nfsA* was 7.9-fold higher than *nupC*. While the

mutation rate was not identical in the two genes, the mutation of *nupC* was not always higher than that of *nfsA*, and their rate difference was never larger by an order of magnitude.

Taken together, the results from multiple experiments suggested that *nupC* was likely repeatedly inactivated across multiple genetic backgrounds since it confers high drug resistance without compromising growth. Experiments focusing on the *nupC* mutation revealed that gene inactivation could take place through multiple alternative mutation mechanisms and that the *nupC* locus is not characterized by an exceptionally high mutation rate (excluding the possibility of a mutational hotspot).

#### **2.4.6. A bacterial evolution experiment against gemcitabine in a mouse model of cancer did not show indications of gemcitabine adaptation**

We next wondered if we could find evidence if adaptation to gemcitabine could happen *in vivo* (Figure 2.12A). We generated subcutaneous tumors in BALB/c mice and colonized the tumors with bioluminescent *E. coli* Nissle 1917 (experiment performed by Leore Geller, Weizmann Institute). Colonization was confirmed by bioluminescent imaging and it was successful in many of the mice. Then we treated the mice with gemcitabine (150 mg/kg) or vehicle every four days up to seven times or until the experimental endpoint was reached (maximum allowed tumor size by IACUC). We could isolate colonies from five gemcitabine-treated and two vehicle-treated mice and we evaluated phenotype of these colonies by growing them in high gemcitabine concentration (Figure 2.12B).

We observed no gemcitabine resistance in any of colonies isolated from the gemcitabine-treated mice. Targeted amplification of *nupC* locus and sanger sequencing showed all of the analyzed *nupC* loci were wild-type (a representative result is shown from mouse #2 in Figure 2.12C). In addition, whole genome sequence analysis of randomly selected colonies also did not show indications of gemcitabine resistance. (No deleterious mutations in coding regions identified compared to the ancestor, see the Supplementary File 6)

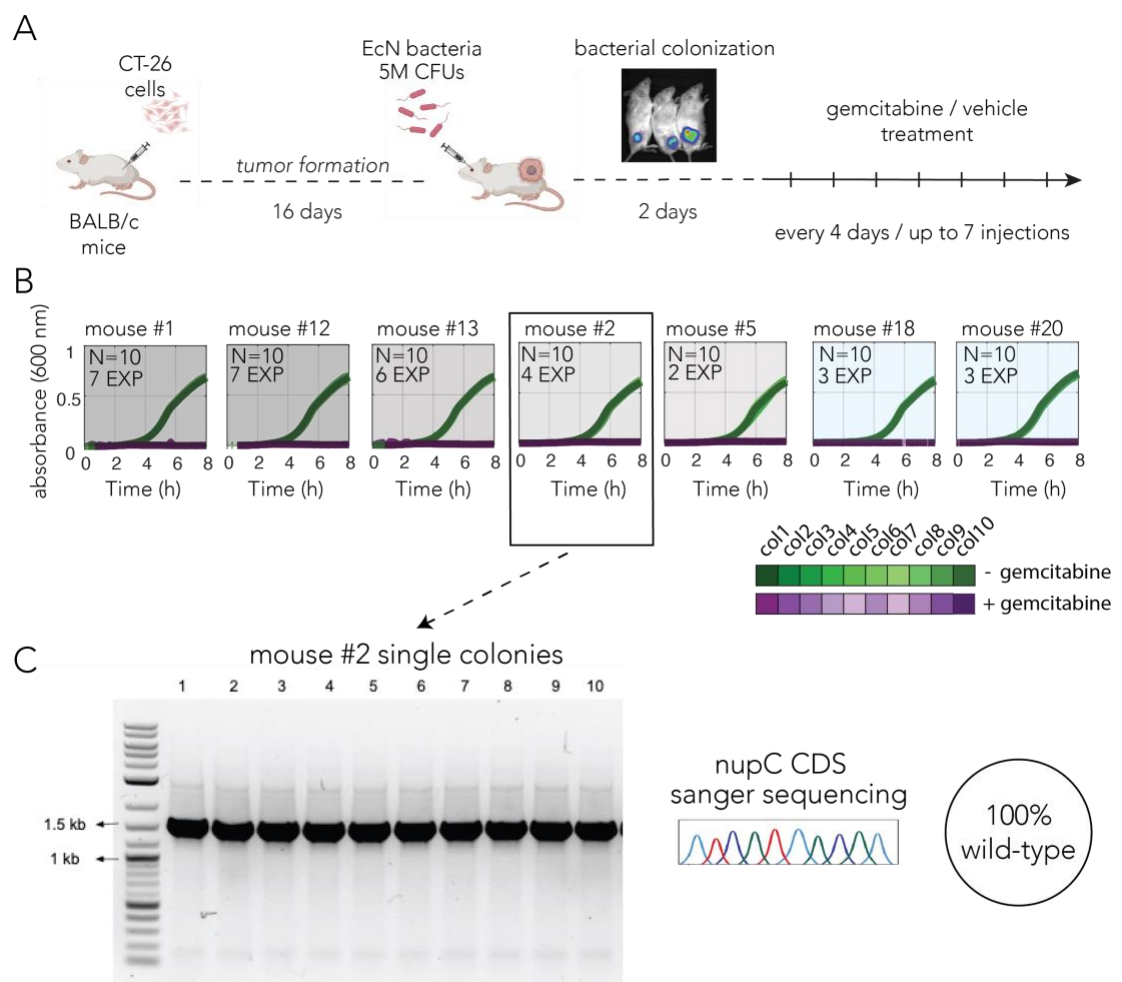


**Figure 2.12: Adaptive bacterial evolution to gemcitabine was not observed *in vivo***

(A) Schematic of the mouse experiment. 6-week old female BALB/c mice (N=20) were injected with one million CT-26 cells on the right flank. After tumors formed and grew for 16 days, mice were injected with five million CFUs of bioluminescent *E. coli* Nissle 1917 retro-orbitally. After two days of bacterial colonization of the tumors (checked with IVIS bioluminescent imaging) mice were treated with vehicle or gemcitabine (150 mg/kg) every four days up to seven exposures or until the experimental endpoint was reached (maximum allowed tumor size). This mouse experiment has been performed by Leore Geller in collaboration with Ravid Straussman's lab at Weizmann Institute, Israel. (B) Growth curves of single bacteria colonies isolated from the mice (10 colony per tumor). Shade of gray background represents the number of gemcitabine exposures, and shade of turquoise background represents the number of vehicle exposures. EXP: exposure). Note that none of the colonies could grow in gemcitabine over the eight hours (C) A single representative result of amplification and sanger sequencing of *nupC* from the colonies isolated from mouse #2. Sanger sequencing showed wild-type *nupC* locus for all of the colonies which aligns with their phenotype in medium with gemcitabine.

## 2.5. DISCUSSION

The recent discovery that bacterial infections are frequent across multiple cancer types suggests that the tumor-microbiome is an important, yet understudied, component of the tumor microenvironment (Cullin et al., 2021; Nejman et al., 2020) Here, we suggest that a key aspect of microbial biology is underexplored in current investigations of the tumor-microbiome – the ability of bacteria to rapidly evolve and adapt to extracellular changes. Within the tumor niche, successful colonization may require bacterial adaptation to the unique conditions of the tumor microenvironment, including adaptation to tumor-targeting therapeutics. A strong selective pressure from chemotherapies likely exists given that multiple antineoplastic drugs are putative antimicrobials at physiological concentrations (Maier et al., 2018). We previously raised the hypothesis that bacterial evolved resistance to tumor-targeting chemotherapies can manifest in changes to bacterial drug metabolism and this type of adaptation can inadvertently influence chemoresistance. Our previous work used the *Caenorhabditis elegans*

model system, its bacterial diet, and two fluoropyrimidine chemotherapy drugs to study this hypothesis (Rosener et al., 2020). In that model system, we estimated that almost 60% of loss-of-function mutations that conferred bacterial resistance would also reduce drug toxicity in a worm host feeding on these bacteria. Here we further study this hypothesis and focus on a different chemotherapy drug and a model system that captures bacterial-drug interactions that may be at play in the tumor microenvironment, rather than in the host gut as in the previous publication.

Research of the bacterial role in pancreatic cancer revealed multiple and independent mechanisms of microbial influence on cancers in this organ (Aykut et al., 2019; Geller et al., 2017; McAllister et al., 2019; Nejman et al., 2020b; Pushalkar et al., 2018; Riquelme et al., 2019). Specifically, recent work suggested that pancreatic colonization by proteobacteria can decrease efficacy of gemcitabine through rapid bacterial drug inactivation (Geller et al., 2017). We used this drug-bacteria-tumor interaction to test our hypothesis by reconstituting similar interactions from individual parts that are well-understood on their own. We first mapped the gemcitabine resistome in *E. coli* and found that changes in multiple cellular processes increase resistance. Importantly, these potential adaptations are easily accessible within short time scales since they only require inactivation of a single gene. A functional assay revealed that one third of these adaptations impact bacterial drug breakdown (Figure 2B). Indeed, gemcitabine administration to co-cultures of cancer spheroids and bacteria demonstrated that two of the top loss-of-function mutations that the screen identified can considerably, and

oppositely, impact drug efficacy in neighboring cancer cells (Figure 2E). While the impact of bacterial resistance on neighboring cells could have been predicted for the *nupC* knockout, it was not trivial for the *cytR* knockout. CytR is a transcription factor that represses at least 14 different operons, including nucleotide transporters and membrane proteins (*nupC*, *nupG*, *tsx*, *ycdZ*), sigma factors (*rpoH*), and metabolic enzymes in the target pathways (*ccd*, *udp*, *deoABCD*) (Keseler et al., 2017). A chemical assay revealed that *cytR* knockdown culminates in increased drug degradation and a co-culture experiment confirmed it increases chemoresistance of neighboring cancer spheroids. It is therefore likely that relief of CytR repression of both *nupC* and *ccd* leads to increased import that is counteracted by even faster gemcitabine deamination. This observation is key since it suggests that mutations conferring gemcitabine resistance in bacteria can both increase and decrease gemcitabine breakdown rate. In the context of the tumor-microbiome, bacterial adaptation to gemcitabine can therefore raise or reduce the tumor's chemoresistance.

A key question that arises from the observation that bacterial resistance can modulate drug availability for neighboring cancer cells, is which adaptations will emerge under drug selection and whether evolution will repeatedly converge to the same resistance mechanism. Results from the serial transfer evolution experiment in three *E. coli* strains showed that drug selection repeatedly yielded adapted clones that disabled the drug permease (Figure 4A). Additional experiments suggested that selection for *nupC* inactivation, at the expense of alternative

resistance mechanisms, is attributed the high resistance this inactivation confers and to the minimal impact it has on growth. Importantly, as the fluctuation experiments reveal, resistant clones can preexist drug exposure and therefore also likely preexist any treatment if the bacterial number in the tumor microbiome is sufficiently large. In such cases, tumor-microbiome adaptation can potentially take place through ecological-like changes and take-over by a resistant bacterial clone. Such clonal expansion in bacteria is reminiscent to the process of clonal expansion and takeover of preexisting resistant cancer cells that is thought to be prevalent in cancer treatment.

Previous research established that the microbiomes, in natural body sites or within tumors, can metabolize tumor-targeting drugs and by doing so influence drug efficacy in the host. Our previous and current studies complement this premise by demonstrating that bacterial evolutionary adaptation to chemotherapies can further influence bacterial drug metabolism and therefore host drug efficacy. Intriguingly, in this work we found that bacterial influence can have opposite effects on drug breakdown and therefore can increase, or decrease, chemoresistance. Moreover, the genetic screens from both works suggest that such occurrences might not be rare, given that such a high fraction of adaptive loss-of-function mutations also alter drug breakdown rates.

While we believe this work illuminates an under-explored and potentially impactful field of research - evolutionary adaptation in the tumor microbiome - we are also excited by the follow-up questions that naturally ensue our in-vitro

findings. Although our *in vivo* evolution experiments did not provide any evidence if bacterial gemcitabine adaptive evolution could happen in actual tumor environments, it still does not conclude this might not happen. Duration of gemcitabine exposure, sensitivity of bacterial strain to gemcitabine, local gemcitabine concentration could have effects on this experimental outcome and more parameters could be further tested (some discussed in appendix) Specifically, following our observations in the model gammaproteobacteria *E. coli*, and the known prevalence of gammaproteobacteria colonization in pancreatic cancer (Geller et al., 2017), it will be intriguing to check if similar adaptations are observed in bacteria isolated from tumors that were resected from pancreatic cancer patients. Identifying convergent adaptation in tumor-microbiome of patients may prove impactful for personalizing anticancer treatment and informing the decision to complement chemotherapy treatment with antibiotics, a decision that is highly consequential for cancer patients and that should therefore be well-justified (Corty et al., 2020; Elkrief et al., 2019; Gao et al., 2020; Meriggi & Zaniboni, 2021).

## Chapter 3. BACTERIAL POPULATION DYNAMICS DURING COLONIZATION OF SOLID TUMORS

### 3.1. SUMMARY

Bacterial colonization of solid cancer tumors is common and can influence disease progression and treatment success. While the clinical implications of intratumor bacteria are widely investigated, little is known about the colonization process itself. We monitored tumor colonization in a mouse model by intravenously injecting of genetically barcoded *E. coli* cells and then sequencing the barcodes of bacteria isolated from the resected tumors. Within a day, intratumor bacterial load reached billions of cells, yet sequencing revealed they originated from only a few dozen of seeding bacteria that generated progenies with highly uneven population sizes. Narrow infection bottlenecks can explain the low progeny number, but not their skewed population sizes. Repeating the experiment with an intratumor injection that circumvents the infection bottleneck still resulted in skewed bacterial populations compared to the inoculum. Our work outlines tumor colonization as a two-phase process: initially, rare and independent infection events allow opportunistic bacteria to rapidly expand and take over the favorable niche, once bacterial load saturates, progenies cycle through rapid growth and contraction cycles culminating in a distinctive population structure.

### 3.2. INTRODUCTION

The human microbiome plays significant roles in cancer progression but it can also influence anti-cancer treatments (Hanahan, 2022; Sivan et al., 2015). Notably, research over the past decade has revealed that solid tumors can frequently harbor their own microbiome (Nejman et al., 2020). Two-thirds of breast and pancreatic tumors harbor intratumor bacteria and even tumors developing in sterile body sites, such as the brain and bones, frequently harbor their own microbiome (Nejman *et al*, 2020). Bacterial presence in tumors is either causative of carcinogenesis (Cummins & Tangney, 2013) or attributed to opportunistic colonization of the immunosuppressive microenvironment that exists after solid tumors have already formed (Niño et al., 2022). The potential importance of intratumor bacteria for anti-cancer treatment has promoted translational and biotechnological research of the tumor microbiome, as well as the use of bacteria to fight cancer. However, the fundamental questions regarding underlying biological processes are still left underexplored. Bacteria gain tumor access either by the direct exposure of a tumor to a natural microbiome site, e.g. retrograde migration of bacteria from the duodenum through pancreatic ducts into pancreatic tumors (Geller et al., 2017; Pushalkar et al., 2018), or through transient translocations through the host's bloodstream (Cummins & Tangney, 2013). Recent work has shown that other microorganisms that commonly compose human microbiomes, including fungi, could also infect tumors (Narunsky-Haziza et

al., 2022). Tumor infection and colonization by other microorganisms might follow similar infection routes as bacterial colonization.

A key gap in knowledge concerns the process of tumor infection and colonization, as existing models remain highly speculative. The suggested models are limited because they rely only on the observed overlap between species composition in specific “natural” microbiome sites and the species identified in tumors in specific body sites (Parhi et al., 2020; Zhu, Wang, Liu, & Wei, 2022). Remarkably little has been empirically observed beyond this association. It therefore remains unclear how bacteria initially colonize the tumor niche and how a multi-species microbiome emerges. It remains unknown if multi-species colonization arises through simultaneous infections by multiple species or whether colonization follows a sequential seeding process reminiscent of gut colonization during development. Moreover, it is unclear if, once established, the tumor-microbiome needs to comprise keystone species that are critical for microbiome maintenance. Lastly, little is known about population turnover of intratumor bacteria, including the growth and death rate of colonizing bacteria and whether population bottlenecks exist in different stages of infection and colonization.

Sequence tag-based analysis of microbial populations (STAMP) has been widely used to understand colonization bottlenecks in many bacterial infection models (Abel et al., 2015; Hullahall & Waldor, 2021; Zhang et al., 2017), and it can also help us understand the bacterial colonization dynamics in solid tumors. In STAMP, a library of bacteria is generated with hundreds to thousands of DNA

barcodes integrated into the genome. All of the bacteria have the same genetic background other than the barcoded region thus they have the same growth dynamics (no barcode induces a fitness advantage). The barcoded region from the DNA can easily be amplified by PCR and sequenced deeply. The number and frequency of barcodes in the sample can be determined computationally from the sequencing data, taking into consideration the sequencing errors. The use of mathematical models allows for the identification of host bottlenecks by calculation of the founding population size (Abel et al., 2015; Hullahalli & Pritchard, 2021; Krimbas & Tsakas, 1971).

Here we tried to answer the following questions regarding the bacterial colonization of solid tumors: i) what is the magnitude of host barriers for colonization of the tumor microenvironment from a systemic infection, ii) how does a bacterial population, once established, expand within the tumor? To achieve this, we first generated a barcoded *E. coli* Nissle 1917 (EcN) library which includes 51,000 unique barcodes. We then colonized mice with subcutaneous colon carcinoma with the barcoded library to study the population dynamics of this tumor colonization. Using intravenous delivery of the bacteria, we first identified the magnitude of the host bottleneck. Then, we used intratumor delivery of bacteria to avoid the colonization bottleneck and studied the dynamics of the bacterial population expansion in the tumor. Our results revealed a very narrow colonization bottleneck in which the number of introduced barcodes was dramatically reduced by 256-fold. In addition, the rank-frequency plot revealed a power law that we are

developing some mathematical models for. We propose that following the extreme colonization bottleneck, bacteria expand within the tumor unequally due to the existence of better and worse niches to thrive.

### **3.3. MATERIALS AND METHODS**

#### **3.3.1. Bacteria and growth conditions**

*E. coli* Nissle 1917 strain (Ardeypharm, GmbH, Germany) was used as a parent strain to build the barcoded library. For all experiments, bacteria were inoculated into Lysogeny Broth (LB) with 50 µg/mL kanamycin and grown overnight at 37°C, 200 rpm orbital shaking.

#### **3.3.2. Construction of the *E. coli* Nissle 1917 Barcoded library**

A kanamycin resistance cassette with 20 random nucleotides, targeting the *lacZ* locus of the *E. coli* Nissle 1917 genome, was amplified using the following forward and reverse primers 5'GTTGTGTGAAATTATGAGCGGATAACAAT TTCACACAGGATACAGCTATTCCGGGGATCCGTCGACC3' and 5'ACGGGC AGACATAGCCTGCCCGGTTATTATTATTTTTGACACCAGACCAANNNNNNNNN NNNNNNNNNNNNTGTAGGCTGGAGCTGCTTCG3'. Genomic DNA from a knockout strain from the KEIO collection was used as a template for the PCR. PCR products were visualized on 1% agarose gel and purified using a commercial kit.

*E. coli* Nissle 1917 cells were transformed with the pSIM6 plasmid by electroporation. These cells with induction of beta, gam, and exo genes, were

prepared from a single transformant as described previously (Datta, Costantino, & Court, 2006; Murphy, 2016) and made competent for future transformations. Multiple transformations were made using 2.5  $\mu\text{g}$  of PCR product per aliquot of competent cells to achieve about 30000 single colonies on LB agar plates with kanamycin after overnight incubation at 37°C. The colonies were then scraped from the agar plates and homogenized in PBS. Frozen glycerol stocks were then stored at -80°C. In order to remove the pSIM6 plasmid, the pooled library was inoculated and grown in liquid LB with kanamycin for three days with daily passaging (1:2000 dilution). The final library was stored as a glycerol stock at -80°C and the experiments were performed using these frozen stocks of the library.

### **3.3.3. Preparation of *E. coli* Nissle 1917 Barcoded library for injection**

100  $\mu\text{L}$  of thawed glycerol stock of the *E. coli* Nissle 1917 barcoded library was inoculated into 20 mL LB with kanamycin (50  $\mu\text{g}/\text{mL}$ ). The culture was grown for 18 hours overnight. In the morning, the culture was diluted 1:100 in 30mL of LB with kanamycin (50  $\mu\text{g}/\text{mL}$ ) and grown until  $\text{OD}_{600}$  of  $\sim 0.5$ . The bacteria were pelleted by centrifugation, and the bacterial pellet was then washed with PBS three times. Washed bacteria were incubated at room temperature for an hour and then the  $\text{OD}_{600}$  was measured. Considering  $\text{OD}_{600}$  of 1 culture contains  $4.71 \times 10^8$  CFU/mL, we diluted the culture for the intratumor (*i.t.*) or intravenous (*i.v.*) injections. For *i.v.* injected conditions, we prepared  $5 \times 10^7$  CFU/mL, and for *i.t.* injected conditions we prepared  $2.5 \times 10^8$  CFU/mL. The timepoint zero samples (T0

sample; total bacteria culture at the time of injection) were frozen as glycerol stocks and gDNA was isolated directly from this stock.

#### **3.3.4. Mouse experiments**

5-week-old female, BALB/cJ mice (Jackson Laboratory, Bar Harbor, Maine) were ordered and acclimated to the new environment for seven days. Next, the mice were injected with  $1 \times 10^6$  CT-26 cells on both flanks subcutaneously. Tumor growth due to injected CT-26 cells was monitored every 2-4 days. When tumor size reached about 300-500 mm<sup>3</sup>, mice were injected with the *E. coli* Nissle 1917 barcoded library as two groups. The intratumorally injected group received  $5 \times 10^6$  CFU per tumor and the intravenously injected group received  $10^7$  CFU per mouse. Mice were euthanized according to experimental endpoints on days 1, 3, or 7 post-bacterial injection. Tumors were immediately processed for CFU plating and the remaining tissue was flash frozen in liquid nitrogen and kept at -80°C. Downstream experiments were performed from the homogenized frozen tumors.

#### **3.3.5. Determination of bacterial CFU in the mouse tumors**

Fresh or previously frozen tumor pieces were chopped into 1-2 mm long pieces using a sterile scalpel in a petri dish. Approximately 200 mg of chopped tumor was added into a lysing matrix I tube (Cat# 6918100, MP Biomedicals) filled with 300 µL PBS. These samples were then homogenized twice at a speed of 6m/s for 40 seconds using the MP Biomedicals Fastprep-24 instrument. The homogenate (20 µL) was serially diluted 1:1000, 1:10000, and 1:100000 in 200 µL

and then 100  $\mu$ L of these serial dilutions was plated on LB+kan plates. Plates were incubated overnight and each plate's colonies were counted the next day. The dilution that had the most reasonable number of colonies (100-500) was used to determine the CFU from the tumor piece homogenate. The weight of the homogenized tumor piece and the total tumor weight were used to calculate the total CFU per tumor.

### **3.3.6. Barcode Sequencing Library Preparation**

Total DNA was purified from the homogenized frozen tumor samples using the Zymo Quick-DNA Midiprep plus kit (Cat# 4075). Precise DNA concentrations were determined using Qubit High Sensitivity DNA reagent (Thermo-fisher, Cat#Q32854). Since the total gDNA contains high amount of host DNA relative to bacterial DNA, we used 10  $\mu$ g of DNA as template for each PCR. A region of ~400 bp around the barcoded region was amplified using 2x KAPA HiFi HotStart ReadyMix (Kapa Biosystems, Cat#KK2602) and the following forward and reverse primers: 5' TCGTCGGCAGCGTCAGATGTGTATAAGAGACAG(1-3N)cctgcccggttattattattttg3' and '5GTCTCGTGGGCTCGGAGATGTGTATAAGAGACAGgattcatcgactgtggcc 3'. The cycling parameters were: 98 °C initial denaturation for 3 min; 23 cycles of 98 °C denaturation for 20 secs, 68.6 °C annealing for 15 secs and 72 °C extension for 30 secs; 72°C final extension for one minute. Four to seven PCR reactions were set up per sample depending on the amount of DNA extracted from the tumor tissue. Each technical replicate PCR was pooled into a single tube (10  $\mu$ L per replicate) and the pooled products were run on a 3% agarose gel. The

amplicon was gel purified, and the concentration was determined using Qubit high-sensitivity DNA reagent. We performed a second 13-cycle PCR using Illumina Nextera XT indexes and 2x KAPA HiFi HotStart ReadyMix for multiplexing. The products were run on a 3% agarose gel and purified. Libraries were normalized to the same concentration, denatured, and diluted according to Illumina NextSeq System Denature and Dilute Libraries Guide. Sequencing was performed using Nextseq 500/550 High Output Reagent Kit, 75 cycles on Illumina NextSeq 500 device.

### **3.3.7. Targeted Barcode Sequencing Analysis**

We used Bartender (L. Zhao, Liu, Levy, & Wu, 2018) to extract and cluster the barcodes from raw fastq files. Multiple technical replicates of time zero injection fastq files were merged together for the analysis. We first ran bartender extractor (bartender\_extractor\_com) with an average base quality score cutoff of 30 and allowing no mismatch on upstream and downstream anchor sequences using the following parameters: “-q ? -p ACCAA[20]TG TAG -m 0”. Next, we ran bartender clustering (bartender\_single\_com) with these parameters: “-c 10 -d 2 -z 10 -l 5 -t 1 -s 1”. After the clustering, we used bartender\_combiner\_com to create outputs with multiple time points combining barcodes from the T0, T1 (day 1), T3 (day 3), and T7 (day 7).

A MATLAB script was used to further organize the barcode clusters. First, common barcodes in technical replicates of timepoint zero samples were identified and then the union of those barcodes was used to get the total time zero barcode

clusters. Then, all of the samples were organized in the same order of barcode clusters and read counts were normalized to reads per million. Technical replicates were averaged and metadata information was incorporated. This data structure referred as “meta” has been used in downstream analyses.

## 3.4. RESULTS

### 3.4.1. Generation of *E. coli* Nissle 1917 barcoded library

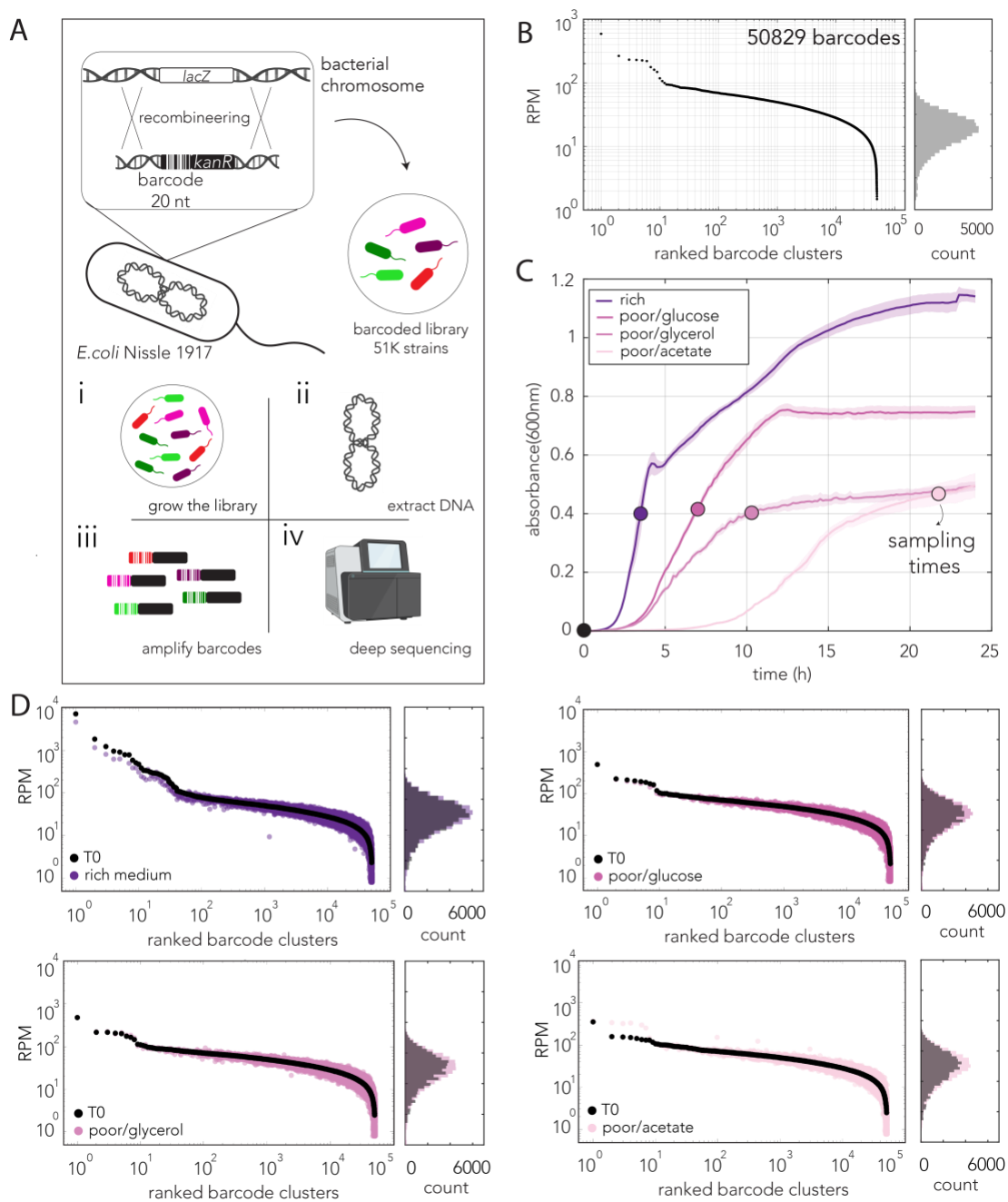
We first generated an isogenic but individually barcoded EcN library. We chose the *lacZ* gene locus as the integration site for the 20-nucleotide random barcode and kanamycin resistance cassette, resulting in a library with the *lacZ* gene deleted. The lambda red recombination method was used to integrate the PCR product pool that contained random barcode sequences, producing thousands of colonies on selective agar plates (Figure 3.1A). We generated a pooled library by scraping the colonies from multiple selective agar plates and growing them for two passages in rich media to remove the retained plasmids. The barcoded region was amplified with specific primers from the extracted gDNA and sequenced deeply using illumina sequencing. We used bartender software previously published to extract and cluster the barcodes, which yielded 50829 individual barcodes (Figure 3.1B). We expected a similar frequency of each barcode in the pool which was represented in the results. Note that the range of barcode frequencies are within one-log-fold higher or lower than the frequency of the majority of barcodes. Next, we wanted to know if differences in growth rates across individual members of the library would affect barcode frequencies when the library is grown in vitro. In order to achieve this, we grew the barcoded library in different media types with varying carbon sources and sampled the cultures when they reached similar densities as shown in

Figure 3.1C. We then analyzed the changes in the barcode frequency distributions (Figure 3.1D). We observed that the overall pattern in barcode frequencies did not dramatically change, however we detected a minor fluctuation. This result shows that each barcoded clone has a similar growth rate in a controlled environment and individually barcoded bacteria populations expand similarly with a minor level of intrinsic noise.

### **3.4.2. Exploring the host bottlenecks during tumor colonization**

After characterizing the barcode frequency distributions and growth dynamics of the library *in vitro*, we performed a mouse experiment to understand the host bottlenecks during bacterial tumor colonization. Schematic representation of the mouse experiment is illustrated in Figure 3.2A. Briefly, immunocompetent BALB/c mice were subcutaneously injected with CT-26 cells to form tumors on both flanks. Once the tumors reached  $\sim 300\text{-}500\text{mm}^3$ , we injected each animal with a total of 10 million CFUs of the EcN barcoded library ( $\sim 200$  bacteria cells per barcode) intravenously into the tail vein. Mice were euthanized on days one, three, and seven post-bacterial injections for analysis of bacterial CFUs and barcodes from the harvested tumors. Figure 3.2B shows the changes in bacterial CFUs and detected barcodes. On day one, we observed a dramatic increase in total CFUs per tumor compared to the injected bacteria count ( $>10^4$  fold). On days three and seven, this bacterial number stayed at similar levels suggesting that the tumors quickly reached the bacterial carrying capacity already by day one. Detected barcodes, in contrast, decreased dramatically after day one, (256-fold reduction

compared to inoculum), and remained steady as similar numbers of barcodes were observed on days three and seven.



### Figure 3.1: Cloning and growth dynamics of *E. coli* Nissle 1917 barcoded library

Generation of the barcoded library (top). PCR product pool containing 20 nucleotide random barcode region, kanamycin resistance gene and homology arms to *lacZ* gene were integrated into the genome of *E. coli* Nissle 1917 using lambda red recombinase. A total pool of ~51,000 barcoded bacteria were generated (bottom) Preparation of the amplicon library. Library is grown in specific media/growth condition (i), genomic DNA is extracted at designated timepoint (ii), barcoded region is amplified with PCR including sequencing adapters and indexes (iii) deep sequencing is performed on Illumina platform (iv) (B) Ranked barcode frequency distribution of the initial library and overlaid histogram of the normalized read counts, RPM: reads per million (C) Growth curves of the library in four media types. Rich: LB medium, poor/glucose: M9 media with 0.4% glucose, poor/glycerol: M9 media with 0.4% glycerol, poor/acetate: M9 media with 0.4% acetate (D) Ranked barcode frequency distributions with overlaid histograms of the library after grown in four media types. Sampling times are shown in C. Initial barcode frequency at timepoint zero is shown in black and the barcodes are ranked according to zero timepoint.

This data suggests that the bacterial population goes through a major bottleneck when colonizing the tumor since the detected number of barcodes is significantly reduced compared to the inoculum even though the number of bacterial cells within the tumor is tremendous. In addition, this data also shows that there are no further bottlenecks in the tumor environment after the initial colonization since the number of detected barcodes remains constant at later time points. We also compared the number of detected barcodes between the right and left flanks and observed a significant correlation (Figure 3.2C). We did not observe any overlap between the detected barcodes from the right and left tumors. Furthermore, we did not observe a correlation between number of detected barcodes and carrying capacity of a tumor neither (Figure 3.2D). A representative mouse from day one is shown in Figure 3.2E. Highly variable frequency distributions of the detected barcodes indicate that there is an unequal expansion of individual barcodes which is different than our *in vitro* results. A great reduction in barcode diversity can be observed by the Shannon entropy index in Figure 3.2F.

In addition, the Shannon equitability index quantitatively shows that the distribution of the barcodes in the inoculum was very even, but this evenness was greatly reduced in the tumors after colonization (Figure 3.2G)

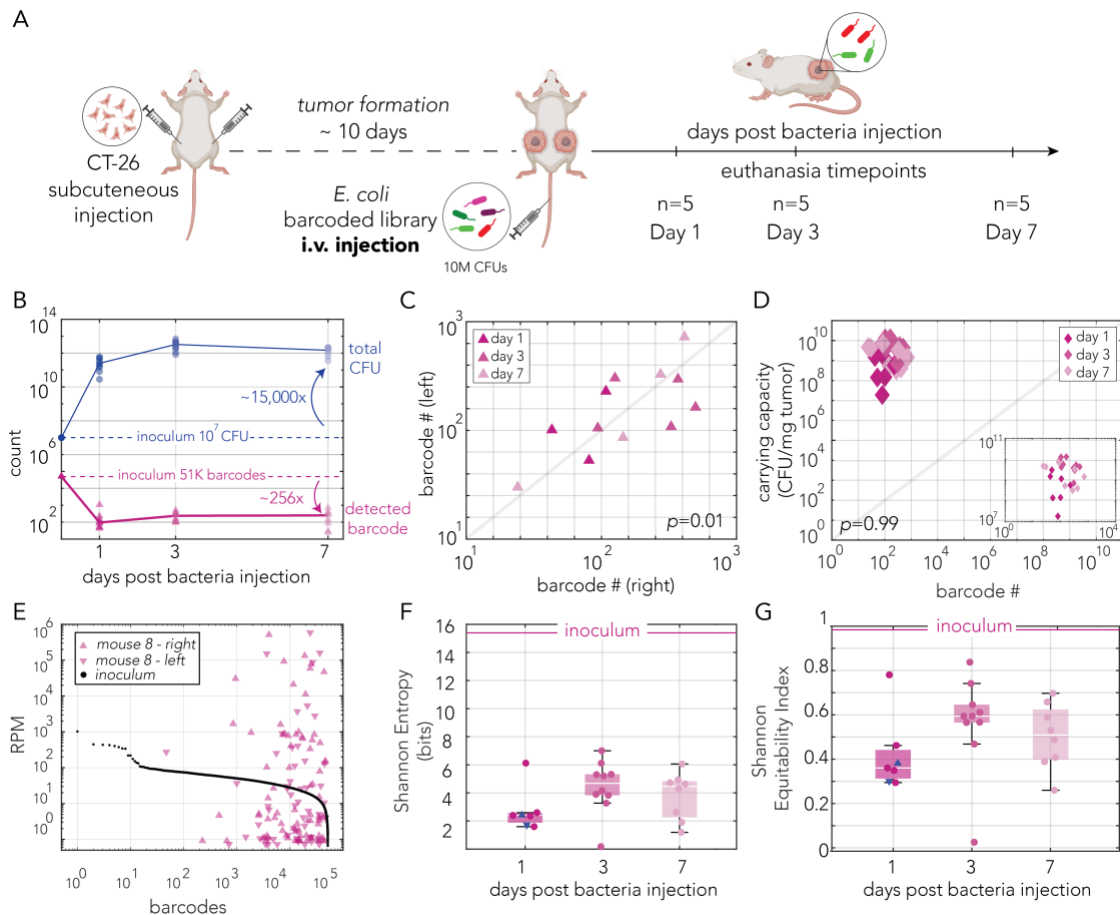


**Figure 3.2: Colonization of the tumor by systemic infection reveals a major host bottleneck**

(A) Schematic illustration of the mouse experiment. Mice were injected on both flanks with one million CT-26 cells subcutaneously. After tumors are formed, ten million CFUs of the EcN barcoded library was delivered by intravenous injection from the tail vein. Mice were euthanized on days 1, 3 and 7 and the tumors were collected. (B) Bacterial population dynamics and detected barcode count across days. CFUs and barcode number in the inoculate population are shown as dashed lines. (C) Number of barcodes plotted from the tumors on the right and left flanks across groups sacrificed on different days. Significant Pearson correlation has been observed ( $p=0.01$ ) (D) Carrying capacity of the right and left tumors from the same mice. ( $p=0.99$ , Pearson Correlation) (E) Ranked barcode distributions from the inoculum and a selected representative mouse (F) Shannon entropy measurement of the barcodes (in bits) Inoculum is shown as a reference. (G) Shannon equitability measurement of the barcodes. Inoculum is shown as a reference.

### 3.4.3. Exploring bacterial population expansion within the tumors

After finding a narrow host bottleneck during bacterial tumor colonization by introducing our barcoded library systemically, we wanted to bypass this initial bottleneck by delivering bacteria intratumorally and analyzing how barcode populations expand within the tumor. This could give us a better understanding of the population dynamics without a reduction in barcode number. Figure 3.3A shows a schematic of the experimental timeline. We generated the same mouse model with subcutaneous colon cancer tumors on both flanks, but this time we delivered bacteria by intratumor injection (5 million CFUs injected into each tumor). We euthanized the mice on days 1, 3, and 7 post-bacteria injection and analyzed the barcodes and bacteria numbers from the tumors. Figure 3.3B shows the changes in bacterial CFUs and detected barcodes. We observed comparable numbers of bacterial load to the *i.v.* experiment within the tumors, and the bacterial population increased to billions of cells even on day one post-injection. Delivering bacteria directly into the tumor removed the narrow bottleneck which existed in *i.v.* administration of bacteria, and we detected only ~3 times fewer barcodes from within tumors compared to the inoculum (Figure 3.3B). A representative mouse from the group sacrificed on day one, is shown in Figure 3.3C. We observed unequal expansion of the barcodes within the tumor which indicates that there could be certain areas within the tumors that provide a better fitness for the bacteria. Rank-frequency plot (Figure 3.4), showed the presence of inverse power

law (Zipf's law), in which the frequency of each clone is inversely correlated with its rank making a slope of -1 as seen in our data (in collaboration with Motasem Elgamel and Andrew Mugler).

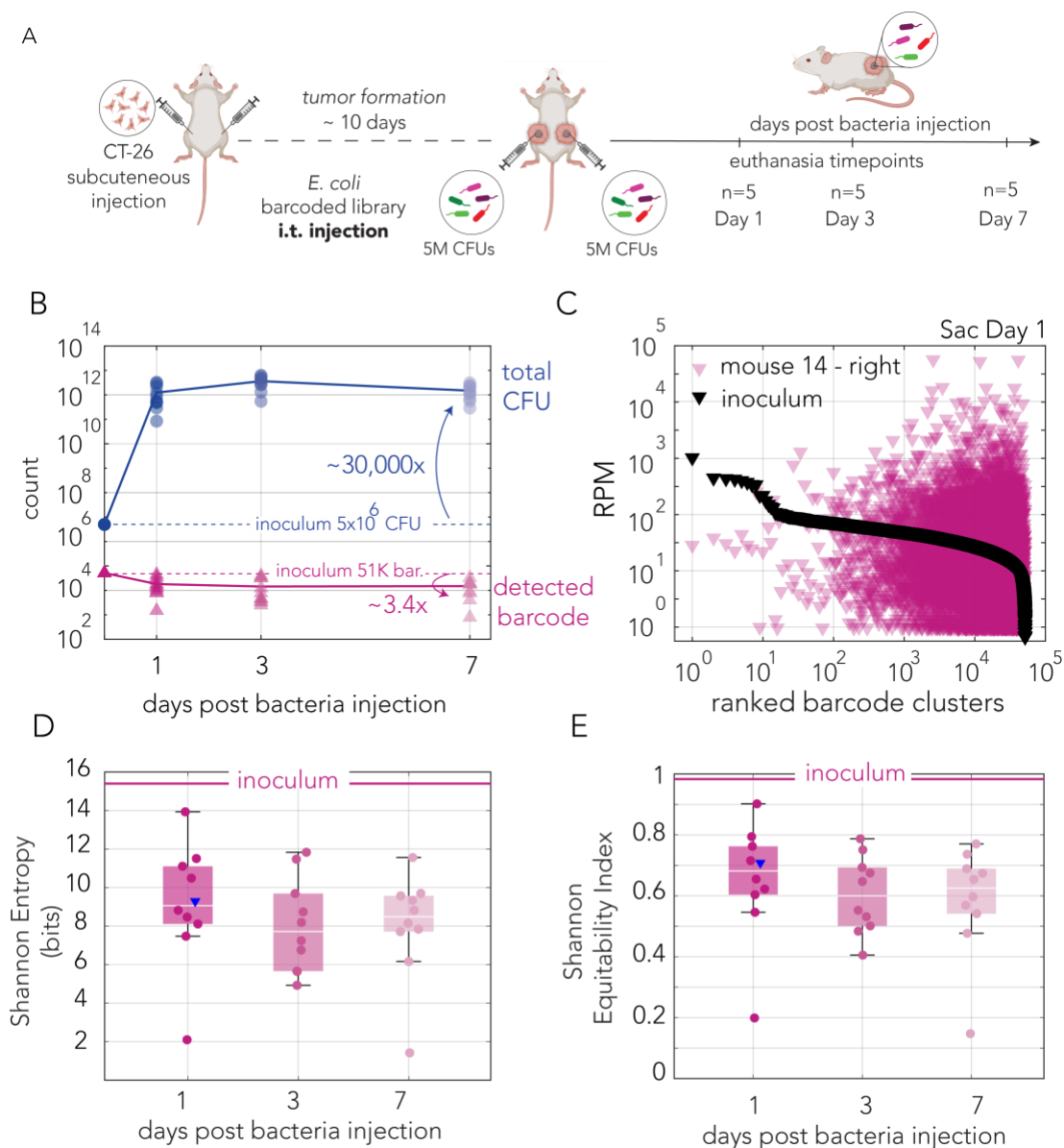


**Figure 3.3 : Unequal barcode expansion in the tumor suggest presence of micro-niches in the tumor which are advantageous for bacterial growth**

(A) Schematic illustration of the mouse experiment. Mice were injected on both flanks with one million CT-26 cells subcutaneously. After tumors were formed, five million CFUs of EcN barcoded library was delivered by intratumor injection. Mice were euthanized on days 1,3 and 7 and the tumors were collected. (B) Bacterial population dynamics and detected barcode count across days. CFU and barcode number in the inoculated population are shown as dashed lines. (C) Ranked barcode distributions from the inoculum and a selected representative mouse (D) Shannon entropy measurement of the barcodes (in bits) Inoculum is shown as a reference. (E) Shannon equitability measurement of the barcodes. Inoculum is shown as a reference.

Furthermore, the Shannon entropy index shows a small reduction in barcode diversity because of *i.t.* injection of the bacteria circumventing the major host colonization bottleneck observed in *i.v.* injection of the bacteria (Figure 3.3E). Lastly, the Shannon equitability index shows a minor reduction in the evenness of barcode frequency distributions, with two outliers. In those specific cases, we observed that the population was dominated by a few barcodes which grew much better than the rest of the population in the tumor environment.

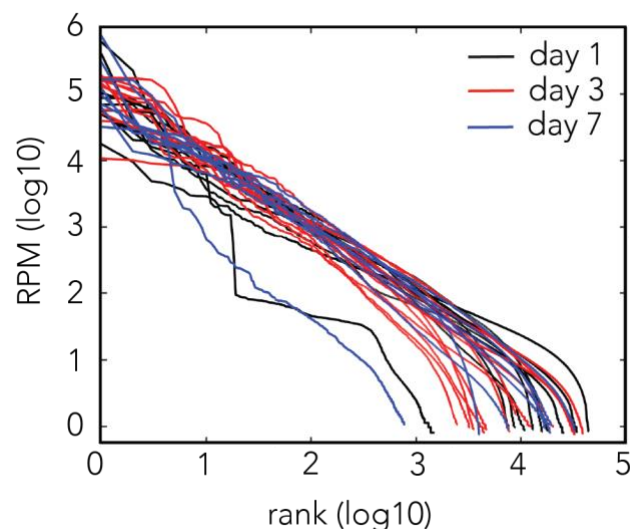


**Figure 3.4: Ranked frequency distribution of barcodes from the *i.t.* experiment with a slope of -1 indicative of power law**

### 3.5. DISCUSSION

Research in recent years has explored many aspects of the microbiome and cancer. Some of the themes that have been explored include the composition of bacteria in tumors, bacterial contribution to tumorigenesis, bacterial interactions with the host cells, and tumor-targeting drugs. Limited evidence shows that in most cases bacteria inside the tumors originate from commensal sites or from infections of the host (Christaki & Giamarellos-Bourboulis, 2014; Cummins & Tangney, 2013). These events potentially could cause homing of the bacteria in the tumor microenvironment, since some bacterial species are naturally attracted to tumors, or some could act opportunistically due to the immunosuppressive nature of the tumors (Cummins & Tangney, 2013; Duong, Qin, You, & Min, 2019). Proposed mechanisms in the literature about how bacteria colonize the tumors specifically provide information about the population sizes and some mechanisms (Leschner et al., 2009; Stritzker et al., 2007), however, they are not sufficient to build a quantitative model of infection and understand the founding population bottlenecks.

In this study, we aimed to define the magnitude of host bottlenecks during bacterial colonization of tumors and explore the growth dynamics of this population. To achieve this, we first generated a library of genetically identical EcN

that only varies in a barcoded 20 nucleotide region in their genomic DNA. This library harbors bacteria cells with ~51,000 unique DNA barcodes (Figure 3.1).

Next, we generated subcutaneous colon cancer tumors on the right and left flanks of BALB/c mice and colonized the tumors with the barcoded bacteria library we generated. We colonized the tumors with our barcoded bacteria library using two different methods: i) via intravenous injection through the tail vein thereby creating a systemic circulation of bacteria cells (referred as i.v. experiment), ii) via intratumor injection which directly delivers the inoculum to the tumor niche (referred as i.t. experiment). By identifying the number of barcodes in the i.v. experiment, we aimed to quantify the bottleneck size that the bacterial population experienced. Out of the 51,000 barcodes we inoculated, we found an average number of 203 barcodes per tumor across all days (Figure 3.2B). This 256-fold reduction in the barcode number indicates that there is an extremely narrow bottleneck during the colonization process. The barcode frequency distribution within the tumors showed a skewed distribution compared to the even expansion of the individual barcodes with a small intrinsic noise in liquid media *in vitro* (Figure 3.2E). There could be multiple reasons that cause this behavior. We thought that some bacteria could have gained adaptive mutations that could give them a better fitness advantage in the tumor environment. To eliminate this possibility, we isolated single colonies with the most abundant barcodes in each tumor (*i.v.* experiment) and performed whole genome sequencing (Supplementary File 7). We did not identify any mutations in these colonies, suggesting that the growth

differences are not due to adaptive mutations (except a 10bp deletion at coding region of sigma-54-dependent Fis family transcriptional regulator, which we think exists in the library ancestor). Another scenario that might explain uneven expansion is that bacteria arrive at the tumor at different time points following the injection. However, this is also very unlikely since previous studies have shown that bacteria are mostly cleared from the blood rapidly in immune-competent mice (Hullahalli & Waldor, 2021). Another plausible explanation could be that there are certain areas within the tumor that provide a better growth advantage for the bacteria given that the tumors are heterogeneous, with areas of hypoxia, altered vascularization, and necrosis present. To focus on the expansion dynamics better, we circumvented this initial tight colonization bottleneck by delivering the bacteria intratumorally in the second experiment. As expected, we detected many more barcodes within the tumor compared to *i.v.* injection of the bacteria (Figure 3.3). However, we still observed uneven expansion of the barcodes within the tumor with comparable levels of bacterial carrying capacity of the tumors to the *i.v.* condition. Ranking the barcode frequency distribution in descending order (Figure 3.4) we have found that a power law exists in this data. The pattern the barcodes show are in alignment with Zipf's law specifically, in which the rank of each barcode is inversely proportional with its frequency (Motasem Elgamel and Andrew Mugler). More advanced mathematical models are required to understand this population structure and why such pattern exists that we are currently developing.

Overall, our study shows that there are extreme colonization bottlenecks during bacterial tumor colonization. Although the bacterial population expands very rapidly within the tumor, this expansion is not even across the individual bacterial cells compared to their frequency in the inoculum. Understanding these bacterial population dynamics in the tumors will allow us to perform further experiments to understand bacterial evolutionary adaptation in tumors and perform *in vivo* genetic screens in the presence of anti-cancer drugs.

## **Chapter 4. DISCUSSION**

### **4.1. INTRA-SPECIES BACTERIAL EVOLUTION AGAINST ANTI-CANCER**

#### **DRUGS**

Humans and the microbiome have coevolved together since the bacteria living in our bodies are intertwined with many host factors, nutrients, xenobiotics, and drugs. Moreover, the bacterial metagenome and metabolome are significant contributors to host health due to novel biotransformation reactions compared to human metabolic capacity. Many researchers showed experimental evidence of microbial biotransformation of host-targeted drugs, changes in the efficacy of the drugs for the host, along with inhibition of the bacterial species of the human microbiome by the host-targeted drugs themselves (García-González et al., 2017; Lehouritis et al., 2015; Maier et al., 2018; Rosener et al., 2020). These complex interactions have been propelling many research projects. 16S rDNA analyses allow researchers to tackle taxonomic changes in the microbiome, gain of function

genetic screens help identify the genes responsible for certain chemical transformations to drug structures, and analytical chemical assays help discover specific functional modifications to drug structures. Analysis of the conditioned supernatants in which bacteria and drugs are coincubated, by mass spectrometry allows for identifying the precise chemical modifications.

One aspect that is often overlooked by many is what kind of genetic diversity exists within a single given species within the microbiome and how this could affect the host treatment. The number of *de novo* mutations arising in the human microbiome daily is enormous and estimated to be  $2 \times 10^9 - 6 \times 10^{12}$  SNP/Microbiome/Day (Barrick & Lenski, 2013; Korem et al., 2015; Nayfach & Pollard, 2015; Sender et al., 2016; S. Zhao et al., 2019). On top of that, some drugs are administered chronically to the patients. If some bacteria species are inhibited by those drugs, this could lead to a positive selection of mutants naturally occurring in that bacterial population. Investigating the adaptation of bacteria to host drugs that potentially have antimicrobial activity might provide insights into how such interactions can change in a longitudinal way over the course of treatment and how treatment strategies should be modified temporally.

Metagenomic datasets with relevant patient cohorts could help discover diversity of intra-species genetic diversity within the microbiome, however, this kind of datasets still has bioinformatics challenges. It is very hard to identify *de novo* mutations when very close species within the sample exist (Schloissnig et al.,

2013). In addition, recent concerns in the field indicate that some databases including bacterial draft genomes could be contaminated with human DNA fragments that cause false positive results (Gihawi et al., 2023). The gold standard in finding naturally occurring genetic variants in the microbiome is culture-based genomic analysis of the bacteria (S. Zhao et al., 2019). Finding mutations in the same set of genes again and again across individuals or dramatic increases in the frequency of mutations at a certain gene could point to such adaptations (Garud et al., 2019; Lieberman et al., 2011; S. Zhao et al., 2019). However, high variability in host genetics and finding enough subjects to gather sufficient specimens could be challenging in such types of studies.

Our work investigated the possibility of bacterial host-targeted drug adaptation using a simple model system of *E. coli* and the antimetabolite gemcitabine. We took a systems biology approach to understand what could be evolutionarily possible and what would the implication be for the cancer cells. Previously, proteobacteria have been described to transform gemcitabine into nontoxic dFdU (Geller et al., 2017; Lehouritis et al., 2015; Voorde et al., 2014). Since *E. coli* is involved in gemcitabine biotransformation, and *E. coli* growth is also inhibited by gemcitabine, we hypothesized that prolonged exposure to gemcitabine could drive the adaptive evolution of *E. coli* (a model proteobacteria). This is especially relevant since proteobacteria are a highly abundant phyla in pancreatic ductal adenocarcinoma cancer patients, in which gemcitabine is frequently used as chemotherapy either alone or in combination with other

chemotherapies. We first mapped the *E. coli* resistome against gemcitabine by performing a genetic screen and found many loss-of-function mutants with various biological functions. Our lab evolution experiments with gemcitabine have shown that *E. coli* can naturally develop resistance to gemcitabine in a very short time scale. Whole genome sequence analysis has shown that this resistance is dictated by a single evolutionary mechanism: loss of function mutations in the nucleoside permease *nupC* but not through other mechanisms found in our genetic screen. We hypothesized that there could be a mutational hotspot in the *nupC* locus that could explain why evolution converges to this gene, but we did not observe a significantly high mutation frequency in this locus. In addition, we could not find any gemcitabine adaptive mutations when we performed our evolution experiment *in vivo* using a syngeneic mouse model with *E. coli* colonized tumors. Possible reasons that could explain this are not having an inhibitory concentration of gemcitabine in the tumor tissue, or not having enough generation times for the bacteria to go through adaptive evolution and selection during the experiment. I discuss alternative experimental strategies to address these points and some preliminary data that we collected from those experiments in the appendix of this thesis. As the next step, bacterial genomes from patients who went through gemcitabine treatment could be used to find evidence of bacterial adaptation to gemcitabine.

## **4.2. DO TUMOR MICROBIOMES IN HUMANS ADAPT TO GEMCITABINE OR OTHER CHEMOTHERAPIES?**

Bacteria go through adaptive evolution in many niches within the human microbiome. For instance, experiments with gnotobiotic mouse models have shown that mutations in the *gat* operon, encoding enzymes for galactitol metabolism, are very essential during gut colonization (Barroso-Batista et al., 2014). Similarly, bacteria in our bodies experience many perturbations that could generate genetic diversity within a single species. Indeed, many studies looked beyond the 16S rDNA data and evaluated intra-species genetic diversity in the human microbiome. While various bacterial species can have a two-fold magnitude difference of SNP per kilobase, functional genes in the categories of conjugation and antibiotic resistance were enriched in their SNP per kilobase value compared to other functional categories (e.g. 38 SNP/kb for clindamycin resistance transfer factor *BtgA*) (Schloissnig et al., 2013). Furthermore, the analysis of the ratio of non-synonymous SNPs to synonymous SNPs could be used to measure the selective constraints on the species. Additionally, looking into genomes of bacteria from the pancreatic tumors of the patients who went through gemcitabine treatment could provide evidence if such adaptations exist in real microbiome niches. Such analyses, if the adaptation is happening, can provide insights into which gene groups we identified in our genetic screen are under selective pressure when gemcitabine is administered in human patients. Since we know the list of genes whose mutations provide gemcitabine resistance from our genetic screen and lab

evolution experiments, we can target those specific regions of the bacterial genomes in the analysis. However, we also need to keep in mind that natural microbiome environments can have more diverse resistance mechanisms since horizontal gene transfer is very common in such environments. Our genetic screen and lab evolution experiments do not capture these mechanisms and yet, we do not have any evidence if these mechanisms actually happen in actual tumor microenvironments. However, our experiments shed light on what could be possible and how it would impact the host through the evolutionary mechanisms that are achieved with a single-step modification.

#### **4.3. UNDERSTANDING BACTERIAL DYNAMICS IN THE TUMORS**

Many independent small- and large-scale studies have reported the presence of microorganisms within solid tumors across many malignancies. While some bacteria and viruses may cause cancer, some colonize the tumors after they are formed due to favorable microenvironments within the tumor for bacterial growth e.g. necrosis, hypoxia, and immune suppression (Cummins & Tangney, 2013). However, recently there has been new evidence that weakens the results of a few major studies that report bacterial presence in solid tumors. For instance, the reproducibility project: Cancer Biology (a collaborative effort between the Center for Open Science, Science Exchange, and eLife magazine) aimed to repeat experiments from 53 cancer biology papers that were published between 2010 and 2012. Surprisingly, while they could replicate some of the results, there were

instances that their replicate experiments yielded weaker and less significant results. Castellarin et al., had reported that *Fusobacterium Nucleatum* was significantly enriched in CRC tumors compared to matched healthy tissues (Castellarin et al., 2012). The replication study showed that not all CRCs had *Fusobacterium Nucleatum* (Repass et al., 2018). Furthermore, among tumors that were positive for *Fusobacterium Nucleatum*, there was an abundance when compared to healthy tissue, but it was not statistically significant (Repass et al., 2018). An eLetter was recently posted as a commentary by Noel Fcc De Miranda and others, claiming that bacteria were present in only 63% of their breast tumor samples and that these bacteria were not, in fact, inside the cancer cells, but only in immune cells and ducts. This result contradicts with the findings of intracellular localization of bacteria (in cancer cells) by Nejman et al., 2020. Poore et al., have used genomic sources and computational approaches to identify microbial signatures from the tumor DNA and RNA sequences from TCGA data by filtering out the contaminating sequences (Poore et al., 2020). This study is an example of how computational approaches could be used to gain insights into the tumor microbiome from sequencing data, however, major concerns about the methodology have recently been identified by others in a preprint, invalidating some of the findings (Gihawi et al., 2023). They claim that the database used by Poore et al., contains draft bacterial genomes with human DNA contamination which yielded false positive identification of bacteria in the samples increasing the bacterial fraction relative to the host cells. In addition, they claim that the

normalization method used in the study has introduced biased bacterial signatures that normally would not exist within the data. Additionally, it's important to keep in mind that TCGA data has not been generated for the purpose of studying the tumor microbiome, so the sample acquisition and processing might not be totally aseptic. The library preparation method also might not capture all microbial genetic products due to differences between eukaryotes and prokaryotes (Ajami & Wargo, 2020).

While these concerns exist in the field, the consensus is that bacteria are present in many types of human tumors at least in some cancer types and some patients. One of the major questions then is where these bacteria originate from. The current understanding is they mostly originate from natural microbiome sites or the infections of the host. In our study covered in chapter 3 of this thesis, we wanted to understand the basic and fundamental features of this process 1) what is the magnitude of host bottlenecks during bacterial colonization of tumors, and 2) how does the bacterial population grow within the tumors. Some preliminary experiments performed in our lab have led us to hypothesize extreme bottlenecks could occur during bacterial colonization of solid tumors. Those experiments are overviewed separately in the Appendix section of this thesis. To study these questions, we chose to use a syngeneic mouse tumor model in which the tumors could be colonized with an *E. coli* library with 51,000 unique DNA barcodes. This mouse model is well established in the field; however the precise dynamics of the bacterial colonization have not been studied. We first generated a systemic

bacterial injection (through *i.v.* route) to colonize the tumor using an individually barcoded *E. coli* Nissle 1917 library. We sequenced the barcodes from the mice euthanized on the 1<sup>st</sup>, 3<sup>rd</sup> and 7<sup>th</sup> days of bacterial injection. The proportion of host DNA to bacteria DNA was very large in these samples which could introduce another bias to the analysis. We overcame this issue by saturating the sequencing library preparation with high amounts of DNA input and performing two technical replicates for the sequencing (in which two replicates correlated with each other). Compared to the inoculum, we only detected a few hundred of the barcodes from the tumors, which showed presence of an extreme host bottleneck. We did not observe a reduction of detected barcodes from the tumors isolated at later time points (Day 3 and 7, suggesting that the host bottleneck only exists during/before the initial colonization. A dramatic increase in bacteria number even on day one already shows that the tumor is a favorable environment for bacterial growth and suggests that the system probably reaches a saturation sooner than one day. Secondly, we found distinctive growth dynamics of bacteria in the *i.t.* condition. The ranked frequency plot of the barcodes detected within the tumor indicated presence of a power law with a slope of -1 (Figure 3.4). Furthermore, changes in barcode frequencies within the tumor compared to the inoculum, shows that the population grows differently than the *in vitro* conditions. This led us to hypothesize that there could be certain areas that bias the population growth by providing unique micro niches with varying fitness advantage. Spatial analysis of the barcodes within the tumor samples could help us to further understand these local

dynamics. More advanced ecological models are required to understand this behavior and the rich data that we collected from these mouse experiments more in more detail.

Studying the population dynamics in these complex environments that bacteria can colonize enhances our understanding of the tumor microbiome and also allows us to develop further experiments to understand bacterial adaptation in this environment. Similar studies in the literature exist to understand bacterial colonization and bottlenecks in the gut environment, as well as pathogen dynamics in systemic infections (Abel et al., 2015; Hullahalli & Waldor, 2021; Mahmutovic et al., 2021). With better understanding of population dynamics in tumors, we can perform *in vivo* genetic screens to find the important mechanisms required for bacterial tumor colonization and also bacterial adaptation to chemotherapies. In these screens, the first step is to be able to colonize the tumor with a genome-wide loss of function or gain of function libraries. Given the size of the bacterial genome and number of genes to be screened, these libraries contain ~ 4000 mutants. What we observed in our experiment, can have a detrimental effect on the experimental results that are not necessarily due to the condition being assayed. Solving the challenges of relaxing this bottleneck to maximize the delivery of all mutants to the tumor, can allow us to study more sophisticated bacterial adaptive evolution strategies in this environment.

#### **4.4. CONCLUSIONS**

Intra-tumor bacteria can affect the efficacy of the anti-cancer treatments. We provided evidence that, bacteria themselves can be inhibited by anti-cancer treatments as well and this growth inhibition could drive adaptive evolution. Evolutionary mechanisms bacteria gain through the adaptation process can change the interaction of bacteria and drugs and eventually alter the efficacy of the treatment for the host (cancer cells). In our model system, we showed that convergent loss of function in nucleoside permease *nupC*, increased the gemcitabine efficacy for the cancer cells. As the next step, it's crucial to explore the cancer patient microbiomes in order to understand if intra-species adaptation to anti-cancer drugs happens in the actual tumor environment with the complex set of bacterial species.

Additionally, we studied bacterial colonization process in tumors using a murine model. We discovered a major host bottleneck during bacterial tumor colonization in which only hundreds of cells out of millions initiate the bacterial population in the tumor. Furthermore, we observed skewed expansion of bacterial clones in the tumor which suggests existence areas with different fitness advantages across the tumor. Advanced mathematical models are required to understand the behavior of bacterial populations from our data.

#### 4.5. IMPLICATIONS OF THIS WORK IN THE TUMOR MICROBIOME FIELD

Studying the tumor microbiome is crucial for developing better treatment strategies for patients since bacteria could modulate the anti-cancer treatments. In the case of PDACs, proteobacteria cause chemoresistance by the breakdown of gemcitabine into an inactive metabolite dFdU (Geller & Straussman, 2018; Voorde, Liekens, & Balzarini, 2013). These effects are significant enough to have clinical implications (Guenther et al., 2020; Mohindroo et al., 2021). For example, in a clinical retrospective study, researchers found that metastatic pancreatic cancer patients who used antibiotics got a better response to treatment with gemcitabine compared to patients who did not use antibiotics (Mohindroo et al., 2021). Gemcitabine may act as an antimicrobial on bacteria, and bacteria can develop resistance to gemcitabine in short timescales. However, the evolutionary adaptation of bacteria to gemcitabine, and how this could affect the existing bacteria-drug interactions has not been studied. My work suggests that there could be adaptations within a single species of the tumor microbiome which can then affect the existing bacteria-drug interactions in extreme directions with implications for the cancer cells. Various resistance mechanisms gained by the bacteria could make bacteria super degraders of the drug or could stop the bacterial drug degradation completely. Overall, we show what's possible rather than what's happening *in vivo* in real patients, and define the next steps to be done to see if this phenomenon happens in real patients. Even though we use a single bacteria-drug interaction in this study as a proof of concept, such adaptations could be

happening among other bacteria species and drugs. The next step should be looking into real pancreatic microbiomes with more diverse bacterial communities from the patients who went through gemcitabine treatment. This could provide evidence if this phenomenon really occurs in natural tumor environments. Understanding these adaptations in patient microbiomes can lead to the development of personalized decisions on treatment schedules or modification of the patient microbiome during the treatment.

Strategies to modify the patient microbiome really depend on understanding the mechanisms of bacteria colonization in the tumors. The second part of this thesis work helps understand those dynamics using a simplified tumor colonization model: subcutaneous syngeneic tumors and a library of *E. coli* Nissle 1917 containing thousands of DNA barcodes. This simple model characterizes fundamental features of bacterial colonization such as the presence of tight host bottlenecks and bacterial dissemination patterns in the tumor. However, it is not representative of the actual tumor microbiome environment which includes multiple species. Next, we can apply this method to study more clinically relevant scenarios using other bacterial species commonly enriched in patient microbiomes (such as *Fusobacterium nucleatum* in CRCs) and tumors that are naturally developing in the origin organ. In addition, we can use communities of bacteria that reflect the actual tumor microbiome. Understanding these mechanisms in more realistic models representing patient microbiomes will help develop strategies to efficiently manipulate the tumor microbiomes of the patients during

the treatment to achieve better therapeutic outcomes. For example, we can intelligently develop strategies to introduce/enrich the bacteria species making the anti-cancer drug more effective or we can remove/deplete bacteria species causing chemoresistance. I hope that in the near future, these kinds of personalized treatment regimens will make the existing anti-cancer therapies more effective for everyone.

## 5. APPENDIX: CHALLENGES IN EXPANDING GEMCITABINE LAB EVOLUTION EXPERIMENTS TO IN VIVO MURINE MODEL

In section 2.4.6, I showed that we could not detect any bacterial gemcitabine adaptive mutations from the evolution experiment performed *in vivo*. The reasons why we could not detect any adaptation to gemcitabine from these bacteria isolated from *in vivo* tumors treated with gemcitabine could be due to the following: gemcitabine levels in tumor tissue might not be inhibitory enough or duration bacteria experience the drug could be too short. To address these points and test additional ideas, we changed the following parameters in the experiment (Figure 5.1). First, we used a more gemcitabine-sensitive mutator strain, *E. coli* F-18 with a deletion in *mutT* (Figure 5.1b). This strain of *E. coli* is more sensitive to gemcitabine compared to EcN, and deletion of the *mutT* gene which is involved in DNA repair, makes it a mutator strain. We thought that these features of the bacteria could help increase the chance of detecting any gemcitabine adaptation. We treated the mice with gemcitabine (150 mg/kg up to seven times maximum) or vehicle and resected the tumors at experimental timepoints. We isolated single bacteria isolates from the tumors, and screened them for gemcitabine resistance. We did not observe gemcitabine resistance at comparable levels to  $\Delta nupC$  controls (results not shown). We also performed whole genome sequencing from selected colonies. We identified many mutations in these colonies (Supplementary File 8) which might be important for tumor colonization, but we did not observe adaptation

to gemcitabine through the loss of function mutations at the *nupC*. Next, we built a community of gemcitabine-resistant *E. coli* mutants (based on our genetic screen and functional gemcitabine breakdown assay), 6 fast gemcitabine degraders, 6 slow gemcitabine degraders, wild-type and non-gemcitabine degrader  $\Delta cdd$  strain (Figure 5.1c). Each mutant in this community had a DNA barcode which allowed us to identify its frequency in the population by deep sequencing. The designated percentage of each mutant in this community is shown in Figure 5.2A, left. Intuitively, we expected the wild-type *E. coli* and the most gemcitabine sensitive strain  $\Delta cdd$  decrease in frequency compared to the gemcitabine resistant mutants in the cohort treated with gemcitabine. We saw reduction in the frequency wild-type and  $\Delta cdd$  mutant in some tumors however, this trend was independent of the gemcitabine treatment Figure 5.2A, right. In addition, some tumors were dominated by a single strain. Furthermore, different parts of the same tumor contained different population profile (spatial effects).

Lastly, we performed a competition between *E. coli* wild-type and  $\Delta nupC$  strains (Figure 5.1d). We expected  $\Delta nupC$  to outcompete wild-type *E. coli* in the gemcitabine treated group since it has a much higher fitness advantage according to our *in vitro* results. However, in some instances they are still in equal frequency or in one mouse wild-type outcompeted  $\Delta nupC$  strain (Figure 5.2C).

Overall, these experiments did not provide evidence about *in vivo* adaptation to gemcitabine however they revealed an interesting observation which

led us to another research question. In the community experiment with many gemcitabine resistant mutant strains and competition experiment with wild-type and  $\Delta nupC$  mutant, we observed distributions of the mutants and wild-type bacteria independent of the gemcitabine treatment. Some tumors were dominated by single bacteria species while some had various inconsistent bacteria compositions. We hypothesized that either a narrow colonization bottleneck or unequal expansion within the tumor could cause such effects. This hypothesis led us to the experiments described in Chapter 3 of this thesis.

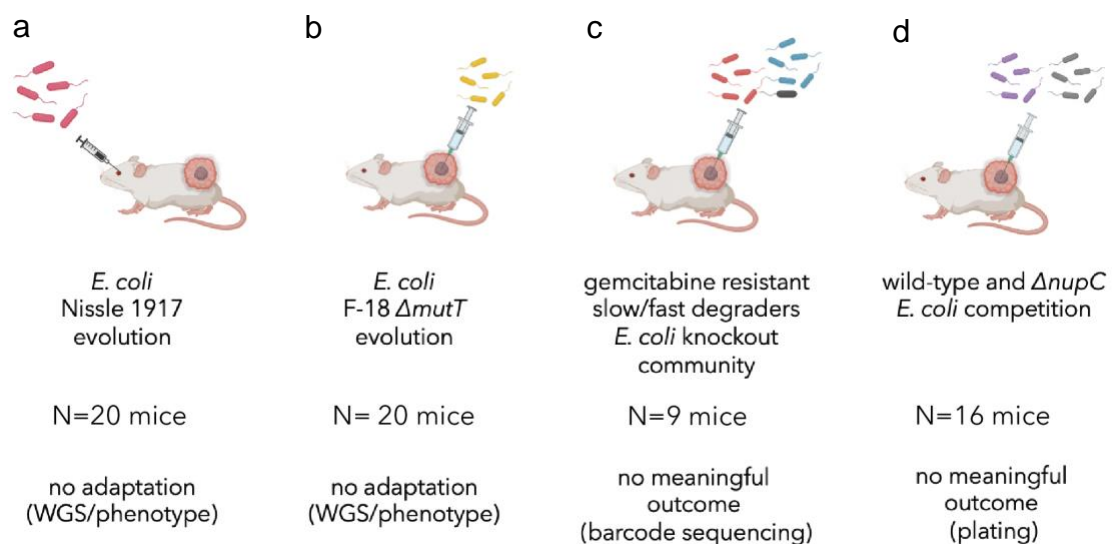


**Figure 5.1: Overview of the preliminary *in vivo* experiments performed**

(a) *In vivo* evolution experiment against gemcitabine using *E. coli* Nissle 1917, discussed in chapter 2. No adaptation to gemcitabine observed (b) *In vivo* evolution experiment against gemcitabine using *E. coli* F-18  $\Delta mutT$ . No adaptation to gemcitabine observed (c) *In vivo* competition experiment with wild-type *E. coli* (BW25113) and gemcitabine-resistant mutant community. No meaningful result was observed (d) *In vivo* competition experiment between wild-type *E. coli* (BW25113) and  $\Delta nupC$  mutant. No meaningful result was observed.

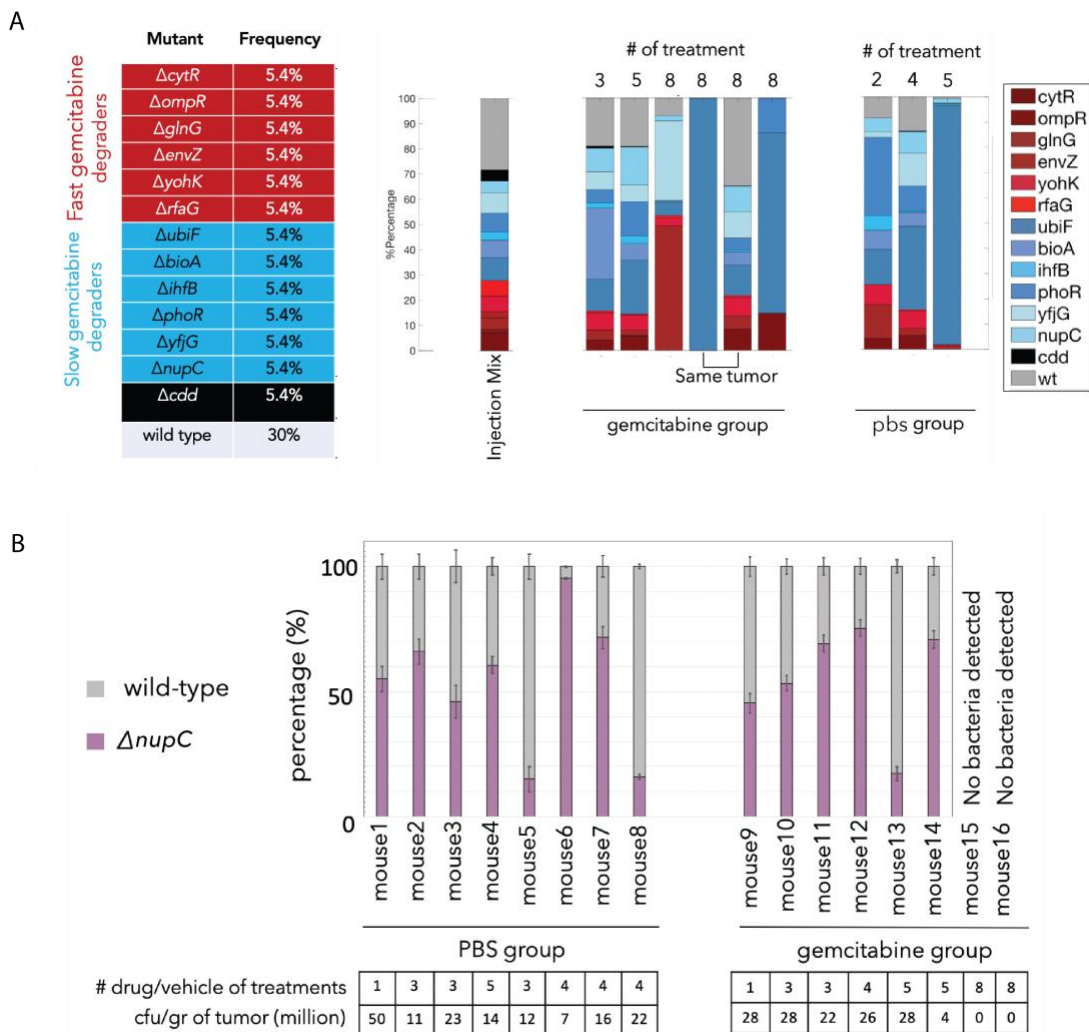


**Figure 5.2 Results of the *in vivo* competition experiments summarized in Figure 5.1.c and 5.1.d**

(A) Left: Composition of the generated bacteria community for injection into the mouse tumors. Right: barcode sequencing results of the injection mix (inoculum) and the bacteria from the resected tumors. The number of gemcitabine and vehicle treatments are indicated as numbers above the bars. (B) Percentage of wild-type and  $\Delta nupC$  bacteria from the tumors resected from gemcitabine or vehicle-treated mice. Colony frequency was determined by blue-white screening on LB agar plates containing X-gal. The number of treatments and carrying capacity (CFU/gr tumor) are indicated below each bar.

## Bibliography

- Abel, S., Abel Zur Wiesch, P., Chang, H. H., Davis, B. M., Lipsitch, M., & Waldor, M. K. (2015). Sequence tag-based analysis of microbial population dynamics. *Nature Methods*, *12*(3), 223–226. <https://doi.org/10.1038/nmeth.3253>
- Ajami, N. J., & Wargo, J. A. (2020). Microbial signatures in tumours and blood A reaction chamber for chromatin modification. *Nature*, *579*, 502–503.
- Akimov, Y., Bulanova, D., Timonen, S., Wennerberg, K., & Aittokallio, T. (2020). Improved detection of differentially represented DNA barcodes for high-throughput clonal phenomics. *Molecular Systems Biology*, *16*(3), 1–18. <https://doi.org/10.15252/msb.20199195>
- Alekshun, M. N., & Levy, S. B. (2007). Molecular Mechanisms of Antibacterial Multidrug Resistance. *Cell*, *128*(6), 1037–1050. <https://doi.org/10.1016/j.cell.2007.03.004>
- Alexander, J. L., Wilson, I. D., Teare, J., Marchesi, J. R., Nicholson, J. K., & Kinross, J. M. (2017). Gut microbiota modulation of chemotherapy efficacy and toxicity. *Nature Reviews Gastroenterology & Hepatology*, *14*(6), 356–365. <https://doi.org/10.1038/nrgastro.2017.20>
- Andreeva, N. V., Gabbasova, R. R., & Grivennikov, S. I. (2020). Microbiome in cancer progression and therapy. *Current Opinion in Microbiology*, *56*, 118–126. <https://doi.org/10.1016/j.mib.2020.09.001>
- Armstrong, H., Bording-Jorgensen, M., Dijk, S., & Wine, E. (2018). The complex interplay between chronic inflammation, the microbiome, and cancer: Understanding disease progression and what we can do to prevent it. *Cancers*, *10*(3), 1–29. <https://doi.org/10.3390/cancers10030083>
- Artacho, A., Isaac, S., Nayak, R., Flor-Duro, A., Alexander, M., Koo, I., ... Scher, J. U. (2021). The Pretreatment Gut Microbiome Is Associated With Lack of Response to Methotrexate in New-Onset Rheumatoid Arthritis. *Arthritis & Rheumatology*, *73*(6), 931–942. <https://doi.org/https://doi.org/10.1002/art.41622>
- Arumugam, M., Raes, J., Pelletier, E., Paslier, D. Le, Yamada, T., Mende, D. R., ... Zeller, G. (2011). Enterotypes of the human gut microbiome. *Nature*, *473*(7346), 174–180. <https://doi.org/10.1038/nature09944>
- Ashkenazy, H., Abadi, S., Martz, E., Chay, O., Mayrose, I., Pupko, T., & Ben-Tal, N. (2016). ConSurf 2016: an improved methodology to estimate and visualize evolutionary conservation in macromolecules. *Nucleic Acids Research*, *44*(W1), W344–W350. <https://doi.org/10.1093/NAR/GKW408>
- Aykut, B., Pushalkar, S., Chen, R., Li, Q., Abengozar, R., Kim, J. I., ... Miller, G. (2019). The fungal mycobiome promotes pancreatic oncogenesis via activation of MBL. *Nature*, *574*(7777), 264–267.

<https://doi.org/10.1038/s41586-019-1608-2>

- Baba, T., Ara, T., Hasegawa, M., Takai, Y., Okumura, Y., Baba, M., ... Mori, H. (2006). Construction of Escherichia coli K-12 in-frame, single-gene knockout mutants: The Keio collection. *Molecular Systems Biology*, 2. <https://doi.org/10.1038/msb4100050>
- Barrick, J. E., Colburn, G., Deatherage, D. E., Traverse, C. C., Strand, M. D., Borges, J. J., ... Meyer, A. G. (2014). Identifying structural variation in haploid microbial genomes from short-read resequencing data using breseq. *BMC Genomics*, 15(1), 1–17. <https://doi.org/10.1186/1471-2164-15-1039>
- Barrick, J. E., & Lenski, R. E. (2013). Genome dynamics during experimental evolution. *Nature Reviews Genetics*, 14(12), 827–839. <https://doi.org/10.1038/nrg3564>
- Barroso-Batista, J., Sousa, A., Lourenço, M., Bergman, M. L., Sobral, D., Demengeot, J., ... Gordo, I. (2014). The First Steps of Adaptation of Escherichia coli to the Gut Are Dominated by Soft Sweeps. *PLoS Genetics*, 10(3). <https://doi.org/10.1371/journal.pgen.1004182>
- Bedoui, Y., Guillot, X., Sélambarom, J., Guiraud, P., Giry, C., Jaffar-Bandjee, M. C., ... Gasque, P. (2019). Methotrexate an old drug with new tricks. *International Journal of Molecular Sciences*, 20(20). <https://doi.org/10.3390/ijms20205023>
- Boekhorst, J., Venlet, N., Procházková, N., Hansen, M. L., Lieberoth, C. B., Bahl, M. I., ... Roager, H. M. (2022). Stool energy density is positively correlated to intestinal transit time and related to microbial enterotypes. *Microbiome*, 10(1), 1–10. <https://doi.org/10.1186/s40168-022-01418-5>
- Bonder, M. J., Kurilshikov, A., Tigchelaar, E. F., Mujagic, Z., Imhann, F., Vila, A. V., ... Zhernakova, A. (2016). The effect of host genetics on the gut microbiome. *Nature Genetics*, 48(11), 1407–1412. <https://doi.org/10.1038/ng.3663>
- Capurso, G., & Lahner, E. (2017). The interaction between smoking, alcohol and the gut microbiome. *Best Practice and Research: Clinical Gastroenterology*, 31(5), 579–588. <https://doi.org/10.1016/j.bpg.2017.10.006>
- Carding, S., Verbeke, K., Vipond, D. T., Corfe, B. M., & Owen, L. J. (2015). Dysbiosis of the gut microbiota in disease. *Microbial Ecology in Health & Disease*, 26(0). <https://doi.org/10.3402/mehd.v26.26191>
- Castellarin, M., Warren, R. L., Freeman, J. D., Dreolini, L., Krzywinski, M., Strauss, J., ... Holt, R. A. (2012). Fusobacterium nucleatum infection is prevalent in human colorectal carcinoma. *Genome Research*, 7, 299–306. <https://doi.org/10.1101/gr.126516.111>
- Chabner, B. A., & Roberts Jr, T. G. (2005). Chemotherapy and the war on cancer

- Roberts et al, 2005. *Nature Reviews Cancer*, 5(January), 65–72.
- Chambers, E. S., Preston, T., Frost, G., & Morrison, D. J. (2018). Role of Gut Microbiota-Generated Short-Chain Fatty Acids in Metabolic and Cardiovascular Health. *Current Nutrition Reports*, 7(4), 198–206. <https://doi.org/10.1007/s13668-018-0248-8>
- Chassard, C., Dapoigny, M., Scott, K. P., Crouzet, L., Del'Homme, C., Marquet, P., ... Bernalier-Donadille, A. (2012). Functional dysbiosis within the gut microbiota of patients with constipated-irritable bowel syndrome. *Alimentary Pharmacology and Therapeutics*, 35(7), 828–838. <https://doi.org/10.1111/j.1365-2036.2012.05007.x>
- Chen, X., & Zhang, J. (2013). No gene-specific optimization of mutation rate in escherichia coli. *Molecular Biology and Evolution*, 30(7), 1559–1562. <https://doi.org/10.1093/molbev/mst060>
- Christaki, E., & Giamarellos-Bourboulis, E. J. (2014). The complex pathogenesis of bacteremia: From antimicrobial clearance mechanisms to the genetic background of the host. *Virulence*, 5(1), 57–65. <https://doi.org/10.4161/viru.26514>
- Christian Milani, Sabrina Duranti, Francesca Bottacini, B., Eoghan Casey, B., Francesca Turroni, Jennifer Mahony, B., Clara Belzer, S. D. P., Silvia Arboleya Montes, E., Leonardo Mancabelli, Gabriele Andrea Lugli, A., ... Lars Bode, Willem de Vos, Miguel Gueimonde, Abelardo Margolles, Douwe van Sinderen, M. V. (2017). The First Microbial Colonizers of the Human Gut: Composition, Activities, and Health Implications of the Infant Gut Microbiota. *Microbiology and Molecular Biology Reviews*, 81(4), 1–67. Retrieved from <https://bit.ly/2rxVSf9>
- Conway, T., Creecy, J. P., Maddox, S. M., Grissom, J. E., Conkle, T. L., Shadid, T. M., ... Wanner, B. L. (2014). Unprecedented high-resolution view of bacterial operon architecture revealed by RNA sequencing. *MBio*, 5(4). <https://doi.org/10.1128/mBio.01442-14>
- Corty, R. W., Langworthy, B. W., Fine, J. P., Buse, J. B., Sanoff, H. K., & Lund, J. L. (2020). Antibacterial Use Is Associated with an Increased Risk of Hematologic and Gastrointestinal Adverse Events in Patients Treated with Gemcitabine for Stage IV Pancreatic Cancer. *The Oncologist*, 25(7), 579–584. <https://doi.org/10.1634/theoncologist.2019-0570>
- Cree, I. A., & Charlton, P. (2017). Molecular chess? Hallmarks of anti-cancer drug resistance. *BMC Cancer*, 17(1), 1–8. <https://doi.org/10.1186/s12885-016-2999-1>
- Cui, J., Ramesh, G., Wu, M., Jensen, E. T., Crago, O., Bertoni, A. G., ... Goodarzi, M. O. (2022). Butyrate-Producing Bacteria and Insulin Homeostasis: The Microbiome and Insulin Longitudinal Evaluation Study (MILES). *Diabetes*,

- 71(11), 2438–2446. <https://doi.org/10.2337/db22-0168>
- Cullin, N., Azevedo Antunes, C., Straussman, R., Stein-Thoeringer, C. K., & Elinav, E. (2021). Microbiome and cancer. *Cancer Cell*, 39(10), 1317–1341. <https://doi.org/10.1016/j.ccell.2021.08.006>
- Cummins, J., & Tangney, M. (2013). Bacteria and tumours: Causative agents or opportunistic inhabitants? *Infectious Agents and Cancer*, 8(1), 1–8. <https://doi.org/10.1186/1750-9378-8-11>
- Datta, S., Costantino, N., & Court, D. L. (2006). A set of recombinering plasmids for gram-negative bacteria, 379(1–2), 109–115. <https://doi.org/10.1016/j.gene.2006.04.018>
- de Martel, C., Georges, D., Bray, F., Ferlay, J., & Clifford, G. M. (2020). Global burden of cancer attributable to infections in 2018: a worldwide incidence analysis. *The Lancet Global Health*, 8(2), e180–e190. [https://doi.org/10.1016/S2214-109X\(19\)30488-7](https://doi.org/10.1016/S2214-109X(19)30488-7)
- De Sousa Cavalcante, L., & Monteiro, G. (2014). Gemcitabine: Metabolism and molecular mechanisms of action, sensitivity and chemoresistance in pancreatic cancer. *European Journal of Pharmacology*, 741, 8–16. <https://doi.org/10.1016/j.ejphar.2014.07.041>
- De Vadder, F., Kovatcheva-Datchary, P., Goncalves, D., Vinera, J., Zitoun, C., Duchamp, A., ... Mithieux, G. (2014). Microbiota-generated metabolites promote metabolic benefits via gut-brain neural circuits. *Cell*, 156(1–2), 84–96. <https://doi.org/10.1016/j.cell.2013.12.016>
- Detert, J., Bastian, H., Listing, J., Weiß, A., Wassenberg, S., Liebhaber, A., ... Burmester, G.-R. (2013). Induction therapy with adalimumab plus methotrexate for 24 weeks followed by methotrexate monotherapy up to week 48 versus methotrexate therapy alone for DMARD-naive patients with early rheumatoid arthritis: HIT HARD, an investigator-initiated study. *Annals of the Rheumatic Diseases*, 72(6), 844–850. <https://doi.org/10.1136/annrheumdis-2012-201612>
- Dragosits, M., & Mattanovich, D. (2013). Adaptive laboratory evolution - principles and applications for biotechnology. *Microbial Cell Factories*, 12(1), 1–17. <https://doi.org/10.1186/1475-2859-12-64>
- Duan, M., Wang, Y., Zhang, Q., Zou, R., Guo, M., & Zheng, H. (2021). Characteristics of gut microbiota in people with obesity. *PLoS ONE*, 16(8 August), 1–15. <https://doi.org/10.1371/journal.pone.0255446>
- Duong, M. T. Q., Qin, Y., You, S. H., & Min, J. J. (2019). Bacteria-cancer interactions: bacteria-based cancer therapy. *Experimental and Molecular Medicine*, 51(12). <https://doi.org/10.1038/s12276-019-0297-0>
- Dziubańska-Kusibab, P. J., Berger, H., Battistini, F., Bouwman, B. A. M., Iftexhar,

- A., Katainen, R., ... Meyer, T. F. (2020). Colibactin DNA-damage signature indicates mutational impact in colorectal cancer. *Nature Medicine*, *26*(7), 1063–1069. <https://doi.org/10.1038/s41591-020-0908-2>
- Elkrief, A., El Raichani, L., Richard, C., Messaoudene, M., Belkaid, W., Malo, J., ... Routy, B. (2019). Antibiotics are associated with decreased progression-free survival of advanced melanoma patients treated with immune checkpoint inhibitors. *Oncot Immunology*, *8*(4), 1–6. <https://doi.org/10.1080/2162402X.2019.1568812>
- Emery, P., Breedveld, F. C., Hall, S., Durez, P., Chang, D. J., Robertson, D., ... Freundlich, B. (2008). Comparison of methotrexate monotherapy with a combination of methotrexate and etanercept in active, early, moderate to severe rheumatoid arthritis (COMET): a randomised, double-blind, parallel treatment trial. *Lancet (London, England)*, *372*(9636), 375–382. [https://doi.org/10.1016/S0140-6736\(08\)61000-4](https://doi.org/10.1016/S0140-6736(08)61000-4)
- Errington, T. M., Mathur, M., Soderberg, C. K., Denis, A., Perfito, N., Iorns, E., & Nosek, B. A. (2021). Investigating the replicability of preclinical cancer biology. *ELife*, *10*, 1–30. <https://doi.org/10.7554/eLife.71601>
- Forbes, N. S. (2010). Engineering the perfect (bacterial) cancer therapy. *Nature Reviews Cancer*, *10*(11), 785–794. <https://doi.org/10.1038/nrc2934>
- Gama-Castro, S., Salgado, H., Santos-Zavaleta, A., Ledezma-Tejeida, D., Muñoz-Rascado, L., García-Sotelo, J. S., ... Collado-Vides, J. (2016). RegulonDB version 9.0: High-level integration of gene regulation, coexpression, motif clustering and beyond. *Nucleic Acids Research*, *44*(D1), D133–D143. <https://doi.org/10.1093/nar/gkv1156>
- Gao, Y., Shang, Q., Li, W., Guo, W., Stojadinovic, A., Mannion, C., ... Chen, T. (2020). Antibiotics for cancer treatment: A double-edged sword. *Journal of Cancer*, *11*(17), 5135–5149. <https://doi.org/10.7150/jca.47470>
- García-González, A. P., Ritter, A. D., Shrestha, S., Andersen, E. C., Yilmaz, L. S., & Walhout, A. J. M. (2017). Bacterial Metabolism Affects the *C. elegans* Response to Cancer Chemotherapeutics. *Cell*, *169*(3), 431–441.e8. <https://doi.org/10.1016/j.cell.2017.03.046>
- Garud, N. R., Good, B. H., Hallatschek, O., & Pollard, K. S. (2019). Evolutionary dynamics of bacteria in the gut microbiome within and across hosts. *PLoS Biology*, *17*(1), 1–29. <https://doi.org/10.1371/JOURNAL.PBIO.3000102>
- Gatt, Y. E., & Margalit, H. (2021). Common Adaptive Strategies Underlie Within-Host Evolution of Bacterial Pathogens. *Molecular Biology and Evolution*, *38*(3), 1101–1121. <https://doi.org/10.1093/molbev/msaa278>
- Geller, L. T., Barzily-Rokni, M., Danino, T., Jonas, O. H., Shental, N., Nejman, D., ... Straussman, R. (2017). Potential role of intratumor bacteria in mediating tumor resistance to the chemotherapeutic drug gemcitabine. *Science*,

- 357(6356), 1–31. <https://doi.org/10.1126/science.aah5043>
- Geller, L. T., & Straussman, R. (2018). Intratumoral bacteria may elicit chemoresistance by metabolizing anticancer agents. *Molecular and Cellular Oncology*, 5(1). <https://doi.org/10.1080/23723556.2017.1405139>
- Genser, L., Aguanno, D., Soula, H. A., Dong, L., Trystram, L., Assmann, K., ... Poitou, C. (2018). Increased jejunal permeability in human obesity is revealed by a lipid challenge and is linked to inflammation and type 2 diabetes. *The Journal of Pathology*, 246(2), 217–230. <https://doi.org/10.1002/path.5134>
- Gihawi, A., Ge, Y., Lu, J., Puiu, D., Xu, A., & Colin, S. (2023). Major data analysis errors invalidate cancer microbiome findings.
- Gilbert, J. A., Blaser, M. J., Caporaso, J. G., Jansson, J. K., Lynch, S. V., & Knight, R. (2018). Current understanding of the human microbiome. *Nature Medicine*, 24(4), 392–400. <https://doi.org/10.1038/nm.4517>
- Gilman, A. (1963). The initial clinical trial of nitrogen mustard. *The American Journal of Surgery*, 105(5), 574–578. [https://doi.org/10.1016/0002-9610\(63\)90232-0](https://doi.org/10.1016/0002-9610(63)90232-0)
- Gingell, R., Bridges, J. W., & Williams, R. T. (1971). The role of the gut flora in the metabolism of prontosil and neoprontosil in the rat. *Xenobiotica; the Fate of Foreign Compounds in Biological Systems*, 1(2), 143–156. <https://doi.org/10.3109/00498257109044386>
- Goodman, A. L., Kallstrom, G., Faith, J. J., Reyes, A., Moore, A., Dantas, G., & Gordon, J. I. (2011). Extensive personal human gut microbiota culture collections characterized and manipulated in gnotobiotic mice. *Proceedings of the National Academy of Sciences of the United States of America*, 108(15), 6252–6257. <https://doi.org/10.1073/pnas.1102938108>
- Goodman, B., & Gardner, H. (2018). The microbiome and cancer. *Journal of Pathology*, 244(5), 667–676. <https://doi.org/10.1002/path.5047>
- Guenther, M., Haas, M., Heinemann, V., Kruger, S., Westphalen, C. B., von Bergwelt-Baildon, M., ... Ormanns, S. (2020). Bacterial lipopolysaccharide as negative predictor of gemcitabine efficacy in advanced pancreatic cancer – translational results from the AIO-PK0104 Phase 3 study. *British Journal of Cancer*, 123(9), 1370–1376. <https://doi.org/10.1038/s41416-020-01029-7>
- Gupta, K. H., Nowicki, C., Giurini, E. F., Marzo, A. L., & Zloza, A. (2021). Bacterial-based cancer therapy (Bbct): Recent advances, current challenges, and future prospects for cancer immunotherapy. *Vaccines*, 9(12), 1–25. <https://doi.org/10.3390/vaccines9121497>
- Haaz, M. C., Rivory, L., Jantet, S., Ratanasavanh, D., & Robert, J. (1997). Glucuronidation of SN-38, the active metabolite of irinotecan, by human hepatic microsomes. *Pharmacology & Toxicology*, 80(2), 91–96.

<https://doi.org/10.1111/j.1600-0773.1997.tb00289.x>

- Haiser, H. J., & Turnbaugh, P. J. (2013). Developing a metagenomic view of xenobiotic metabolism. *Pharmacological Research*, 69(1), 21–31. <https://doi.org/10.1016/j.phrs.2012.07.009>
- Hanahan, D. (2022). Hallmarks of Cancer: New Dimensions. *Cancer Discovery*, 12(1), 31–46. <https://doi.org/10.1158/2159-8290.CD-21-1059>
- Haraga, A., Ohlson, M. B., & Miller, S. I. (2008). Salmonellae interplay with host cells. *Nature Reviews Microbiology*, 6(1), 53–66. <https://doi.org/10.1038/nrmicro1788>
- Harimoto, T., Singer, Z. S., Velazquez, O. S., Zhang, J., Castro, S., Hinchliffe, T. E., ... Danino, T. (2019). Rapid screening of engineered microbial therapies in a 3D multicellular model. *Proceedings of the National Academy of Sciences of the United States of America*, 116(18), 9002–9007. <https://doi.org/10.1073/pnas.1820824116>
- Hatakeyama, M. (2017). Structure and function of helicobacter pylori caga, the first-identified bacterial protein involved in human cancer. *Proceedings of the Japan Academy Series B: Physical and Biological Sciences*, 93(4), 196–219. <https://doi.org/10.2183/pjab.93.013>
- Hallahall, K., & Waldor, M. K. (2021). Pathogen clonal expansion underlies multiorgan dissemination and organ-specific outcomes during murine systemic infection. *ELife*, 10, 1–29. <https://doi.org/10.7554/eLife.70910>
- Hallahalli, K., & Pritchard, J. R. (2021). Refined Quantification of Infection Bottlenecks and Pathogen Dissemination with STAMPR. *MSystems*, 6(4), 1–16.
- Hallahalli, K., & Waldor, M. K. (2021). Pathogen clonal expansion underlies multiorgan dissemination and organ-specific outcomes during murine systemic infection. *ELife*, 10, e70910. <https://doi.org/10.7554/eLife.70910>
- Huttenhower, C., Gevers, D., Knight, R., Abubucker, S., Badger, J. H., Chinwalla, A. T., ... White, O. (2012). Structure, function and diversity of the healthy human microbiome. *Nature*, 486(7402), 207–214. <https://doi.org/10.1038/nature11234>
- Iyer, N. V., Kotch, L. E., Agani, F., Leung, S. W., Laughner, E., Wenger, R. H., ... Semenza, G. L. (1998). Cellular and developmental control of O<sub>2</sub> homeostasis by hypoxia-inducible factor 1 $\alpha$ . *Genes & Development*, 12(2), 149–162. <https://doi.org/10.1101/gad.12.2.149>
- Kanehisa, M., Sato, Y., Kawashima, M., Furumichi, M., & Tanabe, M. (2016). KEGG as a reference resource for gene and protein annotation. *Nucleic Acids Research*, 44(D1), D457–D462. <https://doi.org/10.1093/nar/gkv1070>
- Keseler, I. M., Mackie, A., Santos-Zavaleta, A., Billington, R., Bonavides-Martínez,

- C., Caspi, R., ... Karp, P. D. (2017). The EcoCyc database: Reflecting new knowledge about *Escherichia coli* K-12. *Nucleic Acids Research*, *45*(D1), D543–D550. <https://doi.org/10.1093/nar/gkw1003>
- Klünemann, M., Andrejev, S., Blasche, S., Mateus, A., Phapale, P., Devendran, S., ... Patil, K. R. (2021). Bioaccumulation of therapeutic drugs by human gut bacteria. *Nature*, *597*(7877), 533–538. <https://doi.org/10.1038/s41586-021-03891-8>
- Koppel, N., Maini Rekdal, V., & Balskus, E. P. (2017). Chemical transformation of xenobiotics by the human gut microbiota. *Science*, *356*(6344), eaag2770. <https://doi.org/10.1126/science.aag2770>
- Korem, T., Zeevi, D., Suez, J., Weinberger, A., Avnit-Sagi, T., Pompan-Lotan, M., ... Segal, E. (2015). Growth dynamics of gut microbiota in health and disease inferred from single metagenomic samples. *Science*, *349*(6252), 1101–1106. <https://doi.org/10.1126/science.aac4812>
- Krimbas, C. B., & Tsakas, S. (1971). THE GENETICS OF DACUS OLEAE. V. CHANGES OF ESTERASE POLYMORPHISM IN A NATURAL POPULATION FOLLOWING INSECTICIDE CONTROL-SELECTION OR DRIFT? *Evolution*, (25), 454–460. <https://doi.org/10.1111/j.1558-5646.1971.tb01904.x>
- Kyono, Y., Ellezian, L., Hu, Y. Y., Eliadis, K., Moy, J., Hirsch, E. B., ... Flowers, S. A. (2022). The Atypical Antipsychotic Quetiapine Promotes Multiple Antibiotic Resistance in *Escherichia coli*. *Journal of Bacteriology*, *204*(5). <https://doi.org/10.1128/jb.00102-22>
- Lehouritis, P., Cummins, J., Stanton, M., Murphy, C. T., McCarthy, F. O., Reid, G., ... Tangney, M. (2015). Local bacteria affect the efficacy of chemotherapeutic drugs. *Scientific Reports*, *5*, 14554. <https://doi.org/10.1038/srep14554>
- Leschner, S., Westphal, K., Dietrich, N., Viegas, N., Jablonska, J., Lyszkiewicz, M., ... Weiss, S. (2009). Tumor invasion of *Salmonella enterica* serovar Typhimurium is accompanied by strong hemorrhage promoted by TNF- $\alpha$ . *PLoS ONE*, *4*(8). <https://doi.org/10.1371/journal.pone.0006692>
- Lieberman, T. D. (2022). Detecting bacterial adaptation within individual microbiomes. *Philosophical Transactions of the Royal Society B: Biological Sciences*, *377*(1861). <https://doi.org/10.1098/rstb.2021.0243>
- Lieberman, T. D., Michel, J. B., Aingaran, M., Potter-Bynoe, G., Roux, D., Davis, M. R., ... Kishony, R. (2011). Parallel bacterial evolution within multiple patients identifies candidate pathogenicity genes. *Nature Genetics*, *43*(12), 1275–1280. <https://doi.org/10.1038/ng.997>
- Liekens, S., Bronckaers, A., & Balzarini, J. (2009). Improvement of purine and pyrimidine antimetabolite-based anticancer treatment by selective suppression of mycoplasma-encoded catabolic enzymes. *The Lancet*

- Oncology*, 10(6), 628–635. [https://doi.org/10.1016/S1470-2045\(09\)70037-3](https://doi.org/10.1016/S1470-2045(09)70037-3)
- Lourenço, M., Ramiro, R. S., Güleresi, D., Barroso-Batista, J., Xavier, K. B., Gordo, I., & Sousa, A. (2016). A Mutational Hotspot and Strong Selection Contribute to the Order of Mutations Selected for during *Escherichia coli* Adaptation to the Gut. *PLoS Genetics*, 12(11), 1–23. <https://doi.org/10.1371/journal.pgen.1006420>
- Luo, W., Friedman, M. S., Shedden, K., Hankenson, K. D., & Woolf, P. J. (2009). GAGE: Generally applicable gene set enrichment for pathway analysis. *BMC Bioinformatics*, 10, 1–17. <https://doi.org/10.1186/1471-2105-10-161>
- Luria, S. E., & Delbrück, M. (1943). Mutations of bacteria from virus sensitivity to virus resistance. *Genetics*, 28(November).
- Ma, J., Zhu, W., & Liu, B. (2021). Role of gut microbiome in the outcome of cancer immunotherapy. *International Journal of Cancer*, 149(4), 760–768. <https://doi.org/10.1002/ijc.33524>
- Mahmutovic, A., Gillman, A. N., Lauksund, S., Robson Moe, N. A., Manzi, A., Storflor, M., ... Abel, S. (2021). RESTAMP – Rate estimates by sequence-tag analysis of microbial populations. *Computational and Structural Biotechnology Journal*, 19, 1035–1051. <https://doi.org/10.1016/j.csbj.2021.01.017>
- Maier, L., Pruteanu, M., Kuhn, M., Zeller, G., Telzerow, A., Anderson, E. E., ... Typas, A. (2018). Extensive impact of non-antibiotic drugs on human gut bacteria. *Nature*, 555(7698), 623–628. <https://doi.org/10.1038/nature25979>
- McAllister, F., Khan, M. A. W., Helmink, B., & Wargo, J. A. (2019). The Tumor Microbiome in Pancreatic Cancer: Bacteria and Beyond. *Cancer Cell*, 36(6), 577–579. <https://doi.org/10.1016/j.ccell.2019.11.004>
- McQuade, J. L., Daniel, C. R., Helmink, B. A., & Wargo, J. A. (2019). Modulating the microbiome to improve therapeutic response in cancer. *The Lancet Oncology*, 20(2), e77–e91. [https://doi.org/10.1016/S1470-2045\(18\)30952-5](https://doi.org/10.1016/S1470-2045(18)30952-5)
- Mercado-Lubo, R., Zhang, Y., Zhao, L., Rossi, K., Wu, X., Zou, Y., ... McCormick, B. A. (2016). A Salmonella nanoparticle mimic overcomes multidrug resistance in tumours. *Nature Communications*, 7. <https://doi.org/10.1038/ncomms12225>
- Meriggi, F., & Zaniboni, A. (2021). Antibiotics and steroids, the double enemies of anticancer immunotherapy: a review of the literature. *Cancer Immunology, Immunotherapy*, 70(6), 1511–1517. <https://doi.org/10.1007/s00262-020-02786-3>
- MIZUNO, T., & MIZUSHIMA, S. (1987). Isolation and Characterization of Deletion Mutants of *ompR* and *envZ*, Regulatory Genes for Expression of the Outer Membrane Proteins *OmpC* and *OmpF* in *Escherichia coli*1. *The Journal of Biochemistry*, 101(2), 387–396.

<https://doi.org/10.1093/oxfordjournals.jbchem.a121923>

- Mohindroo, C., Hasanov, M., Rogers, J. E., Dong, W., Prakash, L. R., Baydogan, S., ... McAllister, F. (2021). Antibiotic use influences outcomes in advanced pancreatic adenocarcinoma patients. *Cancer Medicine*, *10*(15), 5041–5050. <https://doi.org/10.1002/cam4.3870>
- Morales, A., Eidinger, D., & Bruce, A. W. (1976). Intracavitary Bacillus Calmette Guerin in the treatment of superficial bladder tumors. *Journal of Urology*, *116*(2), 180–182. [https://doi.org/10.1016/s0022-5347\(17\)58737-6](https://doi.org/10.1016/s0022-5347(17)58737-6)
- Murphy, K. C. (2016).  $\lambda$  Recombination and Recombineering. *EcoSal Plus*, *7*(1). <https://doi.org/10.1128/ecosalplus.esp-0011-2015>
- Narunsky-Haziza, L., Sepich-Poore, G. D., Livyatan, I., Asraf, O., Martino, C., Nejman, D., ... Straussman, R. (2022). Pan-cancer analyses reveal cancer-type-specific fungal ecologies and bacteriome interactions. *Cell*, *185*(20), 3789–3806.e17. <https://doi.org/10.1016/j.cell.2022.09.005>
- Nayfach, S., & Pollard, K. S. (2015). Average genome size estimation improves comparative metagenomics and sheds light on the functional ecology of the human microbiome. *Genome Biology*, *16*(1), 1–18. <https://doi.org/10.1186/s13059-015-0611-7>
- Nejman, D., Livyatan, I., Fuks, G., Gavert, N., Zwang, Y., Geller, L. T., ... Straussman, R. (2020a). The human tumor microbiome is composed of tumor type-specific intracellular bacteria. *Science (New York, N.Y.)*, *368*(6494), 973–980. <https://doi.org/10.1126/science.aay9189>
- Nejman, D., Livyatan, I., Fuks, G., Gavert, N., Zwang, Y., Geller, L. T., ... Straussman, R. (2020b). The human tumor microbiome is composed of tumor type-specific intracellular bacteria. *Science*, *368*(6494), 973–980. <https://doi.org/10.1126/science.aay9189>
- Niño, J. L. G., Wu, H., LaCourse, K. D., Kempchinsky, A. G., Baryiames, A., Barber, B., ... Bullman, S. (2022). Effect of the intratumoral microbiota on spatial and cellular heterogeneity in cancer. *Nature* *2022*, *611*(March), 1–8. <https://doi.org/10.1038/s41586-022-05435-0>
- Noto Guillen, M., Rosener, B., Sayin, S., & Mitchell, A. (2021). Assembling stable syntrophic *Escherichia coli* communities by comprehensively identifying beneficiaries of secreted goods. *Cell Systems*, *12*(11), 1064–1078.e7. <https://doi.org/10.1016/j.cels.2021.08.002>
- Nougayrède, J.-P., Homburg, S., Taieb, F., Boury, M., Brzuszkiewicz, E., Gottschalk, G., ... Oswald, E. (2006). *Escherichia coli* induces DNA double-strand breaks in eukaryotic cells. *Science (New York, N.Y.)*, *313*(5788), 848–851. <https://doi.org/10.1126/science.1127059>
- Oliva, M., Mulet-Margalef, N., Ochoa-De-olza, M., Napoli, S., Mas, J., Laquente,

- B., ... Moreno, V. (2021). Tumor-associated microbiome: Where do we stand? *International Journal of Molecular Sciences*, 22(3), 1–25. <https://doi.org/10.3390/ijms22031446>
- Papac, R. J. (2001). Origins of cancer therapy. *Yale Journal of Biology and Medicine*, 74(6), 391–398.
- Parhi, L., Alon-Maimon, T., Sol, A., Nejman, D., Shhadeh, A., Fainsod-Levi, T., ... Bachrach, G. (2020). Breast cancer colonization by *Fusobacterium nucleatum* accelerates tumor growth and metastatic progression. *Nature Communications*, 11(1), 1–12. <https://doi.org/10.1038/s41467-020-16967-2>
- Penders, J., Thijs, C., Vink, C., Stelma, F. F., Snijders, B., Kummeling, I., ... Stobberingh, E. E. (2006). Factors influencing the composition of the intestinal microbiota in early infancy. *Pediatrics*, 118(2), 511–521. <https://doi.org/10.1542/peds.2005-2824>
- Peppercorn, M. A., & Goldman, P. (1972). The role of intestinal bacteria in the metabolism of salicylazosulfapyridine. *The Journal of Pharmacology and Experimental Therapeutics*, 181(3), 555–562.
- Pérez-Cobas, A. E., Artacho, A., Knecht, H., Ferrús, M. L., Friedrichs, A., Ott, S. J., ... Gosalbes, M. J. (2013). Differential effects of antibiotic therapy on the structure and function of human gut microbiota. *PLoS ONE*, 8(11). <https://doi.org/10.1371/journal.pone.0080201>
- Piche, T., Barbara, G., Aubert, P., Bruley des Varannes, S., Dainese, R., Nano, J. L., ... Neunlist, M. (2009). Impaired intestinal barrier integrity in the colon of patients with irritable bowel syndrome: involvement of soluble mediators. *Gut*, 58(2), 196–201. <https://doi.org/10.1136/gut.2007.140806>
- Pleguezuelos-Manzano, C., Puschhof, J., Rosendahl Huber, A., van Hoeck, A., Wood, H. M., Nomburg, J., ... Clevers, H. (2020). Mutational signature in colorectal cancer caused by genotoxic pks + *E. coli*. *Nature*, 580(7802), 269–273. <https://doi.org/10.1038/s41586-020-2080-8>
- Pommier, Y. (2006). Topoisomerase I inhibitors: Camptothecins and beyond. *Nature Reviews Cancer*, 6(10), 789–802. <https://doi.org/10.1038/nrc1977>
- Poore, G. D., Kopylova, E., Zhu, Q., Carpenter, C., Fraraccio, S., Wandro, S., ... Knight, R. (2020). Microbiome analyses of blood and tissues suggest cancer diagnostic approach. *Nature*, 579(7800), 567–574. <https://doi.org/10.1038/s41586-020-2095-1>
- Proctor, L. M., Creasy, H. H., Fettweis, J. M., Lloyd-Price, J., Mahurkar, A., Zhou, W., ... Huttenhower, C. (2019). The Integrative Human Microbiome Project. *Nature*, 569(7758), 641–648. <https://doi.org/10.1038/s41586-019-1238-8>
- Pushalkar, S., Hundeyin, M., Daley, D., Zambirinis, C. P., Kurz, E., Mishra, A., ... Miller, G. (2018). The pancreatic cancer microbiome promotes oncogenesis

- by induction of innate and adaptive immune suppression. *Cancer Discovery*, 8(4), 403–416. <https://doi.org/10.1158/2159-8290.CD-17-1134>
- Qin, J., Li, R., Raes, J., Arumugam, M., Burgdorf, K. S., Manichanh, C., ... Zoetendal, E. (2010). A human gut microbial gene catalogue established by metagenomic sequencing. *Nature*, 464(7285), 59–65. <https://doi.org/10.1038/nature08821>
- Ramakrishna, B. S. (2013). Role of the gut microbiota in human nutrition and metabolism. *Journal of Gastroenterology and Hepatology (Australia)*, 28(S4), 9–17. <https://doi.org/10.1111/jgh.12294>
- Repass, J., Iorns, E., Denis, A., Williams, S. R., Perfito, N., & Errington, T. M. (2018). Replication study: *Fusobacterium nucleatum* infection is prevalent in human colorectal carcinoma. *eLife*, 7, 299–306. <https://doi.org/10.7554/eLife.25801>
- Rinninella, E., Raoul, P., Cintoni, M., Franceschi, F., Miggiano, G. A. D., Gasbarrini, A., & Mele, M. C. (2019). What is the healthy gut microbiota composition? A changing ecosystem across age, environment, diet, and diseases. *Microorganisms*, 7(1). <https://doi.org/10.3390/microorganisms7010014>
- Riquelme, E., Zhang, Y., Zhang, L., Montiel, M., Zoltan, M., Dong, W., ... McAllister, F. (2019). Tumor Microbiome Diversity and Composition Influence Pancreatic Cancer Outcomes. *Cell*, 178(4), 795-806.e12. <https://doi.org/10.1016/j.cell.2019.07.008>
- Rolston, K. V. I. (2017). Infections in Cancer Patients with Solid Tumors: A Review. *Infectious Diseases and Therapy*, 6(1), 69–83. <https://doi.org/10.1007/s40121-017-0146-1>
- Rosener, B., Sayin, S., Oluoch, P., García-González, A. P., Mori, H., Walhout, A. J. M., & Mitchell, A. (2020). Evolved bacterial resistance against fluoropyrimidines can lower chemotherapy impact in the *Caenorhabditis elegans* host. *eLife*, 9, 1–57. <https://doi.org/10.7554/eLife.59831>
- Roy, S., & Trinchieri, G. (2017). Microbiota: A key orchestrator of cancer therapy. *Nature Reviews Cancer*, 17(5), 271–285. <https://doi.org/10.1038/nrc.2017.13>
- Said, H. M., & Mohammed, Z. M. (2006). Intestinal absorption of water-soluble vitamins: An update. *Current Opinion in Gastroenterology*, 22(2), 140–146. <https://doi.org/10.1097/01.mog.0000203870.22706.52>
- Satoh, T., Hosokawa, M., Atsumi, R., Suzuki, W., Hakusui, H., & Nagai, E. (1994). Metabolic activation of CPT-11, 7-ethyl-10-[4-(1-piperidino)-1-piperidino]carbonyloxycamptothecin, a novel antitumor agent, by carboxylesterase. *Biological & Pharmaceutical Bulletin*, 17(5), 662–664. <https://doi.org/10.1248/bpb.17.662>

- Schloissnig, S., Arumugam, M., Sunagawa, S., Mitreva, M., Tap, J., Zhu, A., ... Bork, P. (2013). Genomic variation landscape of the human gut microbiome. *Nature*, *493*(7430), 45–50. <https://doi.org/10.1038/nature11711>
- Schoultz, I., & Keita, Å. V. (2020). The Intestinal Barrier and Current Techniques for the Assessment of Gut Permeability. *Cells*, *9*(8), 1–30. <https://doi.org/10.3390/cells9081909>
- Sender, R., Fuchs, S., & Milo, R. (2016). Revised Estimates for the Number of Human and Bacteria Cells in the Body. *PLoS Biology*, *14*(8), 1–14. <https://doi.org/10.1371/journal.pbio.1002533>
- Sepich-Poore, G. D., Zitvogel, L., Straussman, R., Hasty, J., Wargo, J. A., & Knight, R. (2021). The microbiome and human cancer. *Science*, *371*(6536). <https://doi.org/10.1126/science.abc4552>
- Siccardi, D., Mummy, K. L., Wall, D. M., Bien, J. D., & McCormick, B. A. (2008). Salmonella enterica serovar Typhimurium modulates P-glycoprotein in the intestinal epithelium. *American Journal of Physiology - Gastrointestinal and Liver Physiology*, *294*(6), 1392–1400. <https://doi.org/10.1152/ajpgi.00599.2007>
- Sieow, B. F. L., Wun, K. S., Yong, W. P., Hwang, I. Y., & Chang, M. W. (2021). Tweak to Treat: Reprogramming Bacteria for Cancer Treatment. *Trends in Cancer*, *7*(5), 447–464. <https://doi.org/10.1016/j.trecan.2020.11.004>
- Simpson, C. A., Diaz-Arteche, C., Eliby, D., Schwartz, O. S., Simmons, J. G., & Cowan, C. S. M. (2021). The gut microbiota in anxiety and depression – A systematic review. *Clinical Psychology Review*, *83*(July 2020), 101943. <https://doi.org/10.1016/j.cpr.2020.101943>
- Sivan, A., Corrales, L., Hubert, N., Williams, J. B., Aquino-Michaels, K., Earley, Z. M., ... Gajewski, T. F. (2015). Commensal Bifidobacterium promotes antitumor immunity and facilitates anti-PD-L1 efficacy. *Science*, *350*(6264), 1084–1089. <https://doi.org/10.1126/science.aac4255>
- Smith, K., McCoy, K. D., & Macpherson, A. J. (2007). Use of axenic animals in studying the adaptation of mammals to their commensal intestinal microbiota. *Seminars in Immunology*, *19*(2), 59–69. <https://doi.org/10.1016/j.smim.2006.10.002>
- Snitkin, E. S., Zelazny, A. M., Gupta, J., Palmore, T. N., Murray, P. R., & Segre, J. A. (2013). Genomic insights into the fate of colistin resistance and *Acinetobacter baumannii* during patient treatment. *Genome Research*, *23*(7), 1155–1162. <https://doi.org/10.1101/gr.154328.112>
- Spanogiannopoulos, P., Bess, E. N., Carmody, R. N., & Turnbaugh, P. J. (2016). The microbial pharmacists within us: A metagenomic view of xenobiotic metabolism. *Nature Reviews Microbiology*, *14*(5), 273–287. <https://doi.org/10.1038/nrmicro.2016.17>

- Stone, T. W., & Darlington, L. G. (2017). Microbial carcinogenic toxins and dietary anti-cancer protectants. *Cellular and Molecular Life Sciences*, *74*(14), 2627–2643. <https://doi.org/10.1007/s00018-017-2487-z>
- Stritzker, J., Weibel, S., Hill, P. J., Oelschlaeger, T. A., Goebel, W., & Szalay, A. A. (2007). Tumor-specific colonization, tissue distribution, and gene induction by probiotic *Escherichia coli* Nissle 1917 in live mice. *International Journal of Medical Microbiology*, *297*(3), 151–162. <https://doi.org/10.1016/j.ijmm.2007.01.008>
- Suzuki, N., Murata-Kamiya, N., Yanagiya, K., Suda, W., Hattori, M., Kanda, H., ... Hatakeyama, M. (2015). Mutual reinforcement of inflammation and carcinogenesis by the *Helicobacter pylori* CagA oncoprotein. *Scientific Reports*, *5*(March), 1–14. <https://doi.org/10.1038/srep10024>
- Takasuna, K., Hagiwara, T., Hirohashi, M., Kato, M., Nomura, M., Nagai, E., ... Kamataki, T. (1996). Involvement of beta-glucuronidase in intestinal microflora in the intestinal toxicity of the antitumor camptothecin derivative irinotecan hydrochloride (CPT-11) in rats. *Cancer Research*, *56*(16), 3752–3757.
- The Gene Ontology Consortium, C. (2000). Gene Ontology: tool for the unification of biology. *Nature Genetics*, *25*, 25–29. <https://doi.org/10.2174/1381612824666180522105202>
- Thomason, L. (2007). *Current Protocols in Molecular Biology*, ed Ausubel FJ. New York: Wiley.
- Turnbaugh, P. J., Ley, R. E., Hamady, M., Fraser-Liggett, C. M., Knight, R., & Gordon, J. I. (2007). The Human Microbiome Project. *Nature*, *449*(7164), 804–810. <https://doi.org/10.1038/nature06244>
- Valdes, A. M., Walter, J., Segal, E., & Spector, T. D. (2018). Role of the gut microbiota in nutrition and health. *BMJ*, *361*. <https://doi.org/10.1136/bmj.k2179>
- van Elsland, D., & Neefjes, J. (2018). Bacterial infections and cancer. *EMBO Reports*, *19*(11), 1–11. <https://doi.org/10.15252/embr.201846632>
- Vande Voorde, J., Vervaeke, P., Liekens, S., & Balzarini, J. (2015). Mycoplasma hyorhinitis-encoded cytidine deaminase efficiently inactivates cytosine-based anticancer drugs. *FEBS Open Bio*, *5*, 634–639. <https://doi.org/10.1016/j.fob.2015.07.007>
- Voorde, J. Vande, Liekens, S., & Balzarini, J. (2013). Mycoplasma hyorhinitis-encoded purine nucleoside phosphorylase: Kinetic properties and its effect on the cytostatic potential of purine-based anticancer drugs. *Molecular Pharmacology*, *84*(6), 865–875. <https://doi.org/10.1124/mol.113.088625>
- Voorde, J. Vande, Sabuncuog, S., Noppen, S., Hofer, A., Ranjbarian, F., Fieuws,

- S., ... Liekens, S. (2014). Nucleoside-catabolizing Enzymes in Mycoplasma-infected Tumor Cell Cultures Compromise the Cytostatic Activity of the Anticancer Drug Gemcitabine <sup>\*</sup>, 289(19), 13054–13065. <https://doi.org/10.1074/jbc.M114.558924>
- Walker, S. P., Tangney, M., & Claesson, M. J. (2020). Sequence-Based Characterization of Intratumoral Bacteria—A Guide to Best Practice. *Frontiers in Oncology*, 10(February), 1–12. <https://doi.org/10.3389/fonc.2020.00179>
- Widemann, B. C., Sung, E., Anderson, L., Salzer, W. L., Balis, F. M., Monitjo, K. S., ... Adamson, P. C. (2000). Pharmacokinetics and metabolism of the methotrexate metabolite 2, 4-diamino-N(10)-methylpteronic acid. *The Journal of Pharmacology and Experimental Therapeutics*, 294(3), 894–901.
- Wilson, M. R., Jiang, Y., Villalta, P. W., Stornetta, A., Boudreau, P. D., Carrá, A., ... Balskus, E. P. (2019). The human gut bacterial genotoxin colibactin alkylates DNA. *Science*, 363(6428). <https://doi.org/10.1126/science.aar7785>
- Yang, W., Soares, J., Greninger, P., Edelman, E. J., Lightfoot, H., Forbes, S., ... Garnett, M. J. (2013). Genomics of Drug Sensitivity in Cancer (GDSC): A resource for therapeutic biomarker discovery in cancer cells. *Nucleic Acids Research*, 41(D1), 955–961. <https://doi.org/10.1093/nar/gks1111>
- Yu, T. C., Guo, F., Yu, Y., Sun, T., Ma, D., Han, J., ... Fang, J. Y. (2017). *Fusobacterium nucleatum* Promotes Chemoresistance to Colorectal Cancer by Modulating Autophagy. *Cell*, 170(3), 548-563.e16. <https://doi.org/10.1016/j.cell.2017.07.008>
- Yue, B., Gao, R., Wang, Z., & Dou, W. (2021). Microbiota-Host-Irinotecan Axis: A New Insight Toward Irinotecan Chemotherapy. *Frontiers in Cellular and Infection Microbiology*, 11(October), 1–15. <https://doi.org/10.3389/fcimb.2021.710945>
- Zhang, T., Abel, S., Wiesch, P. A., Sasabe, J., Davis, B. M., Higgins, D. E., & Waldor, M. K. (2017). Deciphering the landscape of host barriers to *Listeria monocytogenes* infection. *Proceedings of the National Academy of Sciences of the United States of America*, 114(24), 6334–6339. <https://doi.org/10.1073/pnas.1702077114>
- Zhao, L., Liu, Z., Levy, S. F., & Wu, S. (2018). Bartender: A fast and accurate clustering algorithm to count barcode reads. *Bioinformatics*, 34(5), 739–747. <https://doi.org/10.1093/bioinformatics/btx655>
- Zhao, S., Lieberman, T. D., Poyet, M., Kauffman, K. M., Gibbons, S. M., Groussin, M., ... Alm, E. J. (2019). Adaptive Evolution within Gut Microbiomes of Healthy People. *Cell Host and Microbe*, 25(5), 656-667.e8. <https://doi.org/10.1016/j.chom.2019.03.007>
- Zheng, Q. (2017). rSalvador: An R package for the fluctuation experiment. *G3: Genes, Genomes, Genetics*, 7(12), 3849–3856.

<https://doi.org/10.1534/g3.117.300120>

Zhu, W., Wang, J. Z., Liu, Z., & Wei, J. F. (2022). The bacteria inside human cancer cells: Mainly as cancer promoters. *Frontiers in Oncology*, 12(August), 1–7. <https://doi.org/10.3389/fonc.2022.897330>

Zimmermann, M., Patil, K. R., Typas, A., & Maier, L. (2021). Towards a mechanistic understanding of reciprocal drug–microbiome interactions. *Molecular Systems Biology*, 17(3), 1–15. <https://doi.org/10.15252/msb.202010116>

Zimmermann, M., Zimmermann-Kogadeeva, M., Wegmann, R., & Goodman, A. L. (2019). Mapping human microbiome drug metabolism by gut bacteria and their genes. *Nature*, 570(7762), 462–467. <https://doi.org/10.1038/s41586-019-1291-3>